Templated Synthesis of Polymer Nanocapsules:

The Role of Template Characteristics in the Efficiency of Drug Delivery Systems

A thesis submitted in fulfilment of the requirements for the degree of

Doctor of Philosophy (Applied Chemistry)

Emma Clare Goethals

School of Applied Sciences

RMIT University

February 2013

Declaration

I certify that except where due acknowledgement has been made, the work is that of the author alone; the work has not been submitted previously, in whole or in part, to qualify for any other academic award; the content of the thesis is the result of work which has been carried out since the official commencement date of the approved research program; and any editorial work, paid or unpaid, carried out by a third party is acknowledged; and ethics, procedures and guidelines have been followed

……

Emma Clare Goethals

……/……/……

Acknowledgements

I would like to thank my supervisors Dr. Vipul Bansal and Professor Suresh Bhargava for offering the opportunity and the financial means to complete my PhD. Thank you for the interesting and challenging research subject, for your patience and the time that you spent working with me throughout my candidature, and for teaching me how to be a good scientist.

I would like to acknowledge a number of colleagues for their valuable collaborations. To Ahmad Esmaielzadeh Kandjani for developing the software used for particle analysis, and for assisting me in the development of the Artificial Neuron Network. To Abdulkareem Elbaz, Ravi Shukla, and Vishal Mistry, many thanks for your assistance in facilitating the cell uptake and cytotoxicity studies.

I would also like thank the staff at RMIT University, including Mr Phillip Francis and Mr. Peter Rummel for the countless hours they spent assisted me during my time in the Microscopy and Microanalysis Facilities. Also to the technical staff at the School of Applied Science, Mrs Zahra Homan, Mrs Nadia Zakhartchouk, Mrs Ruth Cepriano-Hall, Mr Howard Anderson, Mr Karl Lang, and Mrs Diane Mileo for all their assistance with the laboratory support.

I would like to add a special thanks to Dr. Selvakannan Periasamy for all your help over the last few years. At times when I could not solve a problem in the laboratory you always helped me find the answer, you spent many hours with me on my thesis, and you would reassure me that everything would work out when I thought it was all too hard.

However, what makes me most appreciative is that you helped me, along with many other students, without ever expecting anything in return.

Most of all, I would like to acknowledge my family and friends from which I received continuous encouragement and support, and without which I never would have found the perseverance to finish. To my wonderful parents, thank you for all your love and patience, your encouragement and commitment to my education, and letting me live at home many more years than I should have! To my wonderful partner Tom, there was never a day when you didn't support me in my PhD. Despite my crazy outbursts and constant lack of money, you always kept a smile on my face and reminded me how good it would be when I eventually finished. And finally to my friends, both the ones I have made at university and the ones from my high school years, thank you for keeping me sane and maintaining fun in my life!

During my years as a PhD student there were many people who contributed directly or indirectly my work. To every one of you I will be forever grateful!

List of Contents

List of Figures

List of Tables

List of Abbreviations

ANN	Artificial Neural Network
BET	Brunauer-Emmett-Teller Surface Analysis
CLSM	Confocal Laser Scanning Microscopy
DDS	Drug Delivery System
DDS	Drug Delivery
DLS	Dynamic Light Scattering
EDX	Energy-Dispersive X-ray Spectroscopy
FEG	Field Emission Gun
LbL	Layer-by-Layer
MS	Mesoporous Shell
ODTMS	Octadecyltrimethoxysilane
PAH	Poly(allylamine) Hydrochloride
PBS	Phosphate Buffer Saline
PGA	Poly(L-glutamic acid)
PLL	Poly(L-lysine)
PSS	Poly(sodium 4-styrene sulfonate)
SC	Solid Core
SC/MS	Solid Core/Mesoporous Shell
SEM	Scanning Electron Microscopy
SSC	Smooth Solid Core
TEM	Transmission Electron Microscopy
TEOS	Tetraethylorthosilicate
TGA	Thermogravimetric Analysis
UV-vis	UV Visable Spectroscopy
XRD	X-ray Diffraction

Abstract

The fabrication and employment of nano-size vehicles for the effective delivery of drugs for therapeutic applications is an emerging and promising field in nanotechnology. Although a diverse range of drug delivery vehicles exist today, most lack the finer control over their size and monodispersity which is essential if they are to be introduced into the body. This thesis exploits template particles for the fabrication of polymeric nanocapsules with structurally unique characteristics. To achieve this, silica nanoparticles acting as templates were first investigated, where the effects of the experimental parameters on the size and monodispersity of the templates was explored and optimized using both single and multivariable experiments, so that the particles could be tailored to their required application. Following template fabrication, a comparison study of two template-facilitated approaches to nanocapsule synthesis were investigated, and the combination of the solid core/mesoporous shell (SC/MS) approach along with the polymer material chitosan was found to be the most effective drug delivery systems (DDS). Through modification of the same SC/MS approach, seven structurally unique chitosan nanocapsules were fabricated, and the size of the vehicle was identified to be the most influential characteristic when comparing the cytotoxic efficiency. The body of this work identifies a promising nanocapsular drug delivery system for the future, which has demonstrated good control over the size and monodispersity of the nanocapsules, a high loading capacity for the water-labile drug curcumin, biocompatibility, and high cytotoxic efficiency when the drug is incorporated.

CHAPTER 1

INTRODUCTION

This chapter provides an overview to the thesis by introducing the field of nanotechnology, current advances in the field of biotechnology, and the way that these two fields are merging together to produce advanced and innovative materials for applications in drug delivery. The chapter also focuses on the approaches currently employed to synthesise a variety of nanoparticles and nanocapsules to act as drug delivery vehicles. Finally, a chapter-wise summary of this thesis has also been provided.

1.1 An Introduction to Nanotechnology

If you have ever become tangled in a spider web and been amazed at how something so small and seemingly so fragile has such strength and flexibility, then you wouldn't be alone. You may not know it at the time but this is due to the phenomena of nanotechnology. When particles (or materials that are made of particles) consist of only a small number of atoms or molecules, the material no longer acts as it would in comparison to its bulk form. Instead, quantum forces begin to dominate and the material can take on surprising new properties.

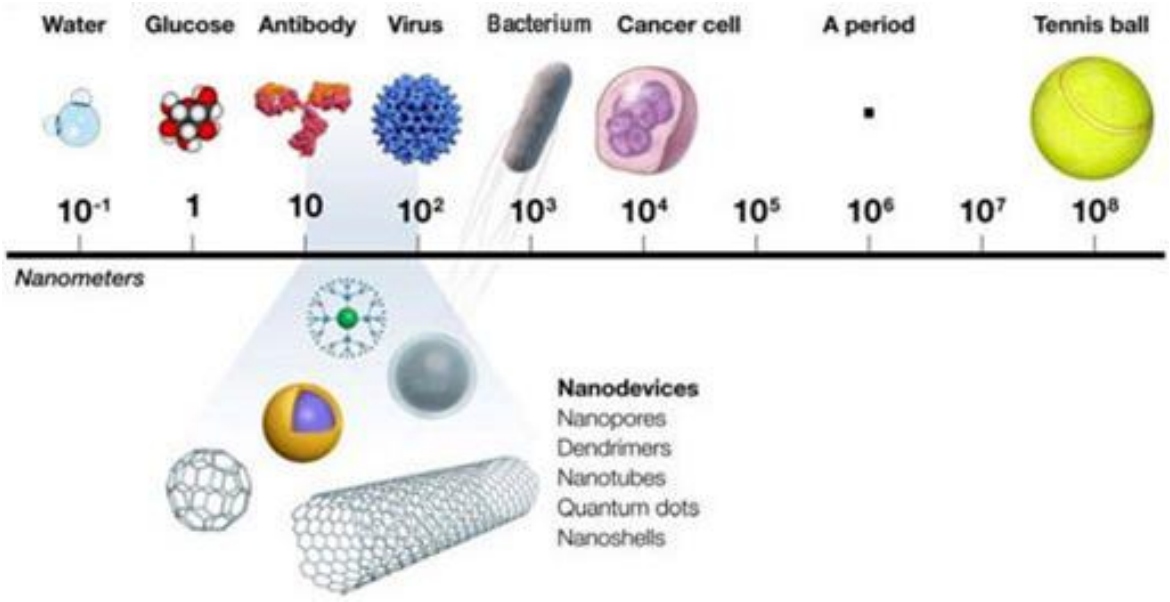

Figure 1: A scale to represent the nano-sized devices compared to other materials. Courtesy of Technologies and Tendencies in Cyberspace.[1]

Nanotechnology is not any particular scientific discipline, nor is it really a field as much a way of thinking about the world around us. The simplest definition of nanotechnology is 'technology at the nanoscale',[2] and encompasses the manipulation of matter on the atomic or molecular level, as well as the technologies and technical processes it employs. The prefix

'nano' originated from the Greek word 'nannos', meaning 'dwarf', which represents one-billionth (10^{-9}) of a base unit. For example, one nanometer is equivalent to 1 x 10^{-9} meters (0.000 000 001 meters). Nanotechnology essentially studies the phenomena that occur in a system when it contains nano-sized features, or features that are typically less than 100 nm in at least one dimension.

Amazingly, the application of 'nano' effects has been traced to glass dating from the 4th century. The famous Roman Lycurgus cup made of a diachronic glass appears green in daylight (when light is reflected off the outer surface), and appears red when lit from within (light transmitted through the vessel). The brilliant optical effects are due to inclusions of minute gold and silver dust particles which undergo surface plasmon resonance.[3-5]

Figure 2: The Lycurgus cup demonstrating different optical effects depending on whether the light is reflected off the glass surface (A) or transmitted through the glass (B). Image adapted from http://www.guardian.co.uk/nanotechnology-world/nanotechnology-is-ancient-history

Mother Nature has also devised nano-sized structures that, due to millions of years of evolution, are so elegant and precise in architecture that engineers today are still unable to

replicate. Nature has successfully developed an impressive and ingenious variety of nano-sized structures including nanocavities in butterflies,[6,7] nanofibers in spider webs,[8] inorganic nanocrystals fabricated by bacteria,[9] and nanorods for superhydrophobic surfaces in lotus leaves.[10]

One of the main ambitions in science is to emulate these intricate and elegant nanostructures already prevalent in nature. Richard Feynman was the first to shed light on the concept in 1959 during his speech "There's plenty of room at the bottom", where he spoke of the possibility of using precise tools to manipulate individual atoms and molecules. Now there seems to be a 'nanotechnology mania' sweeping through the scientific and commercial world, with the National Institute of Health stating in a report in 2000 that 'Every once in a while, a new science and technology emerges that enables the development of a new generation of scientific and technological approaches. Nanotechnology holds such promise'.[11]

One peculiar advantage of nano-sized materials is that their chemical, optical, magnetic and electronic properties can be drastically altered by slight modifications in their physical structure.[12-14] This is because the physical or chemical laws on which macroscopic materials rely do not always translate to the nano world, and as such nanoscaled systems with a scale length in the order of the electron de Broglie wavelength have to be considered to behave within quantum mechanical limits. As one approaches the range of the nano world, the mass of objects becomes increasingly negligent, therefore gravitational forces become less influential while electrostatic attractions and van der Waals forces become increasingly important.[2,15]

The factors that can strongly affect these properties include the material size,[16-21] shape,[22-24] surface composition,[25-28] interparticle interactions,[29-33] and dielectric conditions in which they are held.[34-36] Such significant variations in the properties of nanomaterials are due to their dimensions being comparable to that of the de Broglie wavelength.[37,38] In addition, their small dimensions allow for fast frequency motion, as well as amplified pressure values due to the small surface areas involved.[2,39]

The most commonly used method for developing structures on the submicrometer scale are the 'top-down' approaches which involve the miniaturization of larger, basic units to smaller units. For example, lithographic techniques project a condensed and shrunken replication of a much larger template from which nanoscaled elements are etched. This approach can be considered to be the way that scientists initially learned to fabricate materials and, after time, engineered the structures at submicron levels. However, on approaching sizes below 100 nm, the resolution and replication speed is severely limited by the available technology. As a result the 'bottom-up' approach becomes more important when reaching sub-micron size regions.

The 'bottom-up' method involves the fabrication of individual units to form a larger subsystem. The synthesised nano-sized articles are formed from atomic or molecular compounds using highly controlled conditions and can be tailored to follow specific growth energetics and kinetics. This approach obtains better defined microscopic growth of nanostructures without the need for subsequent manipulation.[39] Within bottom-up methods, two different approaches exist. The first is through understanding and attempting to imitate the complex systems already manifested by Nature, which is capable of feats far beyond what

is currently possible in the laboratory. The second approach is through non-biological molecular mechanisms where a controlled reaction occurs at either a surface or in a liquid, producing complex structures that are influenced at the atomic scale.[40] Using the second approach, new and unique nanostructures can be developed for innovative applications.

1.2 Nanotechnology for Cancer Therapy

One of the most intensively studied areas in nanotechnology is in the engineering of nanoparticles for biomedical applications, with nanoparticles for cancer therapies and diagnostics being one of the fastest expanding fields.[41] Nowadays these engineered particles are multifunctional with abilities to not only encapsulate and release anticancer drugs in a highly controllable way, but also specifically target cancerous tissue for drug release while enhancing contrast for diagnostic purposes.[42]

Cancer is a major public health issue that at some point will directly or indirectly affect every person in their lifetime. One in two Australians are diagnosed with cancer by the age of 85, and out of those cancer patients more than 30% do not survive five years after diagnosis.[43] Furthermore, cancer treatment in Australia costs the government approximately $3.8 billion annually. However, according to Cancer Council Australia the survival rate for many common cancers has increased by 30 % due to recent advancements in cancer research and newly available treatments.[43]

Cancer is a general term used to characterise any disease that arises due to the uncontrolled proliferation of abnormal cells.[45] As these cancerous cells can be generated from almost any type of tissue cell in the body, the collective term ‘cancer’ can refer to more than

200 different diseases.[46] This also makes it extremely difficult in treating cancerous malignancies as they can vary significantly. Effective treatments that are currently employed include surgery, radiotherapy, chemotherapy, hormone therapy and immunotherapy.[47]

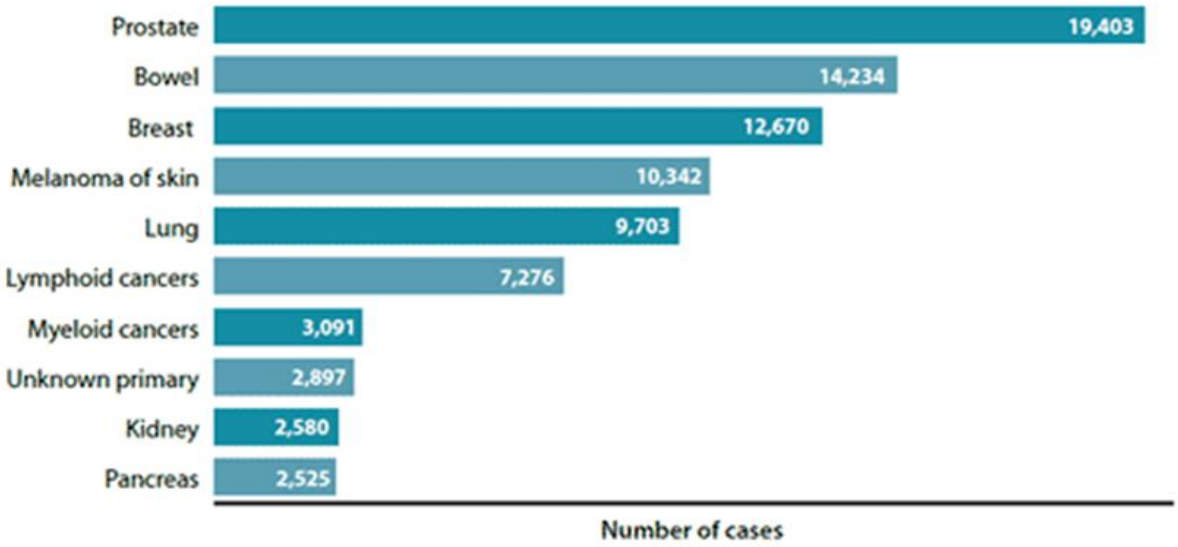

Figure 1.3: A representation of the number of cancers most commonly diagnosed in Australia (2007), courtesy of the Australian Institute of Health and Welfare.[44]

Unfortunately there are several drawbacks with all these conventional cancer therapies. The surgical option is often a very effective method in removal of a cancerous tumour. However, this method is not always viable due to the location of the tumour, or if it is viable it can be very invasive. In addition, surgery often fails in removing 100% of affected cells that can potentially spread and grow into secondary tumours.[48] In contrast, the majority of non-surgical therapies (radio-, chemo-, and immuno-therapy) cannot appreciably differentiate between normal and tumour cells and consequently, although these therapies are

very effective at killing cancer cells, they may also be very toxic to normal cells in the process, causing severe systemic toxicity and adverse side effects.[48]

There have been several approaches to improve the effectiveness and selectivity of anticancer drugs. One approach has been to develop new and innovative drugs that interfere with specific pathways only active in cancerous cells.[49,50] Another method is the development of systems that deliver currently employed anticancer drugs more effectively and selectively by means of drug carrier vehicles,[47,51] where the aim is to ensure acute toxicity to the target cells, while the normal cells remain unaffected. This latter approach is known as a drug delivery system or DDS.

1.3 Controlled Drug Delivery Systems

A drug delivery system (DDS) is a catch-all term used to describe the encapsulation or attachment of drugs to optimised carriers, which modify its pharmacokinetics, its localization in the body, and its uptake into different cells and tissues.[52] The development of controllable drug delivery systems has recently received increased focus in an effort to overcome the drawbacks that continue to plague current cancer therapies. Over the past few decades, a variety of multifunctional and/or biocompatible drug delivery systems with increased drug encapsulation, release kinetics and targeting abilities have been fabricated.

Nano-sized drug delivery systems have received the greatest attention due to the advantages of their sub-cellular size and high surface area to volume ratio.[53,54] In addition, depending on the components of the vehicle, these nano-systems have shown increased drug specificity, efficacy, tolerability and therapeutic index.[55-61] The concept of using nano-sized

carriers for the delivery of drugs was first employed by Speiser and Kopf in the 1970s,[62] with the field rapidly expanding since to include a wide variety of organic, inorganic and hybrid drug delivery vehicles, including but not limited to micelles,[63,64] liposomes,[65,66] solid lipid nanoparticles,[67,68] polymeric nanoparticles,[51,53,69] polymerosomes,[70,71] capsosomes,[72,73] carbon nantotubes,[74,75] and gold nanoparticles.[76-79]

Specifically, a variety of silica-based particles have become more abundant in DDSs due to the materials inert nature, low toxicity, low susceptibility to microbial attack, and its demonstrated ability to be easily fabricated and conjugated to a range of biocompatible components.[80,81] Such drug-loadable silica-based particles include hollow silica nanocapsules,[82] polymer-coated silica nanoparticles,[83] mesoporous silica nanoparticles,[80,81] and multifunctional magnetic and fluorescent silica nanoparticles.[84-86]

1.4 Silica

Silicon dioxide, also known as silica, is composed of oxygen and silicon and is one of the main components of the Earth's crust. It is most commonly found in nature as sand or quartz, and is often manufactured in the forms of fused quartz, crystal, fused silica, silica gel, aerogel, and colloidal silica.[87] Without it many of our modern day technologies would be very different, with silica used in modern day glass and ceramics, as catalysts in oil refineries, microelectronics and fibre optics,[87] and is more recently finding a broad range of potential applications in the world of nanobiotechnology.[88]

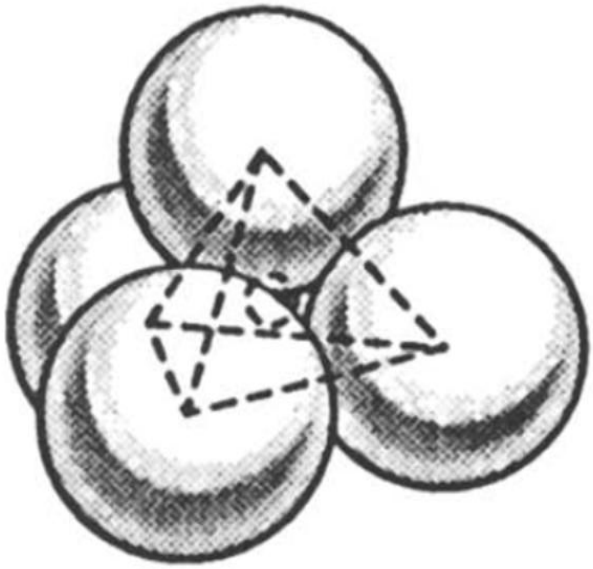

Figure 1.4: Space-filled representation of the tetrahedral coordination of oxygen ions with silicon, figure appropriated from Breck[89]

Although the building block of silica is consisted of a silicon atom surrounded by four oxygen atoms (Figure 1.4), the chemical formula of silica is SiO_2 as the oxygen atoms are shared through either a crystalline or amorphous network. The differences in the way that the tetrahedral $[SiO_4]^{-4}$ units are linked together is described by polymorphism. Quartz has the densest structure as all four oxygen atoms are shared to create a three-dimensional network (Figure 1.5A) and is an example of a highly ordered crystalline silica form. Contrastingly, in amorphous silica the packing of $[SiO_4]^{-4}$ units is random, resulting in a non-periodic structure where the subunits come together by either sharing two oxygen atoms with adjacent groups to form a chain, or three oxygen atoms are shared to form a sheet-like structure (Figure 1.5B).

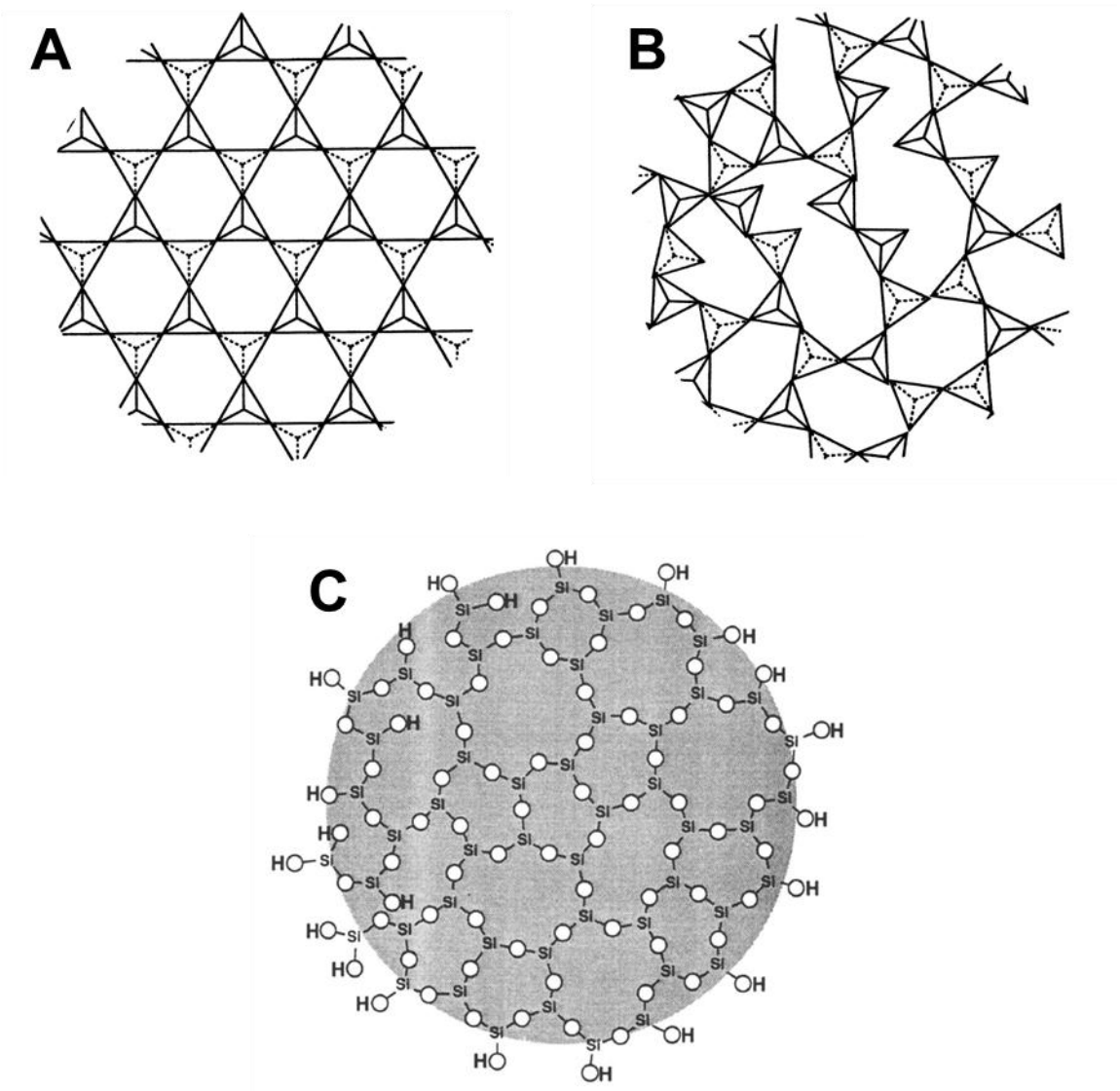

Figure 1.5: Two-dimensional schematic representation for crystalline (A) and amorphous (B) packing of SiO_4 subunits. (C) Two-dimensional schematic representation of a fully hydroxylated colloidal silica particle. Courtesy of Pauling and Bergna.[87,90]

1.5 Colloidal Silica

As areas in science and technology grow, so does the demand for uniform and monodispersed particles. Colloidal silica is of special interest as the system is dominated by short-range forces such as van der Waals and surface forces.[91] The term colloidal typically

refers to particles dispersed in a solvent that have the dimensions of 1-1000 nm in at least one direction. The most important characteristic of colloidal particles is that they are larger than the molecules of the surrounding solvent, allowing them to diffuse via thermal motion. During this diffusive movement the particles undergo fluctuations in their motions due to random collisions with the solvent molecules, this is usually referred to as "Brownian motion".[92,93] As a result the colloidal particles exhibit similar phase behaviour to that of molecules and atoms, however the main advantages of colloidal particles is that their diffusion is orders of magnitude slower than atoms, making them easier to observe and study. Colloidal materials can be referred to as 'soft' as they respond to small external forces,[94] and they can be studied using light scattering and optical techniques since their size is comparable to the wavelength of visible light. Furthermore, the structural characteristics of colloidal particles such as sizes, shapes and chemical properties have been shown to be readily tunable during synthesis.[34,87,95]

Colloidal silica synthesis is expanding with increasing demand for industrial uses such as pigments,[96] stabilizers,[97] catalysis,[98] chemical mechanical polishing,[99] and in numerous scientific fields.[66,93] There has been extensive investigation into broadening the size of particles, improving uniformity and monodispersity, and simplifying the synthesis processes. Colloidal silica has been fabricated via a variety of methods and from a variety of raw materials such as silicon,[100] silicon tetrachloride,[101] water glass,[102] silica powder,[103] and alkoxysilanes.[104,105] However, while the many possibilities for colloidal synthesis are acknowledged, this thesis focuses only on the synthesis of colloidal silica from alkoxysilanes.

In 1956, Kolbe was the first to report on the synthesis of solid, non-porous, monodispersed silica particles through the hydrolysis and subsequent condensation of silicon

alkoxides in a short-chain alcohol solvent.[104] Later in 1968, Werner Stöber expanded Kolbe's work further in a pioneering study where he investigated the reaction conditions and their effects on particle size, and in doing so, was able to synthesize highly homogenous and monodispersed particles in the sub-micron range.[105] To this day the study is regarded as providing the simplest and most robust method for producing colloidal silica.

The experimental procedure for the Stöber method is relatively straight forward, however, the mechanisms responsible for the nucleation and growth of the particles are not. The synthesis involves the ammonia-catalysed reaction between tetraethylorthosilicate (TEOS) and water in a low-molecular weight alcohol solvent. There have been numerous research groups investigating the complex mechanisms of nucleation and the influence of the reaction conditions on the particle size.[106-114]

In brief, the overall conversion of TEOS into SiO_2 can be described as;

$$\mathbf{Si(OR)_4 + 2H_2O \rightarrow SiO_2 + ROH} \qquad \text{Eq. 1.1}$$

where R represents the alkoxy group of a low molecular weight alcohol.

Controlling the size and monodispersity of solid silica particles is of the upmost importance due to the high demand for such particles, where the size can dictate their future applications. Furthermore, the ability to predict particle size based on the experimental parameters is even more sought after as a specific size may be required for a desired application.

Many trends of the effects of the experimental parameters on the sizes of the particles have been proposed. These parameters include the reaction solvent,[105,113-115] TEOS

concentration,[113-116] ammonia,[105,110,113-115] water quantity,[110,113-115] and reaction temperature.[113,115] Many of these studies are in agreement that a general trend of smaller particle formation is observed when a lower molecular weight solvent is used, when there is a decrease in TEOS concentration and when the reaction temperature is increased. Whereas the effect of ammonia and water content are not as predictable and have not always been consistent in the literature.[114,115] However, these investigations required single variable changes and therefore numerous experiments were necessary and laborious, furthermore, when multiple variables are changed it is extremely difficult to predict the final particle size due to the complex changes occurring in the experimental solution, such as interparticle forces, viscosity, zeta potential and pH.[117] One method to overcome this is by employing computing models which can simulate multiple effects of the parameter during a reaction. These models can generate more comprehensive conclusions about the system, while also reducing the number of experimental investigations required to be performed.

1.6 Artificial Neural Networks (ANN)

Through millions of years of evolution, the human brain has been developed into an "organic computer" capable of performing complex tasks simultaneously and many times throughout a day. Without a brain we would not be able to recognise the people around us, drive a car, write an essay, or even perform the simplest of actions. Our brains are a component of a very complex and elegant nervous system, yet when broken down it consists of relatively simple units called neurons. Neurons are small single cell structures that enable the transmission of electrical signals around the body, enabling it to function. The brain gains it's abilities through the massively interconnected network of these neurons, with

approximately 15-30 billion neurons in the human brain that is each connected to several thousand other neurons through synapse pathways. The massively interconnected system allows for complex tasks/pathways to be processed by analysing the information received through the senses, and combining this with information available about the needs of the organism, along with previous memories of success or failure.

Inspired by the learning capabilities of the human brain and their structures, mathematical functions were developed to mimic and act as "artificial neurons". An Artificial Neural Network (ANN) is an interconnected framework of these 'artificial neurons', or nodes, which can be seen as computational units that receive and process inputs, and in doing so produce outputs to create a computational pathways capable of solving complex and extensive problems that linear computing cannot.[118] Similar to human brains, ANNs are typically adaptive systems that can "learn" and change the way the neurons are connected, which in turn can change the way inputs are processed.

ANNs consist of multiple layers of artificial neurons, including the input neurons, a specified number of processing neurons, and the output neurons (Figure 1.6). Since the input and output layers are the most important to the user, the middle neurons are typically referred to as the hidden layer despite performing the most important tasks. Depending on the complexity of the task, the hidden layer can consist anywhere from 1 to any number of "neurons".

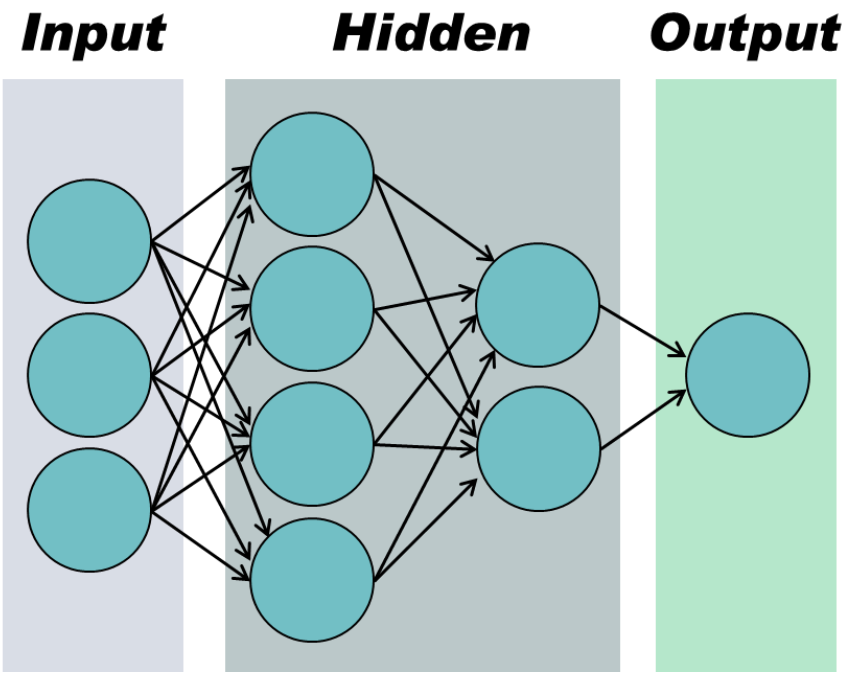

Figure 1.6: A simplified model of the layer of neurons in an artificial neuron network.

As the neurons are interconnected and receive signals from multiple sources, they can judge each input based on applied mathematic functions and decide which signals are more important and require more 'weight' during processing before the output is transmitted to the next node. This continues until the final outputs have been produced, however the first attempts by the nodes to process information is often not accurate. To increase accuracy the ANNs must learn through a technique called back propagation. This is done by comparing the desired (or expected) outputs with the outputs received, and adjusting the "weights" of the neurons back though the layers in an effort to reduce erroneous values. Back propagation is typically repeated many times until the outputs resemble the desired outcomes very closely. The closeness to the desire value is referred to as its precision and denoted as a fraction of one. However, as ANN only process algorithms and identify patterns in systems, they must first be adapted to an experimental situation in some way.

In scientific studies, experiments are often carried out in a full factorial manner, where one variable is changed at a time while all other variables are kept constant. In very complex or large studies where there can be any combination of the parameter values which can be virtually plotted out in a 3 dimensional matrix. For example, if there are three parameters that require investigation, their combinations can be visualised within a 3-dimentianal cube, or a matrix, where the axis x, y, and z represent the parameters. This can create an overwhelming number of sample points, and if one wants to try and test each sample point, they could be there for a very, very, *very* long time. Therefore statistical experimental designs are often implemented.

Experimental designs involve fitting sample points in an even distribution over the matrix of variables in a system, and identifying the experiments required to extract the most information out of the smallest number of experiments. In contrast to full factorial experiment designs, Box-Behnken,[119] and Doehlert,[120] are multivariable experiment designs, and they involve two or more variables changing between each experiment. These multivariable techniques offer the advantage of further reducing the number of experiments required, and also generate more information on the interactive effects among the variables.

As the experiment design only defines the experiments which are required, it is the ANN which correlates the variables to the results to generate information which can be interpreted. The ANNs then correlates the multiple experimental values to the results in a virtual 3 dimensional map using specified algorithms. The computer model then recognises patterns in the 3D projection (something that is a little too complex for the human mind), and creates a continuous map that precisely forecasts the position of results with regards to the

parameters. In some cases, ANNs have been applied to systems where the size of a fabricated particle is affected by certain experimental conditions.[121-123] Using this combination of experimental design and ANNs, investigations into the dynamic effects of a system can be observed, and particles sizes based on those conditions can be predicted. Due to the complexity of ANNs, only a brief introduction has been included in this section, however for more information please refer to the ANN review by Basheer *et al*,[124] or the short video available at youtube.[125]

1.7 Core-Shell Silica

The design and controlled fabrication of core-shell colloidal materials has also been explored, wherein core-shell colloids demonstrate unique optical, structural and surface properties that are dictated as a function of their size, composition and structural order.[94] A core-shell particle is defined as having an internal material composed of a different substance, or having different properties to, an outer (encapsulating) material to form a dual component system. The synthesis of core-shell particles with defined morphologies and properties can be described as particle engineering.[126,127] Composite colloids have been used in coatings, electronics, catalysis, separations and diagnostics.[80,87,88,95,128] The addition of an outer shell onto a particle is typically performed to enable tailoring of the surface properties without losing the initial properties of the encapsulated particle. Often the shell is achieved by coating or encapsulating the core particle with a preferred material in an attempt to alter the charge, functionality, and reactivity, and/or enhance the stability and dispersion of the particles (See Figure 1.7).[127] Consequently, core-shell particles often exhibit improved chemical and

physical properties in comparison to their single-component counterparts, and offering potential in a broader range of applications.[127]

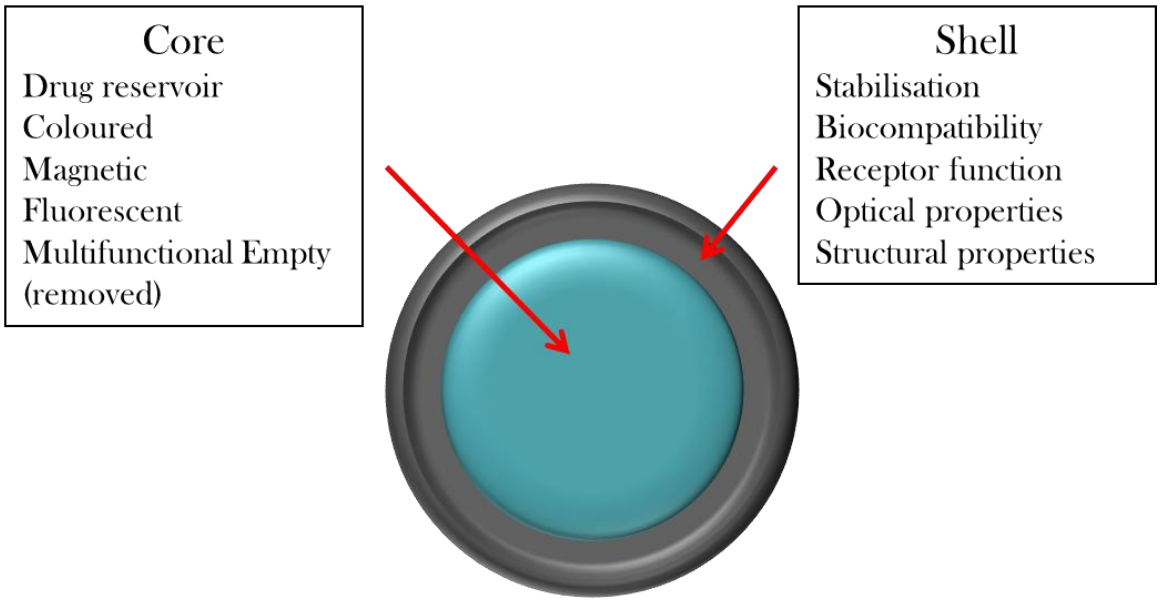

Figure 1.7: A simplified representation of Core/Shell particles and the potential properties of the components.

In the literature there has been a plethora of core-shell particles reported in which silica acts as the shell or coating.[129-132] This is usually to increase stability, biocompatibility, functionalisation capabilities and enhance optical properties. However, there have been relatively fewer core-shell particles where colloidal silica is utilised as the core, surrounded by a secondary material. Such silica core-shell particles that have so far been fabricated include shells of various polymers for enhanced biocompatibility and stealth characteristics,[104,105] and enhanced optical, electric, magnetic, catalytic and absorbent properties.[101,133]

An additional type of core-shell particle that is possible is a solid silica core surrounded by a mesoporous silica shell, or an SC/MS. This was developed in 1998 by Büchel *et al*, who adapted the Stöber method to synthesise a solid silica core (SC), but added a

subsequent step where a mesoporous silica shell (MS) is grown onto the solid core. The mesoporous shell step follows similar Stöber mechanisms where TEOS is hydrolysed onto the silica surface; however there is an addition of the porogen substance octyltrimethoxysilane in the secondary silica mixture which is later removed by calcination to create pores in the outer silica shell, resulting in the formation of solid silica cores with outer mesoporous silica shells.[134] The SC/MS particles have received a great deal of interest in more recent years as promising candidates for multimodal nanoparticle systems,[84,129-131,135,136] especially in biological applications due to their relatively simple fabrication, controllable structural properties, and their ability to be easily functionalised.[87,98,105,116,137,138]

Despite the high potential of silica nanoparticles, whether they are only solid cores, fully mesoporous or solid core/mesoporous shell silica nanoparticles, concerns have been expressed about the possible hazards of utilising inorganic nanoparticles in biological systems, and the toxic affects they could potentially incur.[98,99,133,139] The fear arises due to a lack of understanding of the interactions that can occur between the silica nanoparticles and cells and cellular membranes.[140,141] As well as the discrepancies between the toxic effects studied *in vitro* and *in vivo*,[142,143] the mechanisms of toxicity are not fully understood.[144]

One solution proposed to overcome this problem has been to coat the various silica nanoparticles in polymeric shells.[100-102] The polymer shells can provide colloidal stability and increase blood circulation time,[145] but as the silica particle is still introduced to the body it will remain a potential hazard until it is excreted. A safer approach is to utilize the highly controllable and monodispersed silica nanoparticles as templates, whereby a polymeric outer shell is grown, deposited or infused, followed by subsequent removal of the silica core matrix

through an etching process. Using this approach all the superior structural characteristics such as homogeneous size, mesoporous shell, and controllability of the silica particle can be retained, while negating the introduction of potentially hazardous silica particles into the body or tissue. This approach results in highly homogeneous polymer-based nanocapsules, which depending on the polymer used, can also be biocompatible and biodegradable in nature.

1.8 Polymeric Nanocapsules for Drug Delivery

Nanocapsules are defined as spherical structures with an ultrathin shell enclosing a solvent-filled interior,[146] and have been the subject of significant investigation in recent years to act as carriers for the controlled release and delivery of pharmaceutical drugs.[69,147-156] They are often described as a 'reservoir' system as the drug is confined to an aqueous or oily cavity.[157,158] When the nanocapsular system is well designed, this delivery vehicle is able to protect the drug from decomposition during transport throughout the body before it is released at the target site. Nanocapsules offer a greater advantage over solid nanospheres in reference to delivery applications as they have a potentially larger capacity to carry drug molecules not only on the capsule surface, but also in the hollow interior.

More specifically, polymeric nanocapsules have been extensively studied as drug carriers given the polymeric material can be selected based on their potential application. Polymers are large macromolecules made up of repeating structural subunits which are typically linked together by covalent bonds to form long, linear chains.[159] The choice of polymeric material is of great importance as this material comes into direct contact with the body, and depending on the desired mode of delivery, the polymeric carrier may either be identified or not identified by the immune system. The biocompatibility, biodegradability, low

immunotoxicity, and longevity in the circulatory systems are all properties which can dictate the polymer selected for a particular treatment.[149,151,160-163]

Biodegradable polymers are highly advantageous in DDS because of their ability to be processed by the body, thereby not accumulating and negating the need to be surgically removed. Biopolymers are a special class of biocompatible and biodegradable polymers which are produced by living organisms. One such biopolymer which has been extensively used in DDSs is chitosan due to its low immunogenicity, high biocompatibility, and it being readily available and cheap.[164-168] Although biopolymers are usually cheap, they can also vary greatly in purity and often require cross-linking which can alter their properties. Therefore, synthetic versions are often used. The most utilized synthetic, biodegradable polymers include poly(lactic acid), poly(glycolic acid), and poly(lactic acid)-poly(glycolic acid) copolymers.[169] However, these polymers are considerably expensive, may not have a long shelf life, and tend to be sensitive to experimental conditions, making them not always feasible.

Synthetic, non-biocompatible polyelectrolytes are another alternative as they tend to be much cheaper and more robust. Furthermore, if a biocompatible material is essential for *in vivo* or *in vitro* research, the preliminary investigations can be carried out using a much cheaper polymer, and later the biocompatible (and more expensive) polymer can be substituted. One such synthetic polymer is poly(allylamine) hydrochloride (PAH), which is cationic in nature due to the presence of an amine group. Another common synthetic polymer is poly(sodium 4-styrene sulfonate) (PSS), but unlike PAH, PSS is anionic in nature due to the presence of the sulfonate group. Although both synthetic polymers are relatively cheap, readily available, and their properties have been heavily studied,[170-173] they do not tend to be

as biocompatible as the biopolymers. Therefore any prospective polymers must be thoroughly investigated, their properties weight up, and chosen based on their suitability to the potential application.

Polymer-based nanocapsules are usually prepared via one of six classical methods; nano-precipitation, emulsion-diffusion, double emulsification, emulsion-coacervation, polymer-coating and layer-by-layer (LbL) assembly methods.[69] Many of these methods have shown to be very successful at producing hollow nanocapsules. However, the self-assembly methods of synthesis that do not utilize a particle template (nano-precipitation, emulsion-diffusion, double emulsification, and emulsion-coacervation) often produce particles with broad size distribution, some of which are in the nano-to-micrometer range. In addition, the experimental conditions in some of these methods are relatively harsh, making them unsuitable for certain materials that are desired for encapsulation. Moreover, the biggest drawbacks in the template-free processes is the lack of control over the capsule's structural characteristics with the occurrence of large distributions in the capsule size, wall thickness and uniformity.[174] These variations can have significant impacts on the consistency of their drug loading and release profiles, rendering them unsuitable for many clinical uses.

To overcome these obstacles, sacrificial template particles, typically silica, of controllable size and structural features can be employed.[105,175-178] The most common templating method that has been used in the past to fabricate polymeric nanocapsules is the LbL approach.[72,120,135,139-142] The LbL approach typically involves the sequential layering of oppositely charge polymers onto a template surface, building up enough polymeric material to form a capsule after template is removed. Another template method is the lesser known

SC/MS approach.[156] This approach involves the infiltration of polymers into tiny mesopores scattered throughout the outer shell of a silica template particle, followed by polymer cross-linking.

The employment of silica template particles to fabricate polymeric nanocapsules allows for improved monodispersity, homogeneity, and capsule integrity. Furthermore, due to the commercial availability and well-established methods to synthesize colloidal silica template particles of near-monodispersed size distribution in a wide size range,[105,107,110,134,138,179] capsules fabricated using the LbL and SC/MS templating methods can achieve an equally broad size range.

Despite the obvious advantages of using templating methods for nanocapsule fabrication, it is unclear which method demonstrates the greatest potential as a drug delivery platform. Furthermore, the polymeric material employed in fabrication is of great significance and needs comprehensive investigation. A superior drug delivery system is developed through the combination of a range of complementary components.

Through systematic investigation in this thesis, an attempt has been made to demonstrate that by employing artificial neural network (ANN) approaches, the fabrication of highly homogenous and controllable template particles was achieved. These particles were then exploited for the fabrication of different polymeric nanocapsules with enhanced and controllable characteristics, ideal for drug delivery applications. Such an approach contributes to the existing knowledge gap in the field of nanocapsule-based drug delivery systems.

1.9 Thesis Overview

The work presented in this thesis describes the synthesis of smooth solid core (SSC) and solid core/mesoporous shell (SC/MS) silica template nanoparticles which can be used to fabricate a variety of nanocapsules of different polymeric material and with several different structural features. The effect of these physical features on the nanocapsules and their efficiency to act as drug delivery vehicles has been investigated.

The chapters in this thesis can be broken down as follows:

Chapter 2 introduces the different instrumental techniques that have been employed for the chacterisation of the materials that had been synthesised. The silica template particles and nanocapsules were investigated using scanning and transmission electron microscopy (SEM and TEM), energy-dispersive X-ray (EDX) spectroscopy, dynamic light scattering (DLS), BET surface analysis (BET), UV visible spectroscopy (UV-vis), confocal laser scanning microscopy (CLSM), and thermogravimetric analysis (TGA).

Chapter 3 discusses the synthesis and characterisation of solid core silica nanoparticles fabricated based on the Stöber method, whereby tetraethylorthosilicate is hydrolysed in an ammonia-catalysed reaction, performed in a low molecular weight alcohol solvent. Through experimental processes, the effects of the solvent, ammonia and water content, and reaction temperature were investigated. Furthermore, these effects which had been found not to be exclusive from one another, were modelled using artificial neuron networks to help explain the complex interaction of these parameter, and to enable the accurate prediction of particle size in multivariable experiments.

Chapter 4 compares two dissimilar templating methods and three polymers to fabricate nanocapsules as drug delivery systems. The first templating method involves solid core/mesoporous shell template particles that are employed to fabricate single component chitosan and poly(allylamine hydrochloride) capsules by way of infusing the polymer into the pores within the template shell. The second method involved the sequential deposition of positively and negatively charged polymers onto a smooth silica templates to fabricate combined poly(allylamine hydrochloride) and poly(sodium 4-styrenesulfonate) nanocapsules using a layer by layer approach. Through the comparison of the drug loading capabilities, the cellular uptake, and the cytotoxicity of the capsules, the chitosan capsules fabricated by the SC/MS method was identified to be the best candidate for further investigation as a drug delivery system.

Chapter 5 carries on from chapter 4, and demonstrates that alterations in the structural features of the SC/MS template particles can be translated to develop structurally unique chitosan nanocapsules. Through modifications of the size of the solid silica core based on investigations carried out in chapter 3, and additional modifications to the mesoporous shell thickness and porosity of the SC/MS template particles, the size, capsules wall thickness and wall porosity of chitosan capsules fabricated using these templates can be controlled. In total, seven structurally unique chitosan capsules were fabricated, their drug loading ability investigated, and *in vitro* cellular uptake and cytotoxicity studies were carried out.

Chapter 6 provides a summary of the research undertaking and the results that were yielded in this PhD candidature. This chapter also provides a scope for future work that could be carried out in the area.

1.10 References

1 Trimegisto. *Nanotechnology: What is nanotechnology?*, <http://networksandservers.blogspot.com.au/2011/01/nanotechnology.html> (2012).

2 Ramsden, J. *Nanotechnology: an introduction*. (William Andrew, 2011).

3 Savage, G. *Glass and Glassware*. (1975).

4 Wagner, F. E. *et al.* Before striking gold in gold-ruby glass. *Nature* **407** 691-692, (2000).

5 Turkevich, J. Colloidal Gold, Part I *Gold Bulletin* **18**, (1985).

6 Anderson, T. F. & Richards, A. G. An electron microscope study of some structural colors of insects. *Journal of applied Physics* **13**, 748-758, (1942).

7 Onslow, H. On a periodic structure in many insect scales, and the cause of their iridescent colours. *Philosophical Transactions of the Royal Society of London. Series B, Containing Papers of a Biological Character* **211**, 1-74, (1923).

8 Ko, F. K. & Jovicic, J. Modeling of Mechanical Properties and Structural Design of Spider Web. *Biomacromolecules* **5**, 780-785, (2004).

9 Prozorov, R. *et al.* Magnetic irreversibility and the Verwey transition in nanocrystalline bacterial magnetite. *Physical Review B* **76**, 054406, (2007).

10 Koch, K. & Barthlott, W. Superhydrophobic and superhydrophilic plant surfaces: an inspiration for biomimetic materials. *Philosophical Transactions of the Royal Society A: Mathematical, Physical and Engineering Sciences* **367**, 1487-1509, (2009).

11 Nanotechnology Symposium Report. (Biomedical Engineering Alliance & Consortium, 2000).

12 Martín-Palma, R. J. & Lakhtakia, A. *Properties of Nanostructures*. (SPIE Press, 2010).

13 Salata, O. Applications of nanoparticles in biology and medicine. *Journal of nanobiotechnology* **2**, 3, (2004).

14 Zheng, J., Nicovich, P. R. & Dickson, R. M. Highly Fluorescent Noble Metal Quantum Dots. *Annual review of physical chemistry* **58**, 409, (2007).

15 Poole, C. P. J. & Owens, F. J. *Introduction to Nanotechnology*. (John Wiley & Sons, 2003).

16 Brust, M. & Kiely, C. J. Some recent advances in nanostructure preparation from gold and silver particles: a short topical review. *Colloids and Surfaces A: Physicochemical and Engineering Aspects* **202**, 175-186, (2002).

17 Buffat, P. & Borel, J. Size effect on the melting temperature of gold particles. *Physical Review A* **13**, 2287, (1976).

18 Dick, K., Dhanasekaran, T., Zhang, Z. & Meisel, D. Size-dependent melting of silica-encapsulated gold nanoparticles. *Journal of the American Chemical Society* **124**, 2312-2317, (2002).

19 Glinka, Y. D., Lin, S. H., Hwang, L. P., Chen, Y. T. & Tolk, N. H. Size effect in self-trapped exciton photoluminescence from SiO_2-based nanoscale materials. *Physical Review B* **64**, 085421, (2001).

20 Link, S. & El-Sayed, M. A. Size and Temperature Dependence of the Plasmon Absorption of Colloidal Gold Nanoparticles. *The Journal of Physical Chemistry B* **103**, 4212-4217, (1999).

21 McHale, J., Auroux, A., Perrotta, A. & Navrotsky, A. Surface energies and thermodynamic phase stability in nanocrystalline aluminas. *Science* **277**, 788-791, (1997).

22 Burda, C., Chen, X., Narayanan, R. & El-Sayed, M. A. Chemistry and properties of nanocrystals of different shapes. *Chemical Reviews-Columbus* **105**, 1025-1102, (2005).

23 El-Sayed, M. A. Some interesting properties of metals confined in time and nanometer space of different shapes. *Accounts of Chemical Research* **34**, 257-264, (2001).

24 Link, S. & El-Sayed, M. A. Spectral Properties and Relaxation Dynamics of Surface Plasmon Electronic Oscillations in Gold and Silver Nanodots and Nanorods. *The Journal of Physical Chemistry B* **103**, 8410-8426, (1999).

25 Chen, S. *et al.* Gold nanoelectrodes of varied size: transition to molecule-like charging. *Science* **280**, 2098-2101, (1998).

26 Chen, S. & Pei, R. Ion-induced rectification of nanoparticle quantized capacitance charging in aqueous solutions. *Journal of the American Chemical Society* **123**, 10607-10615, (2001).

27 Quinn, B. M., Liljeroth, P., Ruiz, V., Laaksonen, T. & Kontturi, K. Electrochemical resolution of 15 oxidation states for monolayer protected gold nanoparticles. *Journal of the American Chemical Society* **125**, 6644-6645, (2003).

28 Zhang, P. & Sham, T. Tuning the electronic behavior of Au nanoparticles with capping molecules. *Applied physics letters* **81**, 736, (2002).

29 Al-Rawashdeh, N. & Foss Jr, C. A. UV/Visible and infrared spectra of polyethylene/nanoscopic gold rod composite films: effects of gold particle size, shape and orientation. *Nanostructured Materials* **9**, 383-386, (1997).

30 Kelly, K. L., Coronado, E., Zhao, L. L. & Schatz, G. C. The optical properties of metal nanoparticles: the influence of size, shape, and dielectric environment. *The Journal of Physical Chemistry B* **107**, 668-677, (2003).

31 Schmid, G. & Simon, U. Gold nanoparticles: assembly and electrical properties in 1–3 dimensions. *Chem. Commun.*, 697-710, (2005).

32 Su, K. H. *et al.* Interparticle Coupling Effects on Plasmon Resonances of Nanogold Particles. *Nano Letters* **3**, 1087-1090, (2003).

33 Xu, H., Bjerneld, E. J., Käll, M. & Börjesson, L. Spectroscopy of single hemoglobin molecules by surface enhanced Raman scattering. *Physical review letters* **83**, 4357-4360, (1999).

34 Itoh, T., Asahi, T. & Masuhara, H. Femtosecond light scattering spectroscopy of single gold nanoparticles. *Applied physics letters* **79**, 1667, (2001).

35 Link, S., Mohamed, M. & El-Sayed, M. Simulation of the optical absorption spectra of gold nanorods as a function of their aspect ratio and the effect of the medium dielectric constant. *The Journal of Physical Chemistry B* **103**, 3073-3077, (1999).

36 Templeton, A. C., Pietron, J. J., Murray, R. W. & Mulvaney, P. Solvent refractive index and core charge influences on the surface plasmon absorbance of alkanethiolate monolayer-protected gold clusters. *The Journal of Physical Chemistry B* **104**, 564-570, (2000).

37 Raimondi, F., Scherer, G. G., Kötz, R. & Wokaun, A. Nanoparticles in energy technology: Examples from electrochemistry and catalysis. *Angewandte Chemie International Edition* **44**, 2190-2209, (2005).

38 Zhang, J. Z. Ultrafast Studies of Electron Dynamics in Semiconductor and Metal Colloidal Nanoparticles: Effects of Size and Surface. *Accounts of Chemical Research* **30**, 423-429, (1997).

39 Rubahn, H.-G. *Basics of Nanotechnology*. 3rd edn, (Wiley-VCH, 2008).

40 Voutou, B. & Stefanaki, E.-C. in *Physics of Advanced Materials Winter School* (Thessaloniki, Greece, 2008).

41 Paddock, C. in *Medical News Today* (4 May 2012).

42 Torchilin, V. P. Multifunctional nanocarriers. *Advanced Drug Delivery Reviews* **58**, 1532-1555, (2006).

43 *Cancer Council Australia: Facts and figures*, <http://www.cancer.org.au/aboutcancer/FactsFigures.htm> (2012).

44 *Cancer survival and prevalence in Australia: cancers diagnosed from 1982 to 2004*, <http://www.aihw.gov.au/cancer/> (2008).

45 Miller, A., Hoogstraten, B., Staquet, M. & Winkler, A. What Is Cancer? *Cancer* **47**, 207-214, (1981).

46 *About Cancer: How many different types of cancer are there?*, <http://www.cancerresearchuk.org/cancer-help/about-cancer/cancer-questions/how-many-different-types-of-cancer-are-there> (2012).

47 Feng, S.-S. & Chien, S. Chemotherapeutic engineering: Application and further development of chemical engineering principles for chemotherapy of cancer and other diseases. *Chemical Engineering Science* **58**, 4087-4114, (2003).

48 Vogel, V. *Nanotechnology: Nanomedicine*. Vol. 5 (VCH, 2009).

49 Bianco, R., Melisi, D., Ciardiello, F. & Tortora, G. Key cancer cell signal transduction pathways as therapeutic targets. *European Journal of Cancer* **42**, 290-294, (2006).

50 Sawyers, C. Targeted cancer therapy. *Nature* **432**, 294-297, (2004).

51 Städler, B., Price, A. D. & Zelikin, A. N. A Critical Look at Multilayered Polymer Capsules in Biomedicine: Drug Carriers, Artificial Organelles, and Cell Mimics. *Advanced Functional Materials* **21**, 14-28, (2011).

52 Monteiro-Riviere, N. A. & Tran, C. L. *Nanotoxicology: characterization, dosing and health effects*. (Informa healthcare, 2007).

53 Johnston, A. P. R., Cortez, C., Angelatos, A. S. & Caruso, F. Layer-by-layer engineered capsules and their applications. *Current Opinion in Colloid & Interface Science* **11**, 203-209, (2006).

54 Merisko-Liversidge, E., Liversidge, G. G. & Cooper, E. R. Nanosizing: a formulation approach for poorly-water-soluble compounds. *European Journal of Pharmaceutical Sciences* **18**, 113-120, (2003).

55 Fassas, A., Buffels, R., Kaloyannidis, P. & Anagnostopoulos, A. Safety of high-dose liposomal daunorubicin (daunoxome) for refractory or relapsed acute myeloblastic leukaemia. *British journal of haematology* **122**, 161-163, (2003).

56 Kreuter, J., Petrov, V., Kharkevich, D. & Alyautdin, R. Influence of the type of surfactant on the analgesic effects induced by the peptide dalargin after its delivery across the blood–brain barrier using surfactant-coated nanoparticles. *Journal of Controlled Release* **49**, 81-87, (1997).

57 Kumari, A., Yadav, S. K. & Yadav, S. C. Biodegradable polymeric nanoparticles based drug delivery systems. *Colloids and Surfaces B: Biointerfaces* **75**, 1-18.

58 Leroux, J. C., Allémann, E., De Jaeghere, F., Doelker, E. & Gurny, R. Biodegradable nanoparticles—from sustained release formulations to improved site specific drug delivery. *Journal of Controlled Release* **39**, 339-350, (1996).

59 Raghuvanshi, R. S. *et al.* Improved immune response from biodegradable polymer particles entrapping tetanus toxoid by use of different immunization protocol and adjuvants. *International Journal of Pharmaceutics* **245**, 109-121, (2002).

60 Safra, T. *et al.* Pegylated liposomal doxorubicin (doxil): reduced clinical cardiotoxicity in patients reaching or exceeding cumulative doses of 500 mg/m2. *Annals of oncology* **11**, 1029-1033, (2000).

61 Schroeder, U., Sommerfeld, P., Ulrich, S. & Sabel, B. A. Nanoparticle technology for delivery of drugs across the blood–brain barrier. *Journal of pharmaceutical sciences* **87**, 1305-1307, (1998).

62 Kopf, H., Joshi, R., Soliva, M. & Speiser, P. Studium der Mizellpolymerisation in Gegenwart niedermolekularer Arzneistoffe. Herstellung und Isolierung der Nanpartikel. *Restmonomerenbestimmung, physikalisch-chemische Daten. Pharm.* **38**, 281-284, (1976).

63 Husseini, G. A. & Pitt, W. G. Micelles and nanoparticles for ultrasonic drug and gene delivery. *Advanced Drug Delivery Reviews* **60**, 1137-1152, (2008).

64 Lukyanov, A. N. & Torchilin, V. P. Micelles from lipid derivatives of water-soluble polymers as delivery systems for poorly soluble drugs. *Advanced Drug Delivery Reviews* **56**, 1273-1289, (2004).

65 Cai, S., Yang, Q., Bagby, T. R. & Forrest, M. L. Lymphatic drug delivery using engineered liposomes and solid lipid nanoparticles. *Advanced Drug Delivery Reviews* **63**, 901-908, (2011).

66 Huang, S.-L. Liposomes in ultrasonic drug and gene delivery. *Advanced Drug Delivery Reviews* **60**, 1167-1176, (2008).

67 Blasi, P., Giovagnoli, S., Schoubben, A., Ricci, M. & Rossi, C. Solid lipid nanoparticles for targeted brain drug delivery. *Advanced Drug Delivery Reviews* **59**, 454-477, (2007).

68 Gasco, M. R., Priano, L. & Zara, G. P. in *Progress in Brain Research* Vol. Volume 180 (ed Sharma Hari Shanker) 181-192 (Elsevier, 2009).

69 Mora-Huertas, C. E., Fessi, H. & Elaissari, A. Polymer-based nanocapsules for drug delivery. *International Journal of Pharmaceutics* **385**, 113-142.

70 Rastogi, R., Anand, S. & Koul, V. Flexible polymerosomes—An alternative vehicle for topical delivery. *Colloids and Surfaces B: Biointerfaces* **72**, 161-166, (2009).

71 Lorenceau, E. *et al.* Generation of Polymerosomes from Double-Emulsions. *Langmuir* **21**, 9183-9186, (2005).

72 Städler, B., Chandrawati, R., Goldie, K. & Caruso, F. Capsosomes: subcompartmentalizing polyelectrolyte capsules using liposomes. *Langmuir* **25**, 6725-6732, (2009).

73 Hosta-Rigau, L. *et al.* Capsosomes with multilayered subcompartments: assembly and loading with hydrophobic cargo. *Advanced Functional Materials* **20**, 59-66, (2010).

74 Chowdhury, D. F. in *Comprehensive Biotechnology (Second Edition)* (ed Moo-Young Murray) 643-655 (Academic Press, 2011).

75 Klumpp, C., Kostarelos, K., Prato, M. & Bianco, A. Functionalized carbon nanotubes as emerging nanovectors for the delivery of therapeutics. *Biochimica et Biophysica Acta (BBA) - Biomembranes* **1758**, 404-412, (2006).

76 Ghosh, P., Han, G., De, M., Kim, C. K. & Rotello, V. M. Gold nanoparticles in delivery applications. *Advanced Drug Delivery Reviews* **60**, 1307-1315, (2008).

77 Papasani, M. R., Wang, G. & Hill, R. A. Gold nanoparticles: the importance of physiological principles to devise strategies for targeted drug delivery. *Nanomedicine: Nanotechnology, Biology and Medicine* 10.1016/j.nano.2012.01.008.

78 Pissuwan, D., Niidome, T. & Cortie, M. B. The forthcoming applications of gold nanoparticles in drug and gene delivery systems. *Journal of Controlled Release* **149**, 65-71, (2011).

79 Pissuwan, D., Valenzuela, S. M. & Cortie, M. B. Therapeutic possibilities of plasmonically heated gold nanoparticles. *TRENDS in Biotechnology* **24**, 62-67, (2006).

80 Slowing, I. I., Trewyn, B. G., Giri, S. & Lin, V. S. Y. Mesoporous silica nanoparticles for drug delivery and biosensing applications. *Advanced Functional Materials* **17**, 1225-1236, (2007).

81 Slowing, I. I., Vivero-Escoto, J. L., Wu, C. W. & Lin, V. S. Y. Mesoporous silica nanoparticles as controlled release drug delivery and gene transfection carriers. *Advanced Drug Delivery Reviews* **60**, 1278-1288, (2008).

82 Chen, J. F., Ding, H. M., Wang, J. X. & Shao, L. Preparation and characterization of porous hollow silica nanoparticles for drug delivery application. *Biomaterials* **25**, 723-727, (2004).

83 Gao, Q., Xu, Y., Wu, D., Sun, Y. & Li, X. pH-responsive drug release from polymer-coated mesoporous silica spheres. *The Journal of Physical Chemistry C* **113**, 12753-12758, (2009).

84 Kim, J. *et al.* Multifunctional uniform nanoparticles composed of a magnetite nanocrystal core and a mesoporous silica shell for magnetic resonance and fluorescence imaging and for drug delivery. *Angewandte Chemie International Edition* **47**, 8438-8441, (2008).

85 Kim, J. *et al.* Magnetic fluorescent delivery vehicle using uniform mesoporous silica spheres embedded with monodisperse magnetic and semiconductor nanocrystals. *Journal of the American Chemical Society* **128**, 688-689, (2006).

86 Liong, M. *et al.* Multifunctional inorganic nanoparticles for imaging, targeting, and drug delivery. *Acs Nano* **2**, 889-896, (2008).

87 Bergna, H. E. in *The Colloid Chemistry of Silica* Vol. 234 *Advances in Chemistry* Ch. 1, 1-47 (American Chemical Society, 1994).

88 Caruso, F., Caruso, R. A. & Möhwald, H. Nanoengineering of inorganic and hybrid hollow spheres by colloidal templating. *Science* **282**, 1111-1114, (1998).

89 Breck, D. W. *Zeolite Molecular Sieves*. 32 (Wiley, 1974).

90 Pauling, L. The nature of the chemical bond 1992. *Journal of chemical education* **69**, 519, (1992).

91 Colic, M., Fisher, M. L. & Franks, G. V. Influence of Ion Size on Short-Range Repulsive Forces between Silica Surfaces. *Langmuir* **14**, 6107-6112, (1998).

92 Mazo, R. M. *Brownian motion: fluctuations, dynamics, and applications*. Vol. 112 (Oxford University Press, USA, 2009).

93 Nelson, E. *Dynamical theories of Brownian motion*. Vol. 17 (Princeton university press Princeton, 1967).

94 Zoldesi, C. I. *Hollow colloidal particles by emulsion templating, from synthesis to self-assembly*, Utrecht University, (2006).

95 Lu, J., Liong, M., Zink, J. I. & Tamanoi, F. Mesoporous silica nanoparticles as a delivery system for hydrophobic anticancer drugs. *SMALL* **3**, 1341-1346, (2007).

96 Unger, K., Jilge, G., Janzen, R., Giesche, H. & Kinkel, J. Non-porous microparticulate supports in high-performance liquid chromatography (HPLC) of biopolymers—concepts, realization and prospects. *Chromatographia* **22**, 379-380, (1986).

97 Hassander, H., Johansson, B. & Törnell, B. The mechanism of emulsion stabilization by small silica (Ludox) particles. *Colloids and surfaces* **40**, 93-105, (1989).

98 Iler, R. *The Chemistry of Silica: Solubility, Polymerization, Colloid and Surface Properties and Biochemical of Silica*. (John Wiley & Sons, New York, NY, 1979).

99 Suratwala, T. *et al.* Effect of rogue particles on the sub-surface damage of fused silica during grinding/polishing. *Journal of non-crystalline solids* **354**, 2023-2037, (2008).

100 Balthis, J. H. & Mendenhall, P. Preparation of sols from finely divided silicon. United States patent (1952).

101 Radczewski, O. & Richter, H. Elektronenmikroskopische Untersuchung von Kieselsäuresolen. *Colloid & Polymer Science* **96**, 1-7, (1941).

102 Bird, C. Draft control and fly ash separator. (1941).

103 Loftman, K. A. Aqueous dispersions of pyrogenic silica. (1961).

104 Kolbe, G. *Das Komplexchemische Verhalten der Kieselsaure* Ph.D thesis, Friedrich-Schiller University Jena, (1956).

105 Stöber, W., Fink, A. & Bohn, E. Controlled growth of monodisperse silica spheres in the micron size range. *Journal of Colloid and Interface Science* **26**, 62-69, (1968).

106 Chen, S. L., Dong, P., Yang, G. H. & Yang, J. J. Kinetics of formation of monodisperse colloidal silica particles through the hydrolysis and condensation of tetraethylorthosilicate. *Industrial & Engineering Chemistry Research* **35**, 4487-4493, (1996).

107 Chou, K. S. & Chen, C. C. The critical conditions for secondary nucleation of silica colloids in a batch Stöber growth process. *Ceramics International* **34**, 1623-1627, (2008).

108 Giesche, H. Synthesis of monodispersed silica powders I. Particle properties and reaction kinetics. *Journal of the European Ceramic Society* **14**, 189-204, (1994).

109 Green, D., Jayasundara, S., Lam, Y. F. & Harris, M. Chemical reaction kinetics leading to the first Stober silica nanoparticles–NMR and SAXS investigation. *Journal of non-crystalline solids* **315**, 166-179, (2003).

110 Green, D. L. *et al.* Size, volume fraction, and nucleation of Stober silica nanoparticles. *Journal of Colloid and Interface Science* **266**, 346-358, (2003).

111 Matsoukas, T. & Gulari, E. Dynamics of growth of silica particles from ammonia-catalyzed hydrolysis of tetra-ethyl-orthosilicate. *Journal of Colloid and Interface Science* **124**, 252-261, (1988).

112 Matsoukas, T. & Gulari, E. Monomer-addition growth with a slow initiation step: A growth model for silica particles from alkoxides. *Journal of Colloid and Interface Science* **132**, 13-21, (1989).

113 Wang, H. C., Wu, C. Y., Chung, C. C., Lai, M. H. & Chung, T. W. Analysis of parameters and interaction between parameters in preparation of uniform silicon dioxide nanoparticles using response surface methodology. *Industrial & Engineering Chemistry Research* **45**, 8043-8048, (2006).

114 Wang, X.-D. *et al.* Preparation of spherical silica particles by Stöber process with high concentration of tetra-ethyl-orthosilicate. *Journal of Colloid and Interface Science* **341**, 23-29, (2010).

115 Tan, C. G., Bowen, B. D. & Epstein, N. Production of monodisperse colloidal silica spheres: Effect of temperature. *Journal of Colloid and Interface Science* **118**, 290-293, (1987).

116 Satoh, T., Akitaya, M., Konno, M. & Saito, S. Particle size distributions produced by hydrolysis and condensation of tetraethylorthosilicate. *Journal of chemical engineering of Japan* **30**, 759-762, (1997).

117 10 Ways to Control Rhenology by Changing Particle Properties (Size, Zeta Potential and Shape). *Advanced Technology Made Simple* (2009). <http://www.malvern.com/common/downloads/campaign/MRK1236-01.pdf>.

118 *Intelligent systems and Neural Networks*, <http://www.learnartificialneuralnetworks.com/> (2012).

119 Box, G. E. & Behnken, D. Some new three level designs for the study of quantitative variables. *Technometrics* **2**, 455-475, (1960).

120 Doehlert, D. H. Uniform Shell Designs. *Journal of the Royal Statistical Society. Series C (Applied Statistics)* **19**, 231-239, (1970).

121 Boso, D. P., Lee, S.-Y., Ferrari, M., Schrefler, B. A. & Decuzzi, P. Optimizing particle size for targeting diseased microvasculature: from experiments to artificial neural networks. *International journal of nanomedicine* **6**, 1517, (2011).

122 Song, K. *et al.* Optimization of the processing parameters during internal oxidation of Cu–Al alloy powders using an artificial neural network. *Materials & Design* **26**, 337-341, (2005).

123 Song, X.-H., Hopke, P. K., Fergenson, D. P. & Prather, K. A. Classification of single particles analyzed by ATOFMS using an artificial neural network, ART-2A. *Analytical Chemistry* **71**, 860-865, (1999).

124 Basheer, I. A. & Hajmeer, M. Artificial neural networks: fundamentals, computing, design, and application. *Journal of Microbiological Methods* **43**, 3-31, (2000).

125 Suarez, J. *Intro to Neural Networks*, <http://www.youtube.com/watch?v=DG5-UyRBQD4&feature=related> (2009).

126 Davies, R. *et al.* Engineered Particle Surfaces. *Advanced Materials* **10**, 1264-1270, (1998).

127 Caruso, F. Nanoengineering of particle surfaces. *Advanced Materials* **13**, 11-22, (2001).

128 Vallet-Regi, M., Rámila, A., del Real, R. P. & Pérez-Pariente, J. A New Property of MCM-41: Drug Delivery System. *Chemistry of Materials* **13**, 308-311, (2000).

129 Gerion, D. *et al.* Synthesis and properties of biocompatible water-soluble silica-coated CdSe/ZnS semiconductor quantum dots. *Journal of Physical Chemistry B-Condensed Phase* **105**, 8861-8871, (2001).

130 Joo, S. H. *et al.* Thermally stable Pt/mesoporous silica core–shell nanocatalysts for high-temperature reactions. *Nature materials* **8**, 126-131, (2008).

131 Liz-Marzán, L. M., Giersig, M. & Mulvaney, P. Synthesis of nanosized gold-silica core-shell particles. *Langmuir* **12**, 4329-4335, (1996).

132 Campbell, J. L. *et al.* Quasi-Cubic Magnetite/Silica Core-Shell Nanoparticles as Enhanced MRI Contrast Agents for Cancer Imaging. *PLoS One* **6**, e21857, (2011).

133 Graham, T. J. *Journal of American Chemical Society* **17**, 318, (1864).

134 Büchel, B., Klaus, K. U., Akihiko, M. & Kazuo, T. A Novel Pathway for Synthesis of Submicrometer-Size Solid Core/Mesoporous Shell Silica Spheres. *Advanced Materials* **10**, 1036-1038, (1998).

135 Hilliard, L. R., Zhao, X. & Tan, W. Immobilization of oligonucleotides onto silica nanoparticles for DNA hybridization studies. *Analytica Chimica Acta* **470**, 51-56, (2002).

136 Zhu, Y. *et al.* Stimuli-Responsive Controlled Drug Release from a Hollow Mesoporous Silica Sphere/Polyelectrolyte Multilayer Core–Shell Structure. *Angewandte Chemie* **117**, 5213-5217, (2005).

137 Bae, J. A. *et al.* Effect of pore structure of amine-functionalized mesoporous silica-supported rhodium catalysts on 1-octene hydroformylation. *Microporous and Mesoporous Materials* **123**, 289-297, (2009).

138 Kneuer, C. *et al.* Silica nanoparticles modified with aminosilanes as carriers for plasmid DNA. *International Journal of Pharmaceutics* **196**, 257-261, (2000).

139 Graham, T. J. *Journal of American Chemical Society* **15**, 216, (1862).

140 Allison, A. C., Harington, J. S. & Birbeck, M. An Examination of the Cytotoxic Effects of Silica on Macrophages. *The Journal of Experimental Medicine* **124**, 141-154, (1966).

141 Fujiwara, K. *et al.* Size-dependent toxicity of silica nano-particles to Chlorella kessleri. *Journal of Environmental Science and Health, Part A* **43**, 1167-1173, (2008).

142 Sager, T. M. *et al.* Improved method to disperse nanoparticles for in vitro and in vivo investigation of toxicity. *Nanotoxicology* **1**, 118-129, (2007).

143 Sayes, C. M., Reed, K. L. & Warheit, D. B. Assessing Toxicity of Fine and Nanoparticles: Comparing In Vitro Measurements to In Vivo Pulmonary Toxicity Profiles. *Toxicological Sciences* **97**, 163-180, (2007).

144 Shi, X. *et al.* Reactive oxygen species and molecular mechanism of silica-induced lung injury. *Journal of environmental pathology, toxicology and oncology: official*

organ of the International Society for Environmental Toxicology and Cancer **20**, 85, (2001).

145 Singh, N. *et al.* Bioresponsive Mesoporous Silica Nanoparticles for Triggering Drug Release. *Journal of the American Chemical Society* (2011).

146 Tiwari, K. R. *Polymer capsules: Fundamental studies and new concepts*. (ProQuest, 2008).

147 Calvo, P., Vila-Jato, J. L. & Alonso, M. J. Evaluation of cationic polymer-coated nanocapsules as ocular drug carriers. *International Journal of Pharmaceutics* **153**, 41-50, (1997).

148 Chen, Y., Lin, X., Park, H. & Greever, R. Study of artemisinin nanocapsules as anticancer drug delivery systems. *Nanomedicine: Nanotechnology, Biology and Medicine* **5**, 316-322, (2009).

149 Fawaz, F. *et al.* Disposition and protective effect against irritation after intravenous and rectal administration of indomethacin loaded nanocapsules to rabbits. *International Journal of Pharmaceutics* **133**, 107-115, (1996).

150 Lambert, G., Fattal, E., Pinto-Alphandary, H., Gulik, A. & Couvreur, P. Polyisobutylcyanoacrylate nanocapsules containing an aqueous core as a novel colloidal carrier for the delivery of oligonucleotides. *Pharmaceutical Research* **17**, 707, (2000).

151 Guterres, S. S., Fessi, H., Barratt, G., Puisieux, F. & Devissaguet, J.-P. Poly(D,L-Lactide) Nanocapsules Containing Non-Steroidal Anti-Inflammatory Drugs: Gastrointestinal Tolerance Following Intravenous and Oral Administration. *Pharmaceutical Research* **12**, 1545-1547, (1995).

152 Preetz, C., Rube, A., Reiche, I., Hause, G. & Mader, K. Preparation and characterization of biocompatible oil-loaded polyelectrolyte nanocapsules. *Nanomedicine: Nanotechnology, Biology and Medicine* **4**, 106-114, (2008).

153 Sablon, K. Single-component polymer nanocapsules for drug delivery application. *Nanoscale Research Letters* **3**, 265-267, (2008).

154 Shu, S. *et al.* Hollow and degradable polyelectrolyte nanocapsules for protein drug delivery. *Acta Biomaterialia* **6**, 210-217.

155 Teixeira, M., Alonso, M. J., Pinto, M. M. M. & Barbosa, C. M. Development and characterization of PLGA nanospheres and nanocapsules containing xanthone and 3-methoxyxanthone. *European Journal of Pharmaceutics and Biopharmaceutics* **59**, 491-500, (2005).

156 Wang, Y., Bansal, V., Zelikin, A. N. & Caruso, F. Templated Synthesis of Single-Component Polymer Capsules and Their Application in Drug Delivery. *Nano Letters* **8**, 1741-1745, (2008).

157 Benita, S. *Microencapsulation: methods and industrial applications*. Vol. 158 (Informa Healthcare, 2006).

158 Brigger, I., Dubernet, C. & Couvreur, P. Nanoparticles in Cancer Therapy and Diagnostics. *Advanced Drug Delivery Reviews* **54**, 631-651, (2002).

159 Stevens, M. P. *Polymer chemistry*. (Oxford University Press New York, NY, 1990).

160 Pinto-Alphandary, H., Aboubakar, M., Jaillard, D., Couvreur, P. & Vauthier, C. Visualization of Insulin-Loaded Nanocapsules: *In Vitro* and *in Vivo* Studies After Oral Administration to Rats. *Pharmaceutical Research* **20**, 1071-1084, (2003).

161 Watnasirichaikul, S., Davies, N., Rades, T. & Tucker, I. Preparation of Biodegradable Insulin Nanocapsules from Biocompatible Microemulsions. *Pharmaceutical Research* **17**, 684-689, (2000).

162 Calvo, P., Alonso, M. J., Vila-Jato, J. L. & Robinson, J. R. Improved Ocular Bioavailability of Indomethacin by Novel Ocular Drug Carriers. *Journal of Pharmacy and Pharmacology* **48**, 1147-1152, (1996).

163 Lenaerts, V. *et al.* Nanocapsules with a reduced liver uptake: targeting of phthalocyanines to EMT-6 mouse mammary tumour in vivo. *European Journal of Pharmaceutics and Biopharmaceutics* **41**, 38-43, (1995).

164 Agnihotri, S. A., Mallikarjuna, N. N. & Aminabhavi, T. M. Recent advances on chitosan-based micro-and nanoparticles in drug delivery. *Journal of Controlled Release* **100**, 5-28, (2004).

165 Felt, O., Buri, P. & Gurny, R. Chitosan: a unique polysaccharide for drug delivery. *Drug development and industrial pharmacy* **24**, 979-993, (1998).

166 Gan, Q. & Wang, T. Chitosan nanoparticle as protein delivery carrier: Systematic examination of fabrication conditions for efficient loading and release. *Colloids and Surfaces B: Biointerfaces* **59**, 24-34, (2007).

167 Goy, R. C., Britto, D. d. & Assis, O. B. G. A review of the antimicrobial activity of chitosan. *Polímeros* **19**, 241-247, (2009).

168 Kumar, M. R. A review of chitin and chitosan applications. *Reactive and Functional Polymers* **46**, 1-27, (2000).

169 Brannon-Peppas, L. Recent advances on the use of biodegradable microparticles and nanoparticles in controlled drug delivery. *International Journal of Pharmaceutics* **116** 1-9, (1994).

170 Alkilany, A. M., Thompson, L. B. & Murphy, C. J. Polyelectrolyte Coating Provides a Facile Route to Suspend Gold Nanorods in Polar Organic Solvents and Hydrophobic Polymers. *ACS Applied Materials & Interfaces* **2**, 3417-3421, (2010).

171 Antipov, A. A., Sukhorukov, G. B., Donath, E. & Möhwald, H. Sustained Release Properties of Polyelectrolyte Multilayer Capsules. *The Journal of Physical Chemistry B* **105**, 2281-2284, (2001).

172 Burke, S. E. & Barrett, C. J. Swelling Behavior of Hyaluronic Acid/Polyallylamine Hydrochloride Multilayer Films. *Biomacromolecules* **6**, 1419-1428, (2005).

173 Trau, D. & Renneberg, R. Encapsulation of glucose oxidase microparticles within a nanoscale layer-by-layer film: immobilization and biosensor applications. *Biosensors and Bioelectronics* **18**, 1491-1499, (2003).

174 Caruso, F. Hollow Capsule Processing through Colloidal Templating and Self-Assembly. *Chemistry - A European Journal* **6**, 413-419, (2000).

175 Ashoori, R. Electrons in artificial atoms. *Nature* **379**, 413-419, (1996).

176 Jamieson, T. *et al.* Biological applications of quantum dots. *Biomaterials* **28**, 4717-4732, (2007).

177 Kasfner, M. A. Artificial atoms. *Physics Today*, 25, (1993).

178 Patel, A. C. Bioapplicable, nanostructured and nanocomposite materials for catalytic and biosensor applications. (2006).

179 Bogush, G. H., Tracy, M. A. & Zukoski Iv, C. F. Preparation of monodisperse silica particles: Control of size and mass fraction. *Journal of non-crystalline solids* **104**, 95-106, (1988).

CHAPTER 2

CHARACTERISATION TECHNIQUES

This chapter examines the various characterisation techniques employed throughout this thesis

2.1 Introduction

The main aim of this thesis is to develop multifunctional nanoparticle templates onto which various biodegradable and biocompatible polymer shells are grown. Followed by the subsequent removal of the silica matrix of the template, various polymer-based nanocapsules with a variety of structural properties have been produced. In order to determine the successful development of the components, testing has been carried out throughout the stages of synthesis, as well as additional investigations into the functionality of the drug delivery system developed. These techniques include Scanning Electron Microscopy (SEM), Transmission Electron Microscopy (TEM), Energy dispersive X-ray analysis (EDX), Dynamic Light Scattering (DLS), BET surface area analysis, UV-visible absorption spectroscopy (UV-vis), Confocal Laser Scanning Microscopy (CLSM), and Thermogravimetric analysis (TGA). This chapter is devoted to explain the basic fundamentals of the techniques used to characterise the materials of this PhD.

2.2 Electron Microscopy (EM)

Both the size and shape of nanoparticles used in drug delivery systems can have a profound effect on their biocompatibility and their ability to hold and release incorporated drug solutions. Although many features of the particles can be revealed by other techniques such as XRD, direct images of the particles and capsules are only possible by using scanning and transmission electron microscopes. The microscope images allow for qualitative and semi-quantitative analysis of particle morphologies (size and shape) and the aggregation states.[1]

Electron microscopes operate on a similar principle to light microscopes but due to limitations of the resolution of optical microscopes, development of alternative techniques was required. In contrast to optical microscopes, the light beam is replaced by an electron beam, and the optical lenses are replaced by magnetic lenses. The electron source is preferentially used due to a direct relationship between the wavelength of the beam and the resolution of the resulting image.[2] A stream of electrons is generated from an electron gun when a potential is applied, which is then confined and focused using metal apertures and magnetic lenses. As the sample is irradiated by the sample beam, interactions occur, affecting the beam in a variety of ways, it is these interactions and effects that are detected and transcribed into an 2-dimensional image (see Figure 2.1).[3]

Electrons can possess significant energy and are capable of removing the tightly bound inner shell electrons from the nucleus by transferring kinetic energy to them.[2] Following the de Broglie concept, the wavelength of an electron decreases as the kinetic energy of the electron increases. The rapidly accelerated electrons have very short wavelengths and consequently, are capable of producing images with a resolution several magnitudes better than that of optical microscopes as determined by the formula:

$$d = 0.5\lambda \sin \alpha$$

Where λ represents the wavelength and α corresponds to one-half the aperture. As electrons have wavelengths 100,000 times shorter than that of visible light (where the wavelength of an electron is 1.54 Å), in principle it is possible to achieve resolution as low as a few Angstroms in electron microscopes.[4]

As the electron beam interacts with the sample, the electrons can undergo either elastic or inelastic scattering. In elastic scattering, only the trajectory changes while the kinetic energy and speed remain constant, conserving the energy of the electron. Conversely during inelastic scattering, some of the electrons from the beam source interact with the electrons in the sample, transferring energy to, and displacing the sample atom's electrons from the shells of the nuclei, these interactions transform the atoms of the sample into an excited and unstable state. It is these inelastic interactions between the beam source and sample that enable electron microscopy to work.

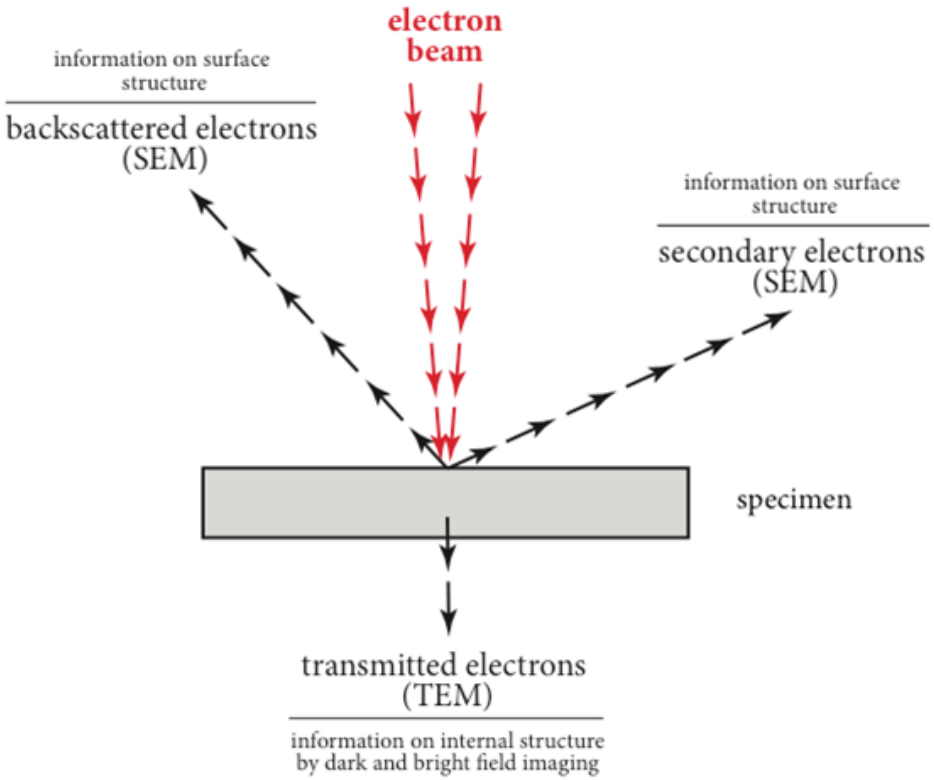

Figure 2.1: A representation of the signals generated when the electron beam interacts with a specimen. Courtesy of https://bsp.med.harvard.edu/node/221[5]

2.2.1 Scanning Electron Microscope (SEM)

The SEM is able to provide extensive information about the surface of a material which can be very useful when determining the sample morphology. The microscope works by passing an electron beam over the sample surface and detecting the energy which is reflected or emitted by the sample. Emitted by either thermionic emission from a Cathode, or from a field emission gun (FEG), the electron beam strikes the sample surface where electrons interact with atoms in the top few layers of the specimen. Some of the electrons are reflected off the surface via elastic scattering, whereas some undergo interactions and inelastic scattering as per the above discussion.

In SEM, the specimen is often sufficiently thick and prevents the electron beam from being transmitted through the sample. Therefore the energy from these electrons is re-emitted from the surface in other forms such as heat, visible light, x-ray emissions, backscattered electrons, diffracted backscattered electrons and low-energy secondary electrons.[3] Although a number of these forms of energy can be used to understand the properties of the sample, the backscattered and secondary electrons are the most commonly detected signals used to construct pseudo 3-dimensional SEM images.

Backscattered electrons consist of high energy electrons which have originated from the beam source but have been reflected or 'back-scattered' from the specimen surface. The production rate of these electrons is highly dependent on the atomic number and therefore can give indications of the density of a material, with denser materials appearing brighter (i.e. heavier elements produce more backscattered electrons).

In contrast, secondary electrons are emitted from the surface of the sample after the incident electron beam dislodges an electron. When an electron from the beam source excites an electron from the sample it transfers energy and allows the electron to move toward the surface as a secondary electron. However, as this secondary electron moves towards the surface it undergoes elastic and inelastic collisions along the way. If it still has sufficient energy it will be ejected from the surface and can be detected. Due to the high energy requirements of escape from the surface, only electrons in the first few layers are emitted (<10 nm). Therefore any changes in the height of the sample will yield differences in the secondary electron intensity. This intensity profile provides the pseudo 3-dimensional detail of the surface,[3,6] and when incorporated with the backscattered electron signal information, a highly resolved pseudo-3D image is created.

SEM analysis of all samples was performed on a FEI NovaSEM, operating at an accelerating voltage of 15 kV, with a spot size of 3.5 nm and a working distance of 5 mm. All samples were drop cast directly onto an aluminium SEM stub.

2.2.2 Transmission Electron Microscope (TEM)

A transmission electron microscope differs from a scanning electron microscope in that the electron beam used to create an image is passed through an ultra-thin sample instead of being reflected or emitted from the sample surface. Therefore, in contrast to SEM, this technique results in a true 2D image and can be utilised to provide information about the structures/components within a sample. In a conventional TEM, a beam of accelerated electrons interacts with the specimen in one of two ways.[2] The electrons transmitted through

the specimen undergo either elastic or inelastic scattering much like in SEM, where elastic scattering conserves all energy and in inelastic scattering a portion of energy is lost.

The electrons that undergo elastic scattering constitute the majority electrons of the electrons that are collected, however, the inelastic scattered electrons that do not lose a significant amount of energy can also contribute to the image of an object. In a TEM contrast is achieved as a result of differences in the density of different areas of the specimen, as it is directly related to the beam interacting with different elements in the sample and causing different scattering potentials. This interaction can be described by the Rutherford formula:

$$K = \frac{-e.eZ}{r^2}$$

Where *K* is the deflection potential, *e* is the electron charge, *Z* is the positive nuclear charge and *r* is the distance between electron and nucleus. As the atomic number of an element increases, so too does the *r* distance. This in turn affects the deflection potential and changes the light intensity (contrast).

All TEM analysis was performed on a Jeol 1010 TEM, operating at an accelerating voltage of 100 kV. All colloidal samples were prepared in solution and drop cast onto copper grids coated with 200 mesh strong carbon. For ultramicrotomed samples, cross sectional slices were placed on copper grids. The samples were imaged after all solvents had evaporated at room temperature.

2.3 Energy-Dispersion X-Ray (EDX) Analysis

Energy-dispersive X-ray (EDX) spectroscopy is a relatively simple yet powerful technique that is used to identify the elemental composition of a material. Often used in conjunction with scanning electron microscopy, a sample surface is bombarded with an electron beam which forces electrons from the innermost orbitals of the sample atoms to be ejected. This causes a momentary electron hole within the sample atom and renders it unstable (as an atom in an excited state). This electron hole then induces an electron from a higher energy shell to relax, or "fall" down to fill the hole within the lower energy shell. During the transition of the electron from a higher energy shell to a lower energy shell, the excess energy is released in the form of a photon, with an energy corresponding to the energy difference between the two orbitals, see Figure 2.2. As all elements have a unique electron configuration,

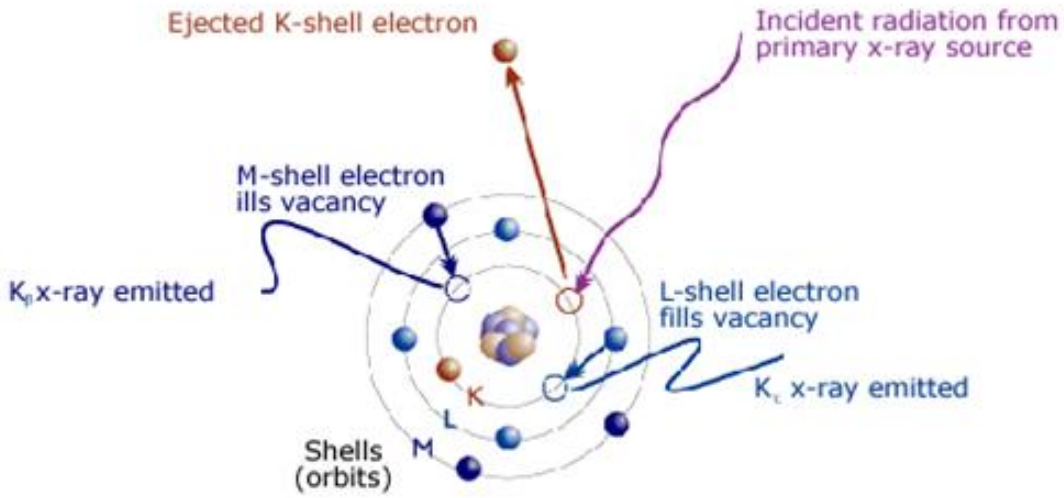

Figure 2.2 Schematic representation of the ejection of a *K*-shell electron to create an electron hole into which an *M*- or *L*- shell electron later fills while emitting the corresponding x-ray in the process. Adapted from http://oxford-labs.com/x-ray-fluorescence/the-basic-process [7]

they generate a unique X-ray spectrum, and therefore, can be identified. In addition, the X-ray spectra produced can be used to semi-quantitatively determine the ratios of elements within a composite.

EDX analysis of the presented work was performed on a FEI Nova NanoSEM instrument coupled with an EDX Si(Li) X-ray detector.

2.4 Dynamic Light Scattering (DLS)

Dynamic light scattering, also known as photon correlation spectroscopy, is one of the most popular methods used to measure the size distribution profile of colloidal particles. The measurements are made by detecting the speed at which particles are diffusing through a fluid due to Brownian motion, and relating the motion to the particle size. Brownian motion occurs due to the collision of the particles with the solvent molecules which themselves are moving due to thermal energy.[8,9] As photons interact with the randomly moving particles they are scattered in all directions, however, due to the motion of the particles the photon undergoes a Doppler shift, changing the wavelength of the incoming photon. This change is detected as a fluctuation of intensity over a time period of nano to milliseconds. The particle size is then determined by the amount of Brownian motion observed, where larger particles undergo slower Brownian motion than smaller particles. The velocity of the particle motion is defined by a property known as the translational diffusion coefficient.

Using the translational diffusion coefficient, the size of the particles can be calculated from the Stokes-Einstein equation:

$$d(H) = kT3\pi\eta D$$

Where *d(H)* is the hydrodynamic diameter, *k* is Boltzmann's constant, *T* the absolute temperature, η is the viscosity, and *D* is the translational diffusion coefficient.

However, as there is often a concentration of ions, or any surface structures around the particles that can affect how the particles diffuse within a fluid, the diameter that is measured in DLS is known as the hydrodynamic diameter and can often be larger than that measured by electron microscopy.

All measurements were carried out on an ALV 5022F Fast DLS particle sizing spectrometer, at 22 °C with a fixed angle of 90° on highly dilute aqueous solutions.

2.5 BET Surface Area Analysis

Surface area analysis was performed using the BET characterisation method first proposed by Stephen Brunauer, Paul Hugh Emmett and Edward Teller.[10] Based on the Langmuir theory of monolayer molecular adsorption, the BET theory describes the changes in pressure during multi-layer adsorption of inert molecules onto a surface.

$$\frac{P}{V(P^\circ - P)} = \frac{1}{CV_m} + \frac{C-1}{CV_m}\frac{P}{P^\circ}$$

And

$$C = e^{(q_2 - q_1)/RT}$$

Where V_m is the monolayer adsorption amount, *V* is the adsorption amount at the equilibrium pressure *P*, and C is a constant

The theory relies on three assumptions in order for the isotherms to be accurate. The analysis assumes that adsorption occurs by multilayer formation and that the number of adsorbed layers is infinite,[11] there is no lateral interaction between layers, and that the Langmuir theory can be applied to each layer.

All measurements were carried out on a Micromeritics ASAP 2000 surface analysis instrument utilising the Brunauer-Emmett-Teller (BET) technique.

2.6 UV-Visible (UV-vis) Spectroscopy

Spectrophotometry, or spectroscopy, is the study of interactions between electromagnetic radiation and matter.[12] When electromagnetic radiation is passed through a solution of particles, the emerging radiation is always less intense than that entering. This is in part due to reflection or scattering of the beam, but is primarily due to absorption by the particles.

When energy is absorbed in the UV or visible regions it results in a change in the electronic energy of the molecule, known as electronic transition. As the radiation energy is absorbed, electrons shift to a higher energy, exited state. The energy required for the transition from the ground state to the excited state is detected, with the depletion in the amount of radiation exiting/transmitted through the solution being inversely related to the amount absorbed at that particular wavelength. The energy absorbed in an electronic transition can be described as:

$$\Delta E = h\nu = \frac{hc}{\lambda} = h\bar{\nu}c$$

Where ΔE is the energy required to induce a molecule from a low energy/ground state to a higher energy/excited state. This is dependent on the frequency (v) and wavelength (λ), where (h = 6.626 x 10^{-34}) is the Planck's constant, (c) is the velocity of light and ($\bar{v}$) is the wavenumber. Therefore, the larger the energy required for electron excitation, the smaller the wavelength absorbed.

The amount of energy required to drive the electrons into this excited energy state is of a unique wavelength for that particular molecule. As the source beam is absorbed, the depletion in the amount of radiation exiting the solution is detected and inversely corresponds to the amount absorbed at that particular wavelength. What is produced is an absorption spectrum which shows the change in degree of absorption as a function of the wavelength at which it was absorbed. The resulting spectrum is characteristic of the material and can therefore be used to identify it.

The principle characteristics of an absorption spectrum are not only the positions of absorption features that correspond to the wavelengths at which electronic transitions are achieved, but also the intensity. The intensity at this point is largely dependent on both the difference between excited and ground states, and the probability of an interaction occurring. If the solution is highly concentrated the probability of absorption by the particles increases proportionally. This relation can be used to determine the concentration of the analyte, and is described in the Beer-Lambert Law:

$$A = e.c.l$$

Where (*A)* is the measured absorbance, (*e)* is the molecular absorptivity which is characteristic of the particular solute and solvent, (*c)* is the analyte concentration and (*l)* is the path length of the cell.

UV-visible spectroscopy (UV-Vis) is often used in analytical chemistry to quantitatively identify analytes, such as conjugated organic compounds, bio-macromolecules, and transition metal ions. UV-vis can also be employed for the characterisation of colloidal particles.[13-15] The optical absorption features of semi-conducting nanoparticles are highly dependent on their electron-hole pairs created by the excitation of the valence shell electrons to the conduction band. Any change in the nanoparticle size has a dramatic effect on the width of the electron bands and therefore on the energies required to shift electrons into excited states. As a result the nanoparticle size can be quantified based on its absorption spectrum. The dependence of the change in the band gap energy (ΔE) in relation to the size of the semiconductor nanoparticle in terms of the radius (R) can be expressed as:

$$\Delta E_{BG} = \frac{h^2\pi^2}{2}\left(\frac{1}{m_e}+\frac{1}{m_h}\right)\frac{1}{R^2} - \frac{1.8e^2}{\varepsilon}\cdot\frac{1}{R}$$

Where m_e and m_h represent the effective masses of electron and hole, respectively, and ε represents the (static) dielectric constant of the semiconducting material.[16]

Absorption spectroscopy in the UV and visible regions is a highly effective tool in the analysis of chemical compounds. In the following thesis, UV-visible spectra were obtained on a Cary 50 Bio spectrometer, operating at a resolution of 1 nm over a wavelength range of 200-800 nm, to determine the extent of loading of a curcumin-in-oil solution into various biocompatible nanocapsules.

2.7 Confocal Laser Scanning Microscopy (CLSM)

Confocal laser scanning microscopy (CLSM) has become an invaluable tool when imaging the subcellular structures of living and fixed cells. It is an optical imaging technique that offers increased optical resolution and contrast in comparison to conventional optical microscopes, as well as the ability to obtain in-focus images from a defined depth. In contrast to the traditional fluorescent microscopy where an entire specimen is illuminated by a light source, confocal imaging uses point-by-point scanning illumination and detection. This is achieved by passing the laser beam through 'pinhole' apertures at both the illumination and detection ends. Typically a laser excitation source is directed through the first of two pinhole apertures (ideally diffraction limited), to eliminate any out-of-focus light rays. Next, the light is reflected off a dichromatic mirror and sent to the objective lens where the beam is refocused onto the specimen. As the excitation beam scans along the specimen in a defined focal plane, secondary fluorescence is emitted from points on the specimen. These fluorescent emission rays then pass back through the dichromatic mirror to be refocused to a second focal point before passing through the second (detector) pinhole aperture, see Figure 3.3. Any emission rays that have come from points too far above or below the objective focal plane are considered to be out-of-focus and are eliminated by the second pinhole aperture. Elimination of these out-of-focus rays enables better quality images of increased contrast and resolution. In addition, this pinhole technique enables collection of a series of optical sections at

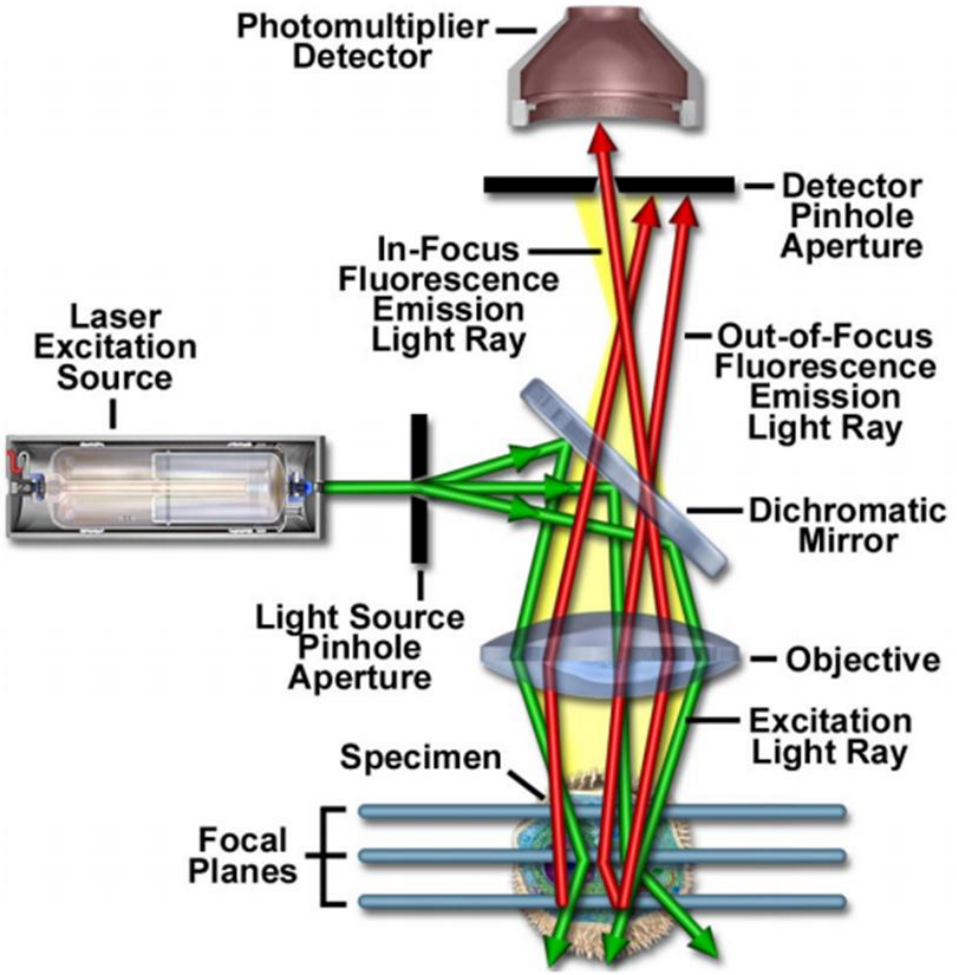

Figure 3.3: Schematic diagram of the components and optical pathway in a laser scanning confocal microscope. Courtesy of Paddock *et al.*[18]

different, and very narrow, depths of a specimen, after which the images can be built up to generate a highly resolved 3-dimentional image. Furthermore, the fluorescent filters can be used on the emission beam to generate fluorescent images of a specific wavelength.[17]

CLSM has been used in this thesis to obtain information about the up-take of nanocapsules *in-vitro*. The nanocapsules were incubated with live cells, and then the cells

were washed and seeded on glass slides for observation using a Nikon, A1 Confocal Microscope.

2.8 Thermogravimetric Analysis

Thermogravimetric Analysis (or TGA) is a thermal analytical technique used to determine the change, and rate of change, in the physical or chemical properties of a material with regards to temperature, and is primarily used to determine the composition and thermal stability of a sample material. The technique involves precise measurement of the percentage weight loss (or in some cases gain) due to dehydration, oxidation, or decomposition of a sample as it is exposed to a controlled temperature profile, in a controlled atmosphere. The percentage weight is then plotted against the temperature to give a curve that can provide information about the composition of multicomponent materials, the thermal or oxidative stability of the sample, as well as any possible intermediates that might form at different temperatures. In this thesis, TGA was used to determine the weight (by mass percentage) of bio-polymer present in the fabricated systems. All analysis was performed on a Pyris-1 TGA Perkin Elmer instrument at a temperature gradient of 20 ºC/min and a flow rate of 20 mL/min in air.

2.9 References

1 Monteiro-Riviere, N. A. & Tran, C. L. *Nanotoxicology: characterization, dosing and health effects*. (Informa healthcare, 2007).

2 Williams, D. B. & Carter, C. B. in *Transmission Electron Microscopy* 3-22 (2009).

3 Voutou, B. & Stefanaki, E.-C. in *Physics of Advanced Materials Winter School* (Thessaloniki, Greece, 2008).

4 Leng, Y. *Materials Characterization: Introduction to Microscopic and Spectroscopic Methods*. (Wiley, 2009).

5 *How Does Elecrton Microscopy Basically Work?*, <https://bsp.med.harvard.edu/node/221> (2010).

6 Zhou, W. & Wang, Z. L. *Scanning Microscopy for Nanotechnology Techniques and Applications*. (Springer New York, 2007).

7 *X-ray Fluorescence, The Basic Process*, <http://oxford-labs.com/x-ray-fluorescence/the-basic-process/> (2009).

8 Mazo, R. M. *Brownian motion: fluctuations, dynamics, and applications*. Vol. 112 (Oxford University Press, USA, 2009).

9 Nelson, E. *Dynamical theories of Brownian motion*. Vol. 17 (Princeton university press Princeton, 1967).

10 Brunauer, S., Emmett, P. H. & Teller, E. *Journal of American Chemical Society* **60**, 309, (1938).

11 Adamson, A. W. & Gast, A. P. *Physical Chemistry of Surfaces, 6th ed*, (1997).

12 Pungor, E. *A Practical Guide to Instramental Analysis*. (CRC Press, 1995).

13 Andrievsky, G., Klochkov, V., Bordyuh, A. & Dovbeshko, G. Comparative analysis of two aqueous-colloidal solutions of C< sub> 60</sub> fullerene with help of FTIR reflectance and UV–Vis spectroscopy. *Chemical Physics Letters* **364**, 8-17, (2002).

14 Grabar, K. C., Freeman, R. G., Hommer, M. B. & Natan, M. J. Preparation and characterization of Au colloid monolayers. *Analytical Chemistry* **67**, 735-743, (1995).

15 Rezwan, K. *et al.* Bovine serum albumin adsorption onto colloidal Al2O3 particles: A new model based on zeta potential and UV-vis measurements. *Langmuir* **20**, 10055-10061, (2004).

16 Brus, L. Chemical approaches to semiconductor nanocrystals. *Journal of Physics and Chemistry of Solids* **59**, 459-465, (1998).

17 Claxton, N. S., Fellers, T. J. & Davidson, M. W. Laser Scanning Confocal Microscopy. (Department of Optical Microscopy and Digital Imaging, National High Magnetic Field Laboratory, The Florida State University, Tallahassee, Florida 3231).

18 Paddock, S. W., Fellers, T. J., Expressions, M., University, F. S. & Nickon. *Confocal Microscopy, Basic Concepts*, <http://www.microscopyu.com/articles/confocal/confocalintrobasics.html> (2010).

CHAPTER 3

SYNTHESIS AND CHARACTERISATION OF SILICA TEMPLATE PARTICLES: THE ROLE OF SOLVENT, TEMPERATURE, AMMONIA AND WATER ON THE PARTICLE SIZE AND DISTRIBUTION

This chapter focuses on the synthesis and optimisation of monodispersed silica spheres to be utilized as template particles for the fabrication of drug delivery vehicles. Experimental parameters such as solvent, temperature, and concentrations of ammonia and water were individually investigated through single variable experiments to determine their effects on particle size and distribution. After the single variable experiments, an additional set of multivariable experiments were performed and the results applied to an artificial neural network (ANN) model in attempts to understand the complex interactions between parameters, that would otherwise be difficult and laborious to achieve through single variable experiments. Through neural network modelling, the way in which the parameters interact and affect one another's ability to influence particle size was investigated in an attempt to more accurately predict particle size based on experimental conditions.

3.1 Introduction

When drug delivery (DD) vehicles are administered into the body, either via intravenous or oral routes, it is essential that they encompass a set of requirements to ensure that they can carry out their function as a therapeutic treatment, while ensuring they cause no unwanted effects due to their physio-chemical properties.

In addition to the carrier materials, the size and distribution of the vehicles play a crucial role in their applicability as DD systems. The size of a particle will control the diffusion, permeation, and aggregation. If the administered particles are above a desired size range, they could become lodged in a passage and potentially cause critical side effects. For example, if the particles are < 6 nm they may be quickly removed by the body before they can achieve the desired function,[1] whereas if the nanoparticles are too large they can become trapped in organs such as the spleen and liver, and if toxic, can cause life threatening complications.[2] For these same reasons, development of optimum sized capsules devoid of the aforementioned is of equal importance. Despite achieving the majority of particles of a desired size, if there is only a very small number of particles that fall above or below the critical size, the vehicles will invade different parts of the body, and dreadful consequences ensue.

In this thesis, the DD vehicles presented are fabricated with a templating approach, where the structural properties of the vehicles correspond to the structural properties of the template particles. Therefore any lack of control in the size and distribution of the template particles, which in this case are silica nanoparticles, is translated to the drug delivery vehicles.

Consequently, it is essential that a high degree of control over the structural properties of the templates must be achieved before the second stage of drug delivery vehicle fabrication is carried out. Silica was chosen as the template material as it has been previously demonstrated to carry the characteristics of a good template particle for the fabrication of capsules through a process called layer-by-layer.[3-6]

To achieve template particles of a desired size and monodispersity, both single and multivariable experiments were undertake to identify the effects the experimental conditions. In the first section of the chapter (Chapter 3.2), traditional, single variable experiments were undertaken to identify the general trends of the parameters, while in the second section (Chapter 3.3), experimental design was used in conjunction with Artificial Neural networks (ANN) to investigate the dynamic interactions that occur between the parameters. Through the use of the two methods, the experimental conditions required to fabricate template particles of a desired size could be predicted.

3.2 Single Variable Investigations

The Stöber method was first developed in 1968,[7] whereby highly monodispersed silica spheres of low polydispersity were synthesised through the hydrolysis and condensation of tetraethyl orthosilicate (TEOS). Since then there have been numerous research efforts investigating the effect of the various experimental parameters, trying to determine the mechanisms by which this method is governed, and in doing so, obtaining a finer control of the size and distribution of the silica particles.

To enhance the ability to fabricate monodispersed particles of a desired size, the reaction mechanisms of particle nucleation and growth need to be understood, yet despite the increasing investigation into Stöber synthesis, the mechanisms still remain vague due to the relatively fast reaction rate and the various intermediates produced.[8] The current consensus is that the Stöber process follows the LaMer model where nucleation occurs very quickly, followed by a longer period of particle growth.[9,10] When these processes are well separated, i.e. there is no secondary nucleation occurring during the growth stage; the particles grow to a uniform size. In comparison, if nucleation continues to occur while some particles are currently undergoing growth, a polydispersed colloidal solution will be formed.

Nucleation occurs on introduction of the precursor into a reaction vessel which induces a sudden increase in precursor concentration (C_{Pre}), see Figure 3.1. If the initial increase in concentration overcomes a threshold value, nucleation will occur. This initial burst

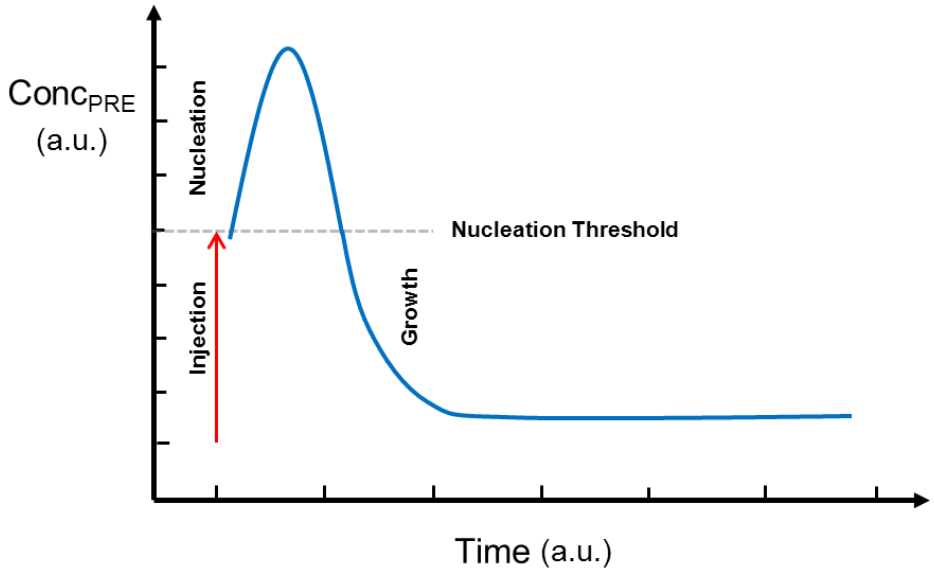

Figure 3.1: A depiction of the LaMer model representing the different stages of nucleation and growth, where Conc$_{PRE}$ represents the concentration of the precursor. Adapted from Capek *et al.*[11]

of nucleation partially reduces the supersaturation ratio, after which the C_{Pre} will eventually drop back below the nucleation threshold, driving the reaction into a growth stage. During the growth stage, as long as the rate of consumption of the reactants for particle growth is faster than the rate that precursors are added to the solution, any secondary nucleation is suppressed, resulting in very uniform particles.[11,12]

The most currently updated mechanism of the reaction which describes the ammonia-catalysed hydrolysis and condensation of tetraethyl orthosilicate (TEOS) with water while in the presence of a low-molecular weight alcohol solvent can be briefly summarised in the following chemical equation:

$$Si(OC_2H_5)_4 + 4H_2O \rightarrow SiO_2 + 4CH_3CH_2OH \qquad \text{(Eq 1)}$$

The reaction can then be further broken down to the following equations where *x, y* and *z* are stoichiometric coefficients;[13]

$$NH_3 + H_2O \rightleftharpoons NH_4OH + OH^- \qquad \text{(Eq 2)}$$

$$Si(OC_2H_5)_4 + OH^- \xrightarrow{\text{Hydrolysis}} (OH)Si(OC_2H_5)_3 + CH_3CH_2O^- \qquad \text{(Eq 3)}$$

$$(OH)Si(OC_2H_5)_3 + Si(OC_2H_5)_4 \xrightarrow{\text{Alcohol Condensation}} (C_2H_5O)_3 -Si-O-Si(OC_2H_5)_3 + CH_3CH_2OH \qquad \text{(Eq 4)}$$

$$(OH)Si(OC_2H_5)_3 + (OH)Si(OC_2H_5)_3 \xrightarrow{\text{Water Condensation}} (C_2H_5O)_3 -Si-O-Si(OC_2H_5)_3 + H_2O \qquad \text{(Eq 5)}$$

From the proposed equations it can be seen that before the TEOS is introduced into the reaction solution, ammonium hydroxide dissociates in water to give ammonium (NH_4^+) and hydroxide (OH^-) ions. The presented mechanism suggests that these hydroxide ions drive the hydrolysis of TEOS through the nucleophilic attack at the Si atom by replacing the alkoxide ions. From these equations we can see that the rate of TEOS hydrolysis is dependant only on the concentration of TEOS and the negatively charged hydroxide group (OH^-). After hydrolysis of the TEOS has occurred, as-formed hydroxyl trimethoxysilane species can undergo either alcohol condensation (*Eq 4*) or water condensation (*Eq 5*). In alcohol condensation the newly acquired hydroxide group of the silicate undergoes deprotonation, allowing it to displace an alkoxide group while attacking the Si atom of another unhydrolysed TEOS molecule, generating alcohol in the process, whereas water condensation involves two hydroxyltrimethoxysilane, with the newly acquired hydroxide groups reacting together to produce water. These processors are further summarised in Figure 3.2. After the formation of dimers through either alcohol or water condensation, the molecules grow through addition of another monomer to form trisilicic acid,[14,15] then oligomerization takes place in order to minimize the abundance of uncondensed Si(OH) bonds in favour of the condensed Si-O-Si bonds.[14,16,17]

The parameters that have been investigated include the reaction solvent,[7,18-20] reaction temperature,[8,18,19] ammonia concentration,[7,8,18-20] water quantity,[8,18-20] TEOS concentration,[8,18-21] the intermediate products,[13,22,23] and the reaction kinetics.[8,13,23-25] Despite the various investigations, many of these studies have not managed to achieve spherical particles in the perfectly tailored size range or with size distributions narrow enough for drug delivery applications. In the study by *Wang and Wu et al* the effects of solvent, TEOS,

ammonia, and water concentration were investigated,[19] however, the particles that were fabricated demonstrated a broad size distribution, with relative standard deviations above 15 % (with most of the deviation ranging between 20–30 % in size). In some particles this corresponded to a distribution of ± 100 nm, a very significant amount when drug delivery applications are considered. In a study by *Wang and Shen et al*, although numerous experiments were undertaken, much of the data produced include bimodal, aggregated or polydispersed particles.[20] Furthermore, many of these studies have used vastly different synthesis conditions from one another, and in some cases have varying multiple parameters

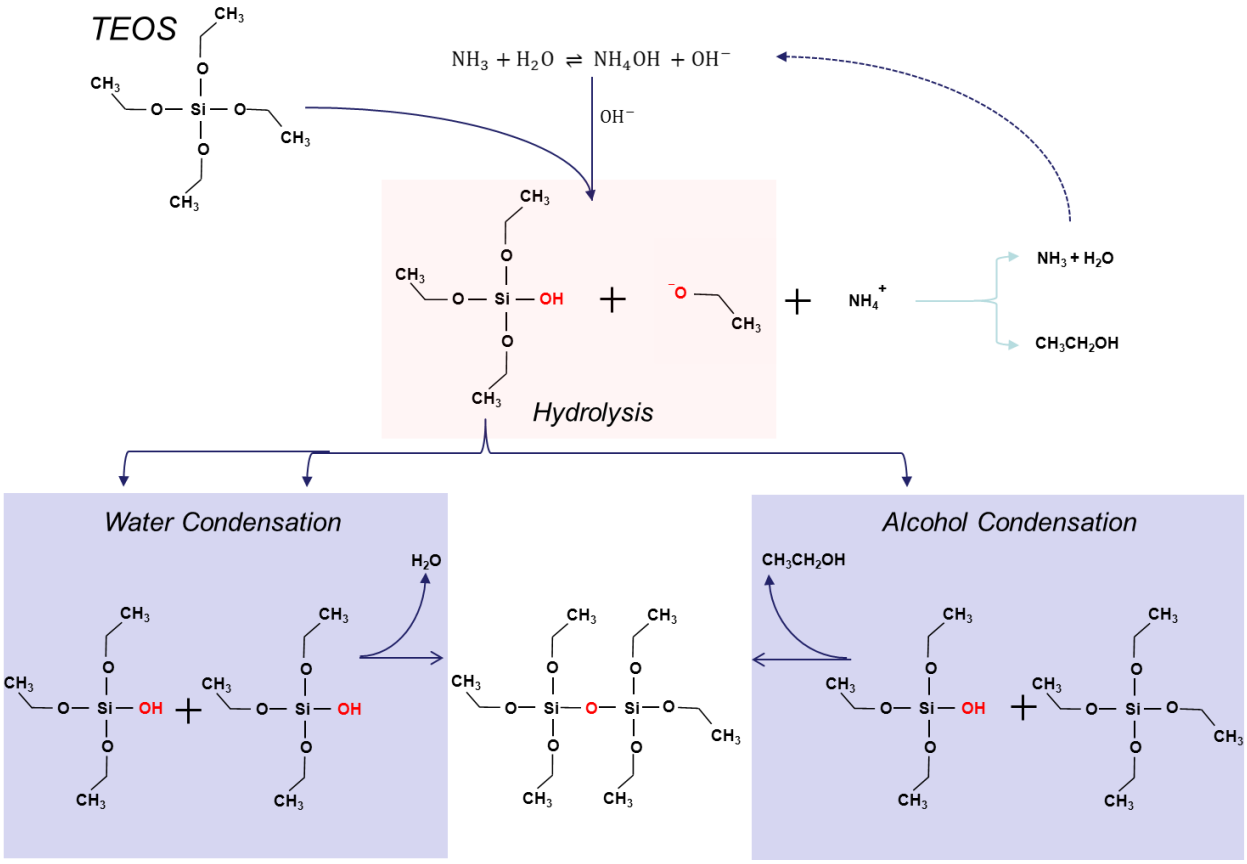

Figure 3.2: The mechanisms of the hydrolysis and condensation of TEOS.

simultaneously, therefore the parameters cannot be effectively correlated with the size and distribution of the particles, nor can the results from different studies be compared.[7,8,13,18-21,26,27]

3.2.0.1 Rationale

As the applicability, effectiveness and safety of drug delivery vehicles has great dependence on their size and distribution, it is essential to control these properties to the best possible degree. The development of the DD vehicles presented in this thesis is through the use of silica spheres acting as template particles, where the size and distribution of the DD vehicles is reflected by the size and distribution of the silica particles, it is of great important to fabricate the particles to a particular size and below critical distributions. Despite the previous investigations, unfortunately it remains exceptionally difficult to accurately produce particles of a desirable size and of narrow distribution due to the complexity of the reaction, with unpredictable patterns in size occurring when any of the experimental conditions are varied due to their effects not being mutually exclusive. Therefore, to fabricate particles required within the correct size range and distributions for the applications of this thesis, the parameter requires new and thorough investigation and optimisation, otherwise, until very thorough investigations into the experimental parameters and their interactions are investigated both individually and simultaneously, the application of these particles will continue to be dictated by, and limited to, the fate of the particles produced.

In this chapter, the reaction solvent, temperature, ammonia and water concentration have been varied, and their effects on the size and distribution are investigated in an effort to identify the optimum parameters required to produce highly monodispersed silica

nanoparticles of a variety of sizes to be employed as templates for the development of drug delivery vehicles.

3.2.1 Experimental Investigations

3.2.1.1 Synthesis of Solid Core Silica Spheres

In the first step, monodispersed, highly homogenous and stable solid silica core particles were prepared through the hydrolysis and condensation of tetraethylorthosilicate in a mixture of low molecular weight solvents such as ethanol, along with ammonia and water.[7] However, several modifications were made to the protocol to investigate their effects on the size of the silica, including variations to the solvent used, ammonia and water content, and reaction temperature. The reaction solutions were prepared using the solvents methanol, ethanol, butanol, n-propanol or pentanol. Different concentrations of both deionised water (MilliQ) and ammonia solution (28%) were used, ranging from 4.11 – 7.13 M and 0.62 – 1.85 M, respectively, as specified in Figure 3.3.

This was followed by mixing of the solution for 1 minute, and then allowing the solution to stabilize at a defined temperature (Figure 3.3) between 5 – 45 °C for 30 minutes in a thermomixer, after which, 75 µL of tetraethoxysilane (TEOS) was added to all the solutions and incubated for 1 hour at the appropriate temperatures without shaking. The resulting spheres were then washed repeatedly with centrifugation and redispersed in ethanol. Finally, to obtain the white powder of silica spheres, the centrifuged pellets were dried in an oven at 100 °C .

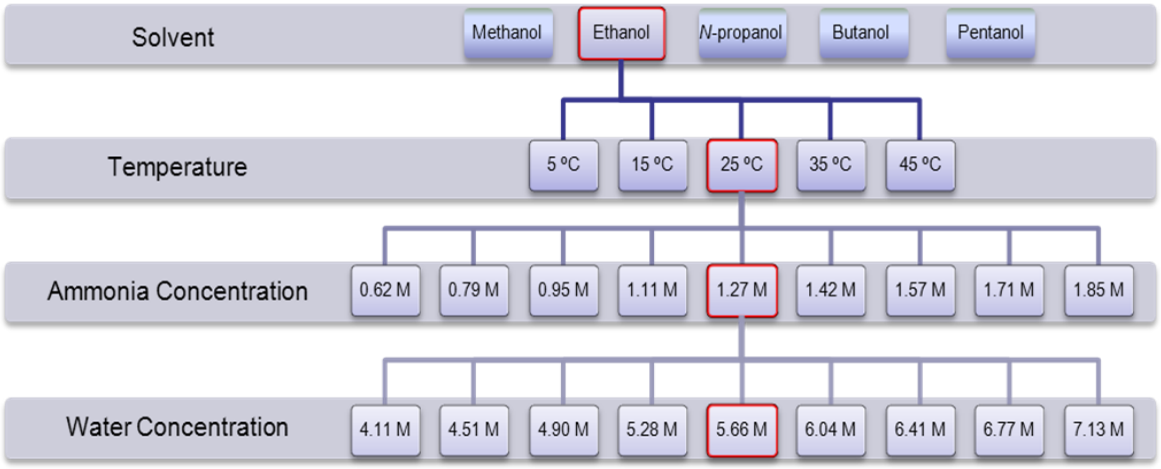

Figure 3.3: The experimental conditions for investigation into the effects of solvent, temperature, ammonia and water concentration.

3.2.1.2 Silica Particle Characterization

Scanning and transmission electron microscopy (SEM and TEM) were used to image and measure the size of the silica sphere templates. SEM images were obtained by drop casting the silica sphere templates directly onto aluminium SEM stubs and analysed using the FEI Nova NanoSEM. TEM images of the silica templates were obtained by air-drying directly onto strong carbon grids and analysed using a Jeol 1010 TEM. In addition to the SEM measurements, the particle size and distribution was also analysed using Dynamic Light Scattering (5022F Fast DLS particle sizing spectrometer).

3.2.2 Results and Discussion

The effect of the synthesis conditions on the resulting diameter and polydispersity has been thoroughly investigated through single variable experimental techniques. During these investigations, one parameter, the solvent, temperature, ammonia or water concentration was varied while all other parameters were kept constant at 1.27 M ammonia and 5.66 M water,

and the reactions were carried out in ethanol at 25 °C. The morphology of the particles was observed with SEM, while their size was measured using both SEM and DLS for better precision. Generally the DLS method measures the hydrodynamic radius of the colloidal particles, therefore it is always slightly higher that the values obtained using the SEM. The polydispersity of the particles was also investigated and determined by the relative deviation of the particles measured by the SEM and displayed as a percentage.

3.2.2.1 Effect of Solvent on the Solid Core

To obtain the most effective silica sphere particles to act as templates for drug delivery vehicles, the best solvent needed to be identified before any further investigation into the effects of temperature, ammonia and water could be undertaken. In this section the solid silica particles synthesised in the different solvents; methanol, butanol, *n*-propanol and pentanol have been investigated while other experimental conditions remained constant (temperature 25 ºC, ammonia 1.27 M, water 5.66 M).

The SEM images displayed in Figure 3.4 revealed that the type of solvent used during the solid core synthesis has a dramatic effect on the outcome of the size and morphology of the particles, with the particles synthesised in methanol found to be very small, intermediate sized particles occurring in ethanol and *n*-propanol, and irregular, polydispersed, and non-spherical particles occurring in butanol and pentanol. The average radii of the spheres are displayed in Figure 3.5.

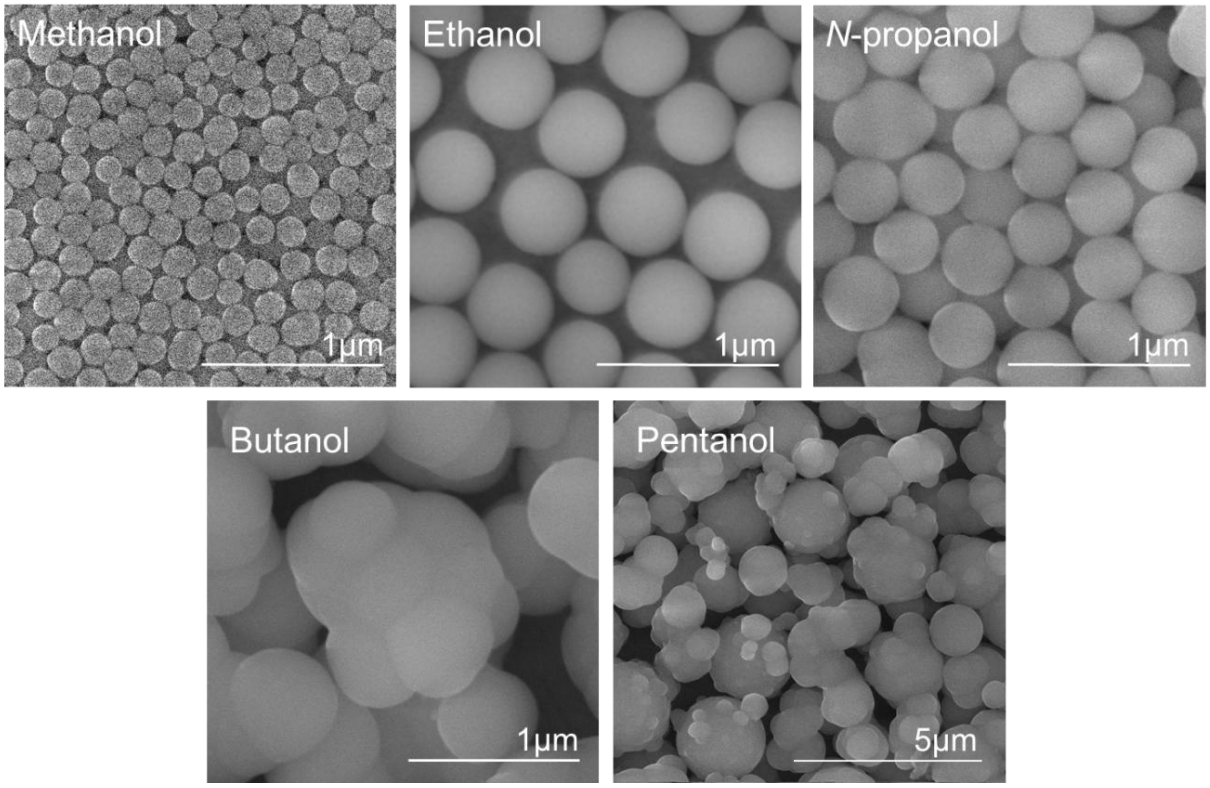

Figure 3.4: SEM images of solid silica nanoparticles synthesised at 25 °C with 1.27 M ammonia and 5.66 M water in different solvents.

As can be seen in the SEM images (Figure 3.4), when butanol is utilized as the primary solvent, the silica particles have grown irregularly, with evidence that some of the particles have not separated properly during growth. Instead the particles demonstrate a 'budding' effect, where they have grown atop each other to produce extremely large but irregular particles. It can be seen from the images that some of the fused particles are ca. 350 nm in radii, while the overall particles are much larger, around 600 nm in radii. As a result the size distribution has suffered considerably, with these particles no longer considered as monodispersed. Although these particles are very large, their shape and size distribution is irregular, limiting their applications in drug delivery systems.

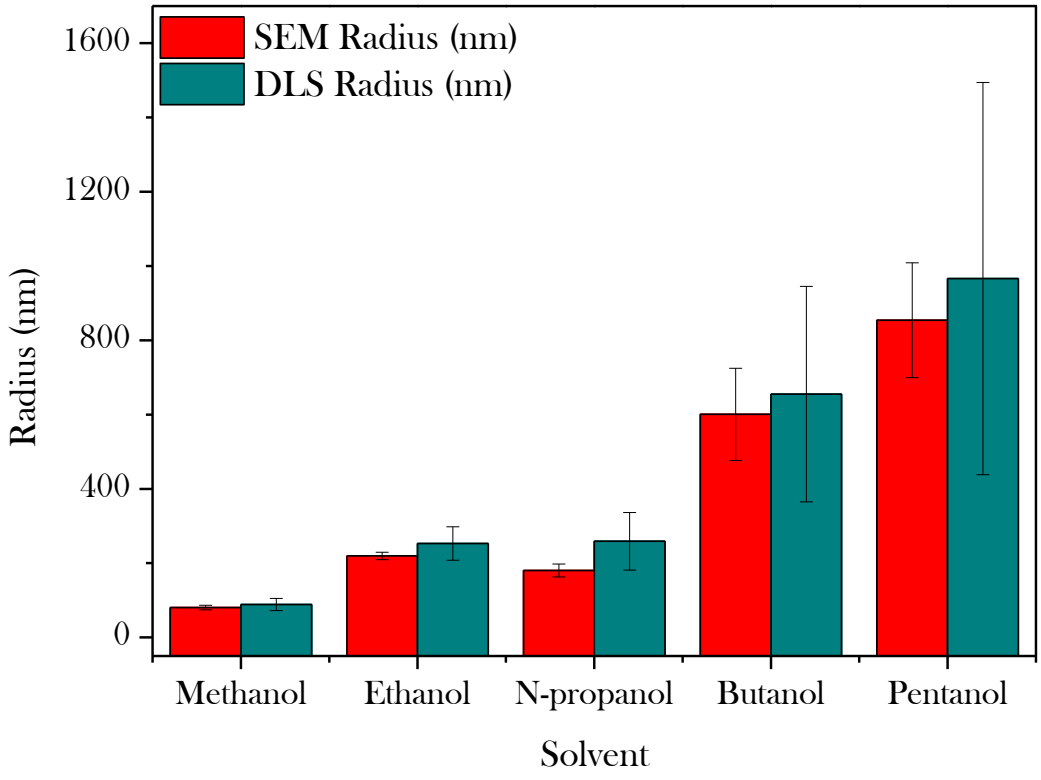

Figure 3.5: The average silica particle radius and standard deviation in the presence of different solvents, as measured by both SEM and DLS.

In pentanol the particles range from ca. 600 nm – 1.05 µm in radius, however, it can also be seen that there are some smaller, fused particles of around 200 nm in radius. Similar to butanol, the particles made in pentanol are not all spherical and range significantly in size and shape. Both the particles formed in butanol and pentanol have very high polydispersity with relative deviations of around 20%, rendering them inappropriate for further investigation as drug delivery template particles.

It is an often reported trend where an increase in the alkyl chain length of the solvent *n*-alcohol can result in larger particles,[7,23,24,28,29] which is the case between particles synthesised in methanol compared to the longer chained ethanol, where the particles in

methanol are shown to have a radius 63% smaller than particles synthesised in ethanol. However this trend does not continue with the longer chained *n*-propanol, with particles produced in ethanol being ~18% larger than those produced in *n*-propanol. Although it would seem that this may be a result of experimental error during synthesis, it is in good agreement with Tan *et al*[18] who also reported a 15% increase in particle size when ethanol was used over *n*-propanol. As *n*-propanol is a longer chained solvent than ethanol it would be expected to produce larger particles, yet the particles produced are smaller. This suggests that the simple statement that longer chained solvent produce larger particles may not be entirely accurate.

The effect of the solvent on the particle size has also been suggested to be related to the dielectric constant of the solvents which causes a variation in the solvents ability to screen the opposite charges in the solution. As silica hydrolysis involves many steps which all contain charged intermediates, employing a solvent with a higher dielectric constant screens their charges and suppresses aggregation of the particle intermediates. This helps to explain the increase in particle size when referring to particles produced in methanol verses ethanol which has the dielectric constants 32.6 and 24.4, respectively (Figure 3.6), as well as the aggregation of nuclei in lower dielectric solvents such as pentanol and butanol. The high dielectric constant helps to explain why isopropanol has been reported to produce larger particles than what we have reported here using *n*-propanol. However, this trend does not coincide with the decrease in particles seen when *n*-propanol was employed which has a dielectric constant of 20.1 (Figure 3.6). It should however be noted that, the formation of ethanol as a side product from the condensation reaction may complicate the process further. This suggests that the outcome of the particle size using the Stöber process is more complex than simply the effect of alkyl chain length and the dielectric constant of the solvent.

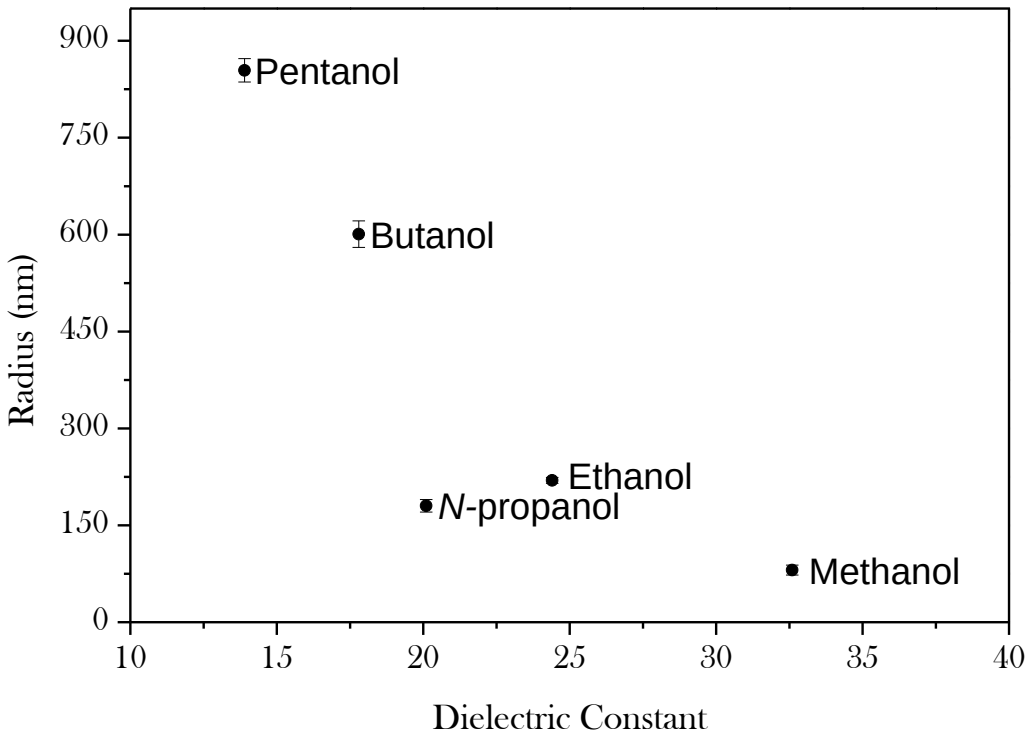

Figure 3.6: The average particle size as a function of the dielectric constant of the solvent.

The viscosity of the solvents is another property which differs between solvents, where the viscosity increases as the alkyl chain increases in size. When a less viscous solvent is used, the rate of the nucleation is fast, allowing for good separation between the nucleation and growth stages. Meanwhile, in a high viscous solution the precursor will take longer to diffuse through the reaction solution. This can create quick nucleation and growth at the interface, while the precursor away from the interface may not undergo nucleation for some time, creating a rather polydispersed colloidal solution.

The size distribution of the particles is also found to be dependent on the solvent that was used. In Figure 3.7 it can be seen that there is an increase in the particle distribution as the molecular weight of the solvent increases, taking into account that the particles produced in both butanol and pentanol have shown polydispersity, it is not surprising that they

demonstrate extremely high distribution values (ca. 20%). The distribution for methanol, ethanol and n-propanol are all relatively low and can be considered monodispersed enough for many applications, with the particles produced in ethanol demonstrating the lowest polydispersity. Furthermore *n*-propanol may not be as good a candidate for producing silica particles of an intermediate size range as their sizes fall within that of methanol and ethanol, while the monodispersity is compromised more than in both other solvents. While the spheres in methanol also demonstrated extremely narrow size distribution, with less than 8% relative variation measured from the SEM data, the particle size range is approaching that where toxicity has been found to increase,[30] making these particles less suitable as templates for synthesis of drug delivery vehicles.

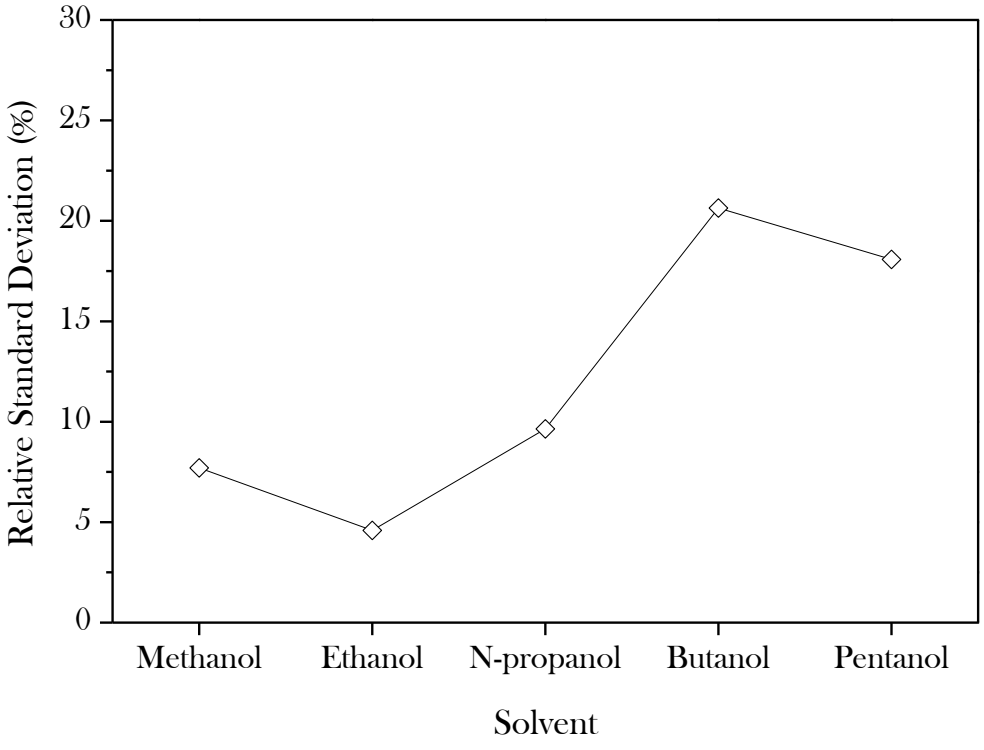

Figure 3.7: The relative standard size distribution of the particles fabricated in the five different solvents.

As a result of these observations, ethanol was chosen as a solvent for particle synthesis due to its good particle production within the size and distribution desirable to be used as templates for the fabrication of monodispersed drug delivery vehicles.

3.2.2.2 Effect of Temperature on the Solid Core

The effect of temperature was investigated and is demonstrated to play a critical role in the outcome of the particle size, where it was determined that the particle size was inversely proportional to the reaction temperature. By altering the reaction temperature from 5 to 45 °C while keeping all other parameters constant, the particle size could be reduced from 533 nm to 104 nm, respectively. All particles with the exception of particles fabricated at 5 °C were extremely spherical and homogeneous, with intermediate particle radii occurring at 15 and 25 °C, and much smaller particle radii occurring above 35 °C (Figure 3.8). Although the

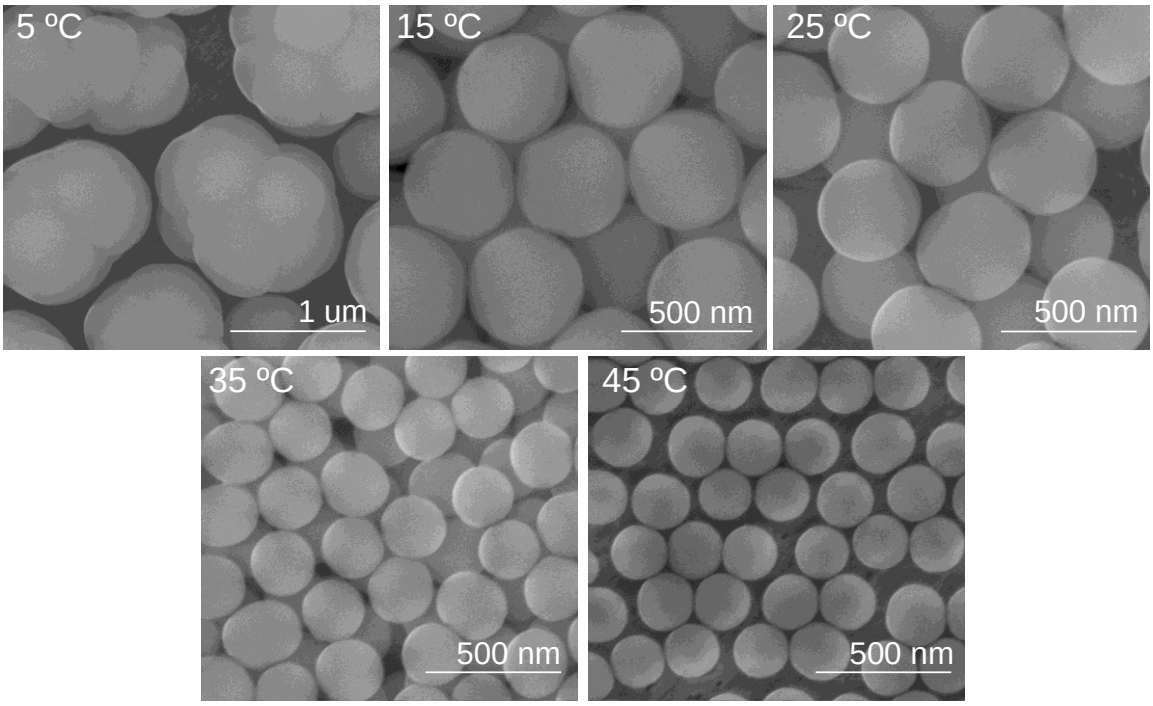

Figure 3.8: SEM images of silica particles synthesised at different temperatures.

relationship between the temperature and particle size was not perfectly linear, a general inverse trend could be seen between temperature and size of the particles.

At the lowest temperature of 5 °C, the particle homogeneity was compromised with large, irregular, and non-spherical particles occurring. From the image at 5 °C (Figure 3.8) it can be seen that many smaller particles fused together into larger particles. In general, the rate of a reaction is controlled by the reaction temperature. At a low temperature the rate of formation of the nuclei and the rate of growth of seed particles would both be very slow, and may occur simultaneously.

Aggregation is also thought to occur if the condensation rate is larger than the hydrolysis rate, which may be a result of the temperature affecting the reactions rates in different ways.[20] Yet despite the aggregation obtained at the low temperature, the fused particle size was still much larger than those grown at higher temperatures, estimated to be around 350 nm. At lower temperatures it has been found that the distance between the vibrating particles becomes greater, permitting space for more monomer addition growth.[20] The radii of the sub-particle size at 5 °C, displayed as a (*) in Figure 3.9, also coincides better in the size verses temperature trend, which would obtain a better line of fit and would support the notion that the larger particles are more likely to have occurred due to the fusing of smaller subparticles. This demonstrated that although there is an increase in particle size by decreasing reaction temperature, there are limits to how far these parameters can be altered before the monodispersity of the colloids are compromised.

Above the temperature of 5 °C, all other particles grown were found to be very monodispersed, with a general decrease in particle size as temperature increases (Figure 3.9).

In previous literature it has often been suggested that the temperature directly affects the rate of hydrolysis, which in turn affects the size of the seed particles, whereby a very fast nucleation rate produces smaller seed particles.[18,20] This is related to the proportional relationship between temperature and diffusion, allowing for the TEOS to diffuse into the solution quicker.

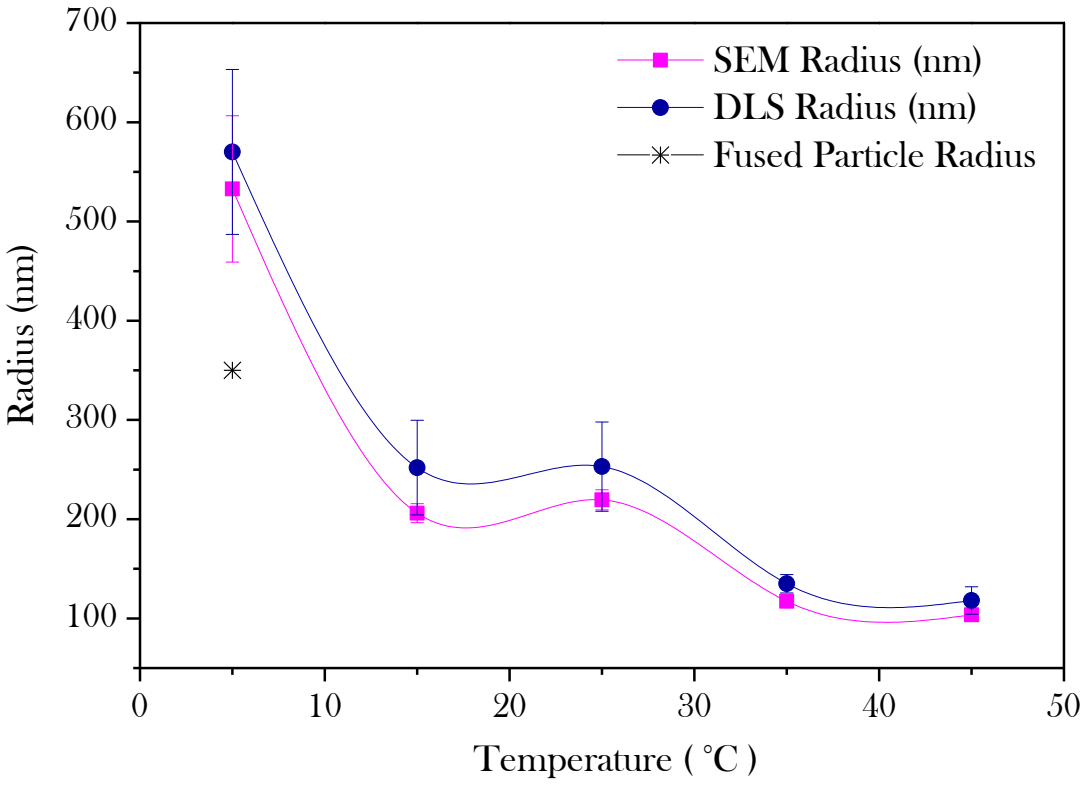

Figure 3.9: The SEM and DLS radii of the silica particles with regards to the reaction temperature.

The relative standard deviation was investigated and shown in Figure 3.10, where the particles produced at 5 °C demonstrated an extremely high polydispersity which is due either to the fusing of unstable particles, uneven growth on the seed particles, or is a reflection of a large size distribution that could have occurred during the initial particle seeding. A large distribution in size renders these particles inefficient for many applications, especially in use

as drug delivery systems as size can have a dramatic and severe effect on the functionality of the particles. In contrast, all particles produced above this temperature demonstrated extremely good monodispersity with relative standard deviations below 5% and can therefore be categorised as highly monodispersed. With the exception of the particles produced at 5 °C, these results demonstrate that not only can silica nanoparticles be produced at a range of temperatures in ethanol, but also in a range of sizes without compromising their monodispersity, making them ideal for further investigation as templates for drug delivery.

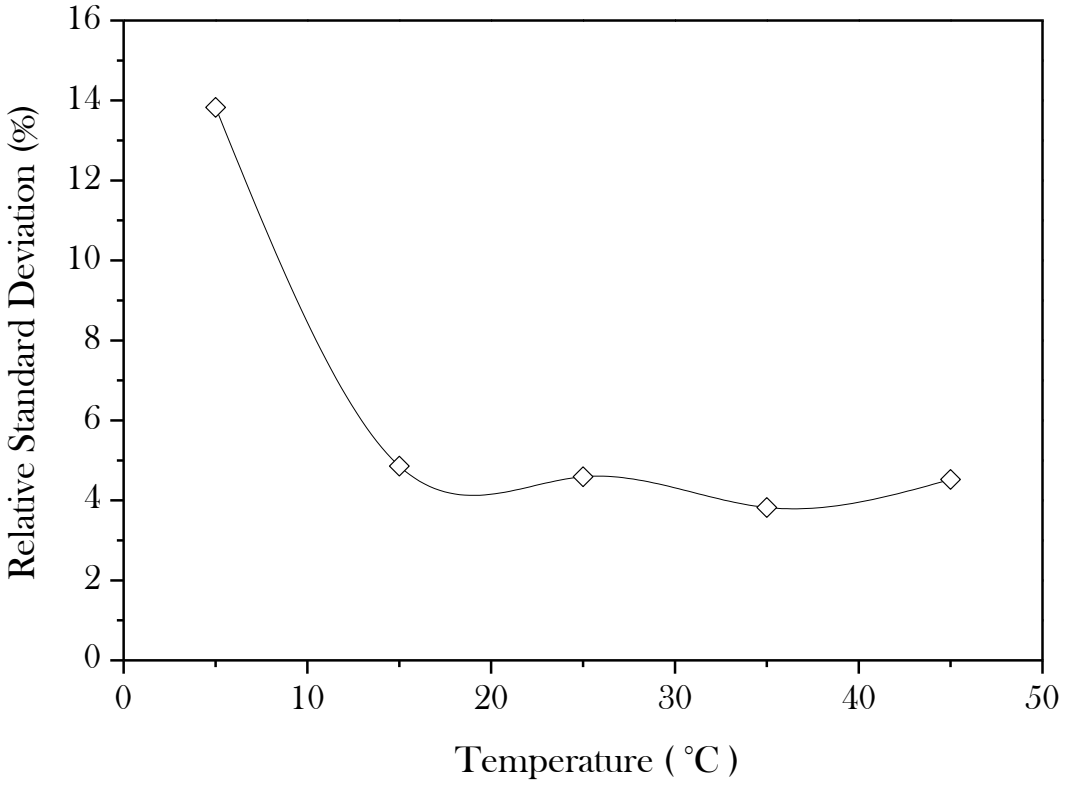

Figure 3.10: The effect of temperature on the relative standard deviation of the particles.

3.2.2.3 Effect of Ammonia on the Solid Core

It is thought that ammonia also has a significant effect on the size and polydispersity, with many previous reports generalising that the particle size increases with ammonia

concentrations,[8,19,26] yet the relationship is not always as sight forward as this statement, with particle size maxima and minima often seen.[31] In this section, the effects of ammonia were systematically investigated over a narrow but relevant concentration range from 0.62-1.85 M ammonia, in which monodispersed growth was seen throughout, yet with fine changes in both particle size and polydispersity.

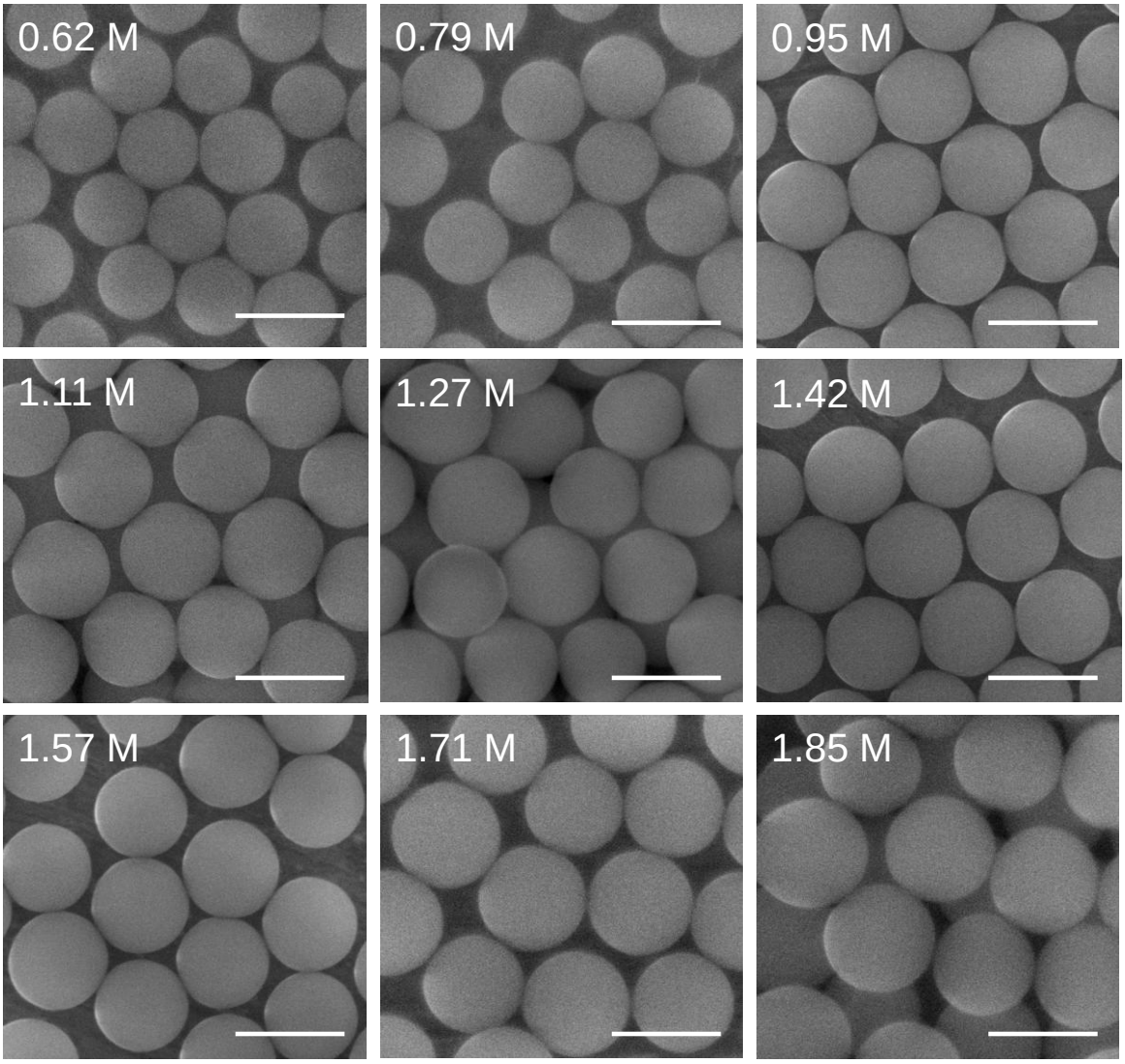

Figure 3.11: SEM images of silica spheres produced at different ammonia concentrations. All scale bars correspond to 500 nm.

As can be seen from Figure 3.11, all the silica spheres fabricated in the ammonia range appear homogenous with only small variations in size and polydispersity. In order to better determine the fine differences that have occurred due to the effects of ammonia, both the SEM and DLS results have been considered. From the graph presented in Figure 3.12 the general trend of particle radius increasing with an increase in ammonia concentration can be seen, however the trend is not entirely linear, with a small but notable drop in particle size at 1.42 M before the increasing trend is re-established.

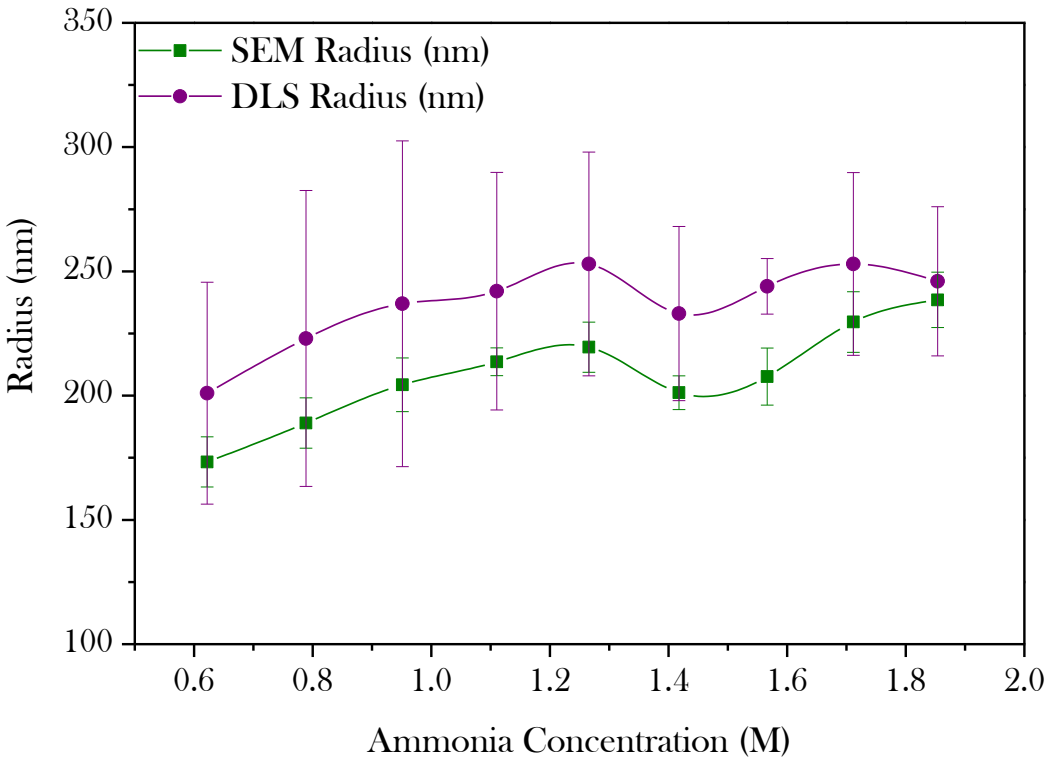

Figure 3.12: The SEM and DLS radii with regards to ammonia concentration.

From the currently proposed mechanisms of TEOS hydrolysis and condensation (Eq 2-5), ammonia clearly plays a crucial role, whereby the ammonia instigates the production of the hydroxide ions (OH^-) either through the deprotonation of water, or through the dissolution

of ammonia hydroxide. These OH^- groups then attack the Si atoms, initiating the hydrolysis of silica precursor (Eq3). Once the reaction is underway, the reaction is self-sufficient until all the TEOS is consumed.

Although OH^- ions are required in catalytic concentrations, ammonia is not part of the rate determining step. Furthermore, since ammonia hydroxide is not a strong base, it will not completely dissociate into OH^- ions, and as the main composition of the reaction solution is ethanol, the pH of the solution would not drastically change as it would in pure water. This helps to explain the small impact of ammonia has on the size of the particles when the ammonia concentration has been increased.

The distribution of the fabricated particles is seen in the relative deviation displayed as a percentage of the total particles size (Figure 3.13). Across this ammonia range the polydispersity is very low, and although there are two local minima in the relative distribution, all are within the range to be considered monodispersed (< 6%). Overall the size of the particles increases slightly with an increase in ammonia concentrations, with very little effect on the polydispersity over a narrow ammonia concentration range, however the trend is not entirely robust, with unexpectedly lower particles sizes occurring at 1.41 and 1.57 M. Therefore the effect of ammonia concentration on the particles size is not as straight forward as it seems, making it an extremely difficult task to accurately fabricate particles of a desired size.

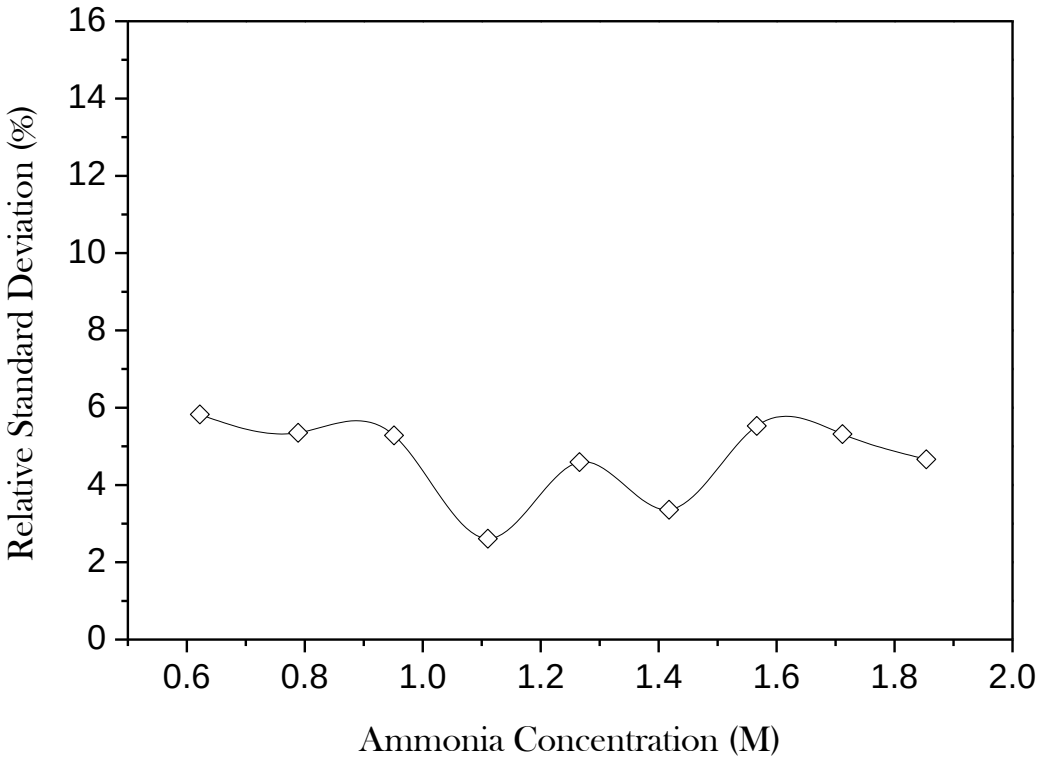

Figure 3.13: The relative standard deviation over the ammonia concentration range.

3.2.2.4 Effect of Water on the Solid Core

The effect of water on the silica particle size and distribution was found to be more unpredictable when compared with all the other reaction parameters. In the investigation presented here, the range of experimental variation was kept narrow, from 4.11 to 7.13 M MilliQ water, where good particle growth was known to occur. The narrow concentration range allows for a more thorough investigation of the behaviour of water, with smaller intervals between sample concentrations than normally presented in many studies.[8,13,19,20] The SEM images of the particles are shown in Figure 3.14.

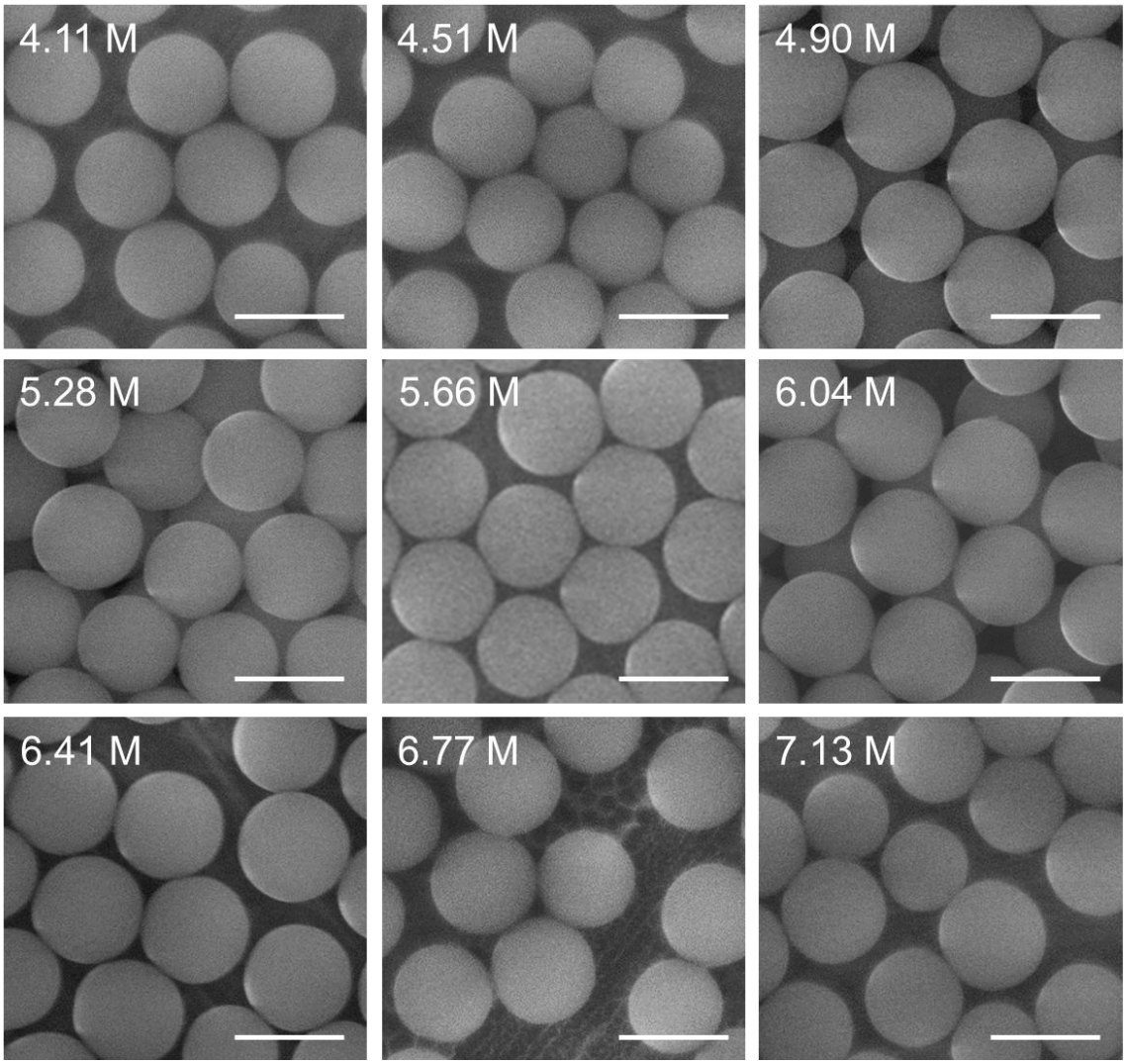

Figure 3.14: SEM images of the silica spheres fabricated with the concentration of MilliQ water ranging from 4.11 M – 7.13 M. All scale bars correspond to 500 nm.

The concentration of water was found to have a much smaller effect on the particles size, with no obvious trend in the radii which ranged from 220-230 nm. Although there was a small local maximum size at 4.90 M water, the overall variation in size was small at ca. ~7%.

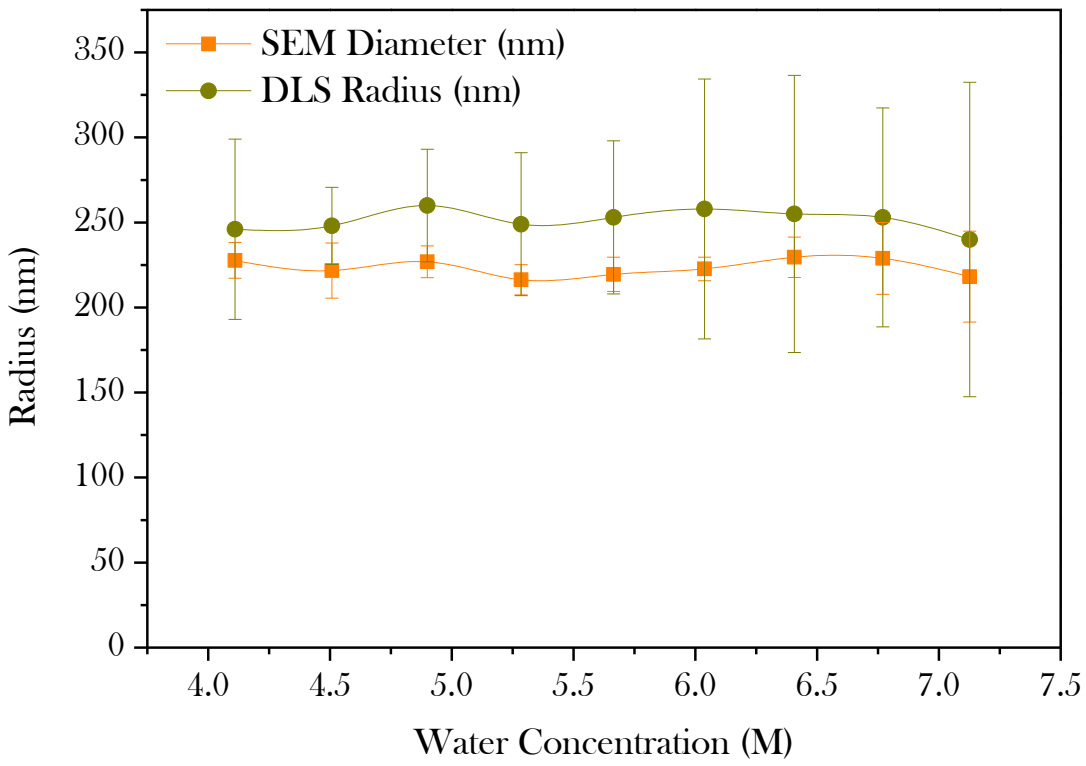

Figure 3.15: The effect of water concentration on silica particle size.

In contrast to a small effect on size, the concentration of water did show a significant effect on the polydispersity of the particles (Figure 3.16), with a steady increase in relative deviation once the water concentration increased from 6.0 M. This increase in deviation is in good agreement with the results obtained by Wang *et al* who also reported an increase in deviation from 4.7, 6.0 and 9 M concentrations.

Since TEOS is immiscible with water, any increase in the water concentration will result in a slower reaction rate as the TEOS molecules will take longer to diffuse into the reaction solution. This will result in polydispersed particles as nucleation and growth are not well separated. Furthermore, similar to ammonia, water facilitates the production of OH^- ions which helps to stabilise the reaction solution of lower ionic strength.[20] However, after a

critical ionic strength the OH^- concentration becomes too high, increasing the pH to a point where the silica particles may begin to dissociate, forming a variety of sizes. The increase in water will also intensify the effects of ammonia, increasing the pH further and resulting in more silica dissolution.

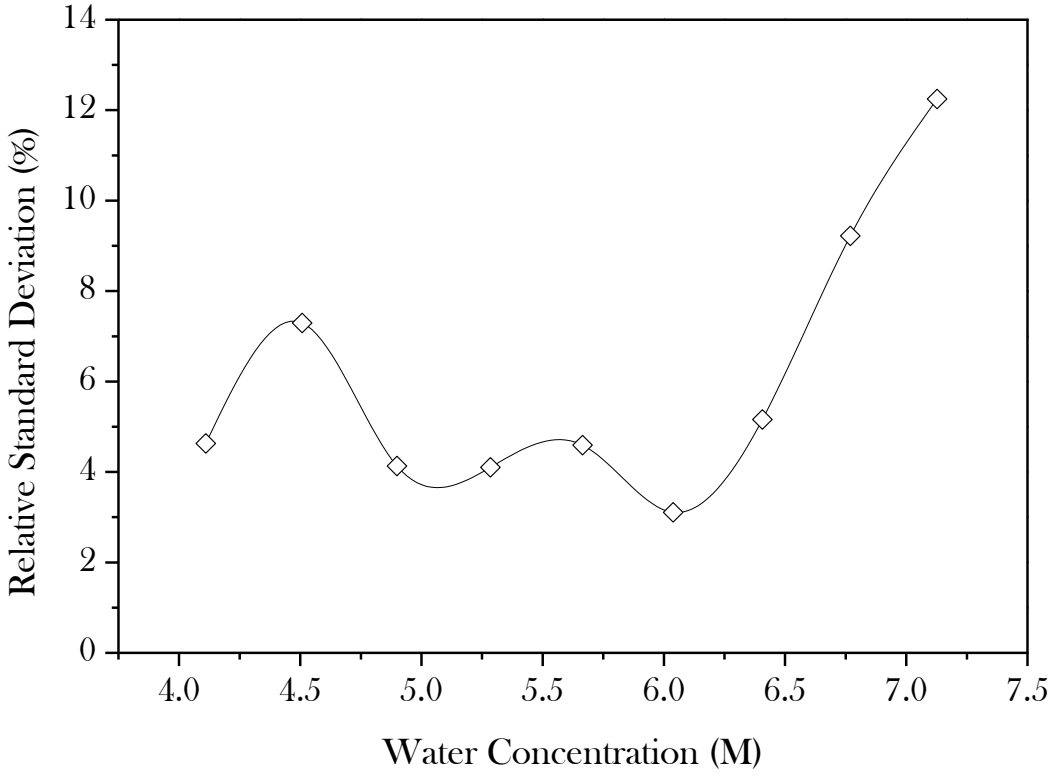

Figure 3.16: The effect of water concentration on the polydispersity of the particles.

A large deviation from monodispersity causes uncertainty and a variation in the properties and effectiveness in biological applications. Therefore a concentration of water around 5.0 to 6.0 M gives the optimum property of monodispersity.

3.2.3 Summary

In summary, the effects of solvent, temperature, water and ammonia concentration were investigated, and it was found that solvent and temperature were demonstrated to have

the largest effect on the particle size, followed by ammonia to a lesser extent. Meanwhile water did not demonstrate a large effect on particle size but did show a stronger influence on the polydispersity of the particles. From these results, it is possible to fabricate highly monodispersed particles of a variety of sizes that are of sufficient quality to be used as template for drug delivery systems.

3.3 Multivariable, Artificial Neural Network Investigations

When it comes to employing nanoparticles in drug delivery systems, therapeutic applications often call for particles to be within a very specific size range. As a result, the ability to identify the experimental parameters required to fabricate silica nanoparticles of a desired size could be invaluable in the scientific world. In the previous section it was shown how variation in one experimental parameter can control the particle size. Since each and every parameter affects the final particle size interdependently, it is extremely difficult to predict or control the particle size in experiments when multiple parameters are varied simultaneously. Furthermore, although it is possible to gain insight into the interactions of the variables through classic, single variable experimental investigations, this process would require an extremely large number of experiments, making it both time consuming and laborious.

Artificial Neuron Networks (ANNs) may offer a solution for particles size prediction without the need for extensive experimental work by exploiting computational modelling programs. ANNs work by solving complex algorithms based on only a small number of experimental results defined by the experimental design, and in doing so, can identify patterns in the particle size. Through the implementation of these computational models, the complex

interactions of the experimental variables and their effects during the synthesis of the particles can be observed. However, the ANNs only relate the results and parameter values using certain algorithms, and do not define the combination of experiments needed to be carried out. Instead, ANNs are often coupled with an experimental design.

Experimental designs are being employed more often in scientific systems due to their increased complexity, where the experiment design involves planning out the experiments to obtain the most amount of information about a system using the least number of experiments. The sample points in these designs are often evenly distributed over the range of variables in the system to cover all the possible interactions. There are numerous different experimental designs that can be applied to systems, including one-variable-changed-at-a-time full factorial designs, or multivariable Box-Behnken and Doehlert designs.[32,33] These experimental design methods differ in the number of experiments required to complete a matrix, as well as their accuracy at interpreting information. As seen in Table 3.1, unlike the other experimental designs, the Doehlert design maintains efficiency while the number of variables and complexity of the system is increased. Therefore the Doehlert design has been implemented in the following section to study the effects of the experimental parameters on the size of the silica particles synthesised.

Variables (K)	Number of coefficients (p)	Number of experiments (N)			Efficiency (p/N)		
		CCD	DM	BBD	CCD	DM	BBD
2	6	9	7	-	0.67	0.86	-
3	10	15	13	13	0.67	0.77	0.77
4	15	25	21	25	0.6	0.71	0.6
5	21	43	31	41	0.49	0.68	0.61
6	28	77	43	61	0.36	0.65	0.46
7	36	143	57	85	0.25	0.63	0.42
8	45	273	73	113	0.16	0.62	0.4

Table 3.1: A comparison of the efficiency of the central composite design (CCD), the Box-Behnken design (BBD) and the Doehlert design (DM). Adapted from Ferreira *et al.*[34]

In the Doehlert design;

$$N = k^2 + k + 1$$

where k is the number of variables, and N is the number of experiments required

When the results from the experimental design are coupled with the algorithms of an ANN, the correlations between the parameter and experimental values are modelled, and the patterns and interactive relationships between them can be visualised in a 3-dimensional response map.

To the best of the author's knowledge, there is only a single report where ANNs have been employed to predict the size of silica nanoparticles based on the experimental parameters as reported by Leparoux *et a.*[35] However, in their investigations they employed an inductively coupled plasma (ICP) process to fabricate the silica nanoparticles. Rather than the Stöber method where the size is a factor of solvent, temperature, ammonia and water concentration, in the ICP process size is a factor of quenching gas flow rates, and precursor feeding rates. Therefore the ANNs in this study were applied to vastly different parameters. Furthermore,

the size distributions of the particles produced in the previous study were far too great to be used as drug delivery vehicles.

In the following section, a multivariable experimental method was employed where the effects of reaction temperature, ammonia and water concentration were varied simultaneously and their resulting effect on the size of the silica particles was investigated. In contrast to single-variable techniques where only one variable is changed per experiment while all others are kept constant, multivariable techniques allow for 2 or more variables to change simultaneously. Using multivariable methods the mutual effects of the variables can be studied, as well as taking into consideration the interconnected effects of experimental conditions. This also allows for a fast and more time effective study than the full factorial or traditional uni-variant methods.

3.3.1 Experimental Theory

In the previous section, the boundary where good silica particle growth was seen for each variable was determined. These results were used to define the following experiments, dictated by the Doehlert design, required to generate an accurate ANN model. After the experiments were carried out, the results were fitted using an artificial neural network (ANN) to obtain a complete 3D map of the size changes with changing synthesis variables.

The experiments required to generate an accurate model are not decided randomly. Instead, the experiments required are based on a structurally symmetrical design which covers a large area of the 3D parameter matrix. Figure 3.17 displays the Doehlert design which required 21 experiments for this study. It is a double shell design with the inner matrix in the shape of a dodecahedron, and the outer matrix in the shape of an icosahedron. Although there

are many other experimental designs,[32-34,36,37] this design was chosen due to its high efficiency at mapping space without overlapping, lower experiments numbers required for an accurate forecast model, and its potential for sequentiality.[34,38] Each point corresponds to a unique combination of the three experimental conditions, defining the experiments required for testing in order to generate an accurate computer model.

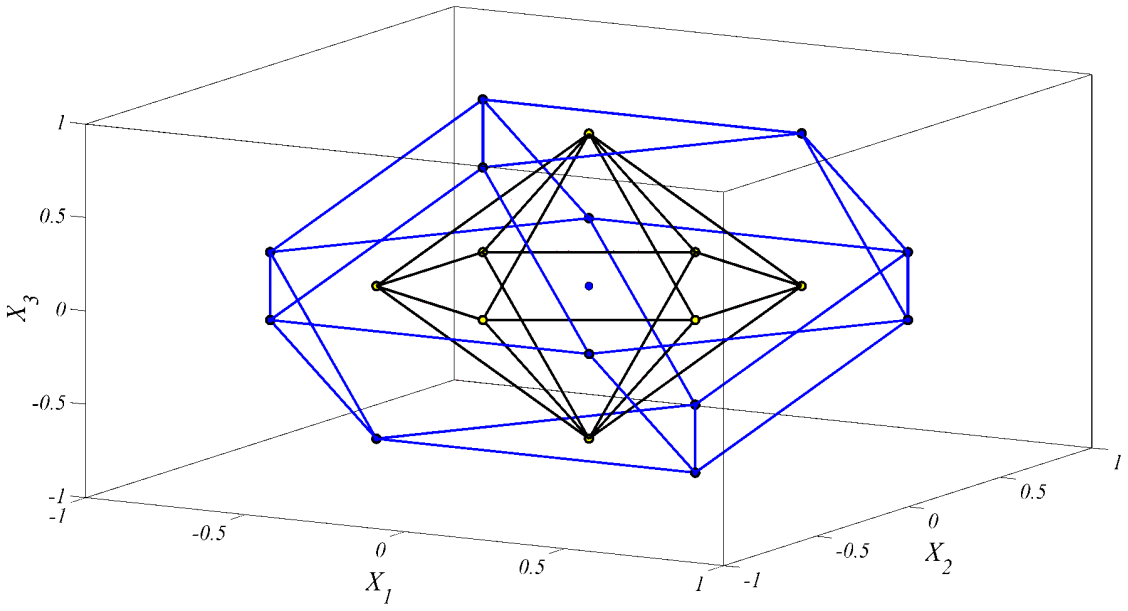

Figure 3.17: A modified version of the Doehlert design, where X_1, X_2, and X_3 represent three experimental variables. Courtesy of Ahmad E. Kandjani in our group at NBRL (NanoBiotechnology Research Laboratory)

The solid silica nanospheres were synthesized based on the same method used in the previous section of this chapter (section 3.2), with the hydrolysis of TEOS in a mixture of ethanol, ammonia and water. The Doehlert design called for 21 experiments to cover the 3D matrix required to accurately model the effects of temperature, ammonia and water concentration. Briefly, the temperature was varied from 10 – 36 ºC, ammonia content from 1.0-1.8 M, and water content from 5.1-6.5 M, however instead of changing one variable per

experiment, multiple variables were changed simultaneously. Table 3.2 describes the experiments that were performed.

Experiment No.	Temp (°C)	NH_4OH (M)	Water (M)
1	23	1.39	5.82
2	23	1.39	6.53
3	23	1.39	5.10
4	23	1.78	6.20
5	23	1.00	5.48
6	23	1.00	6.20
7	23	1.78	5.48
8	36	1.52	5.48
9	10	1.25	6.20
10	10	1.25	5.48
11	36	1.52	6.20
12	36	1.12	5.82
13	10	1.65	5.82
14	23	1.52	6.20
15	23	1.25	6.20
16	23	1.25	5.48
17	23	1.52	5.48
18	36	1.39	5.82
19	10	1.39	5.82
20	23	1.39	5.82
21	23	1.39	5.82

Table 3.2: The experimental parameters for the 21 samples required to generate the artificial neural network.

3.3.2 Particle Characterisation and Application of the Artificial Neural Network

The particles were imaged using TEM, and the 2D images were used to determine the size of the particles with image processing software developed by Ahmad E. Kandjani in our group at NBRL (NanoBiotechnology Research Laboratory), displayed in Figure 3.18.

In the first box the TEM image of the particles is shown, however, as some particles exist along the frame of the image, their size is truncated, therefore the image processing software was programed to omit these particles. The red box in the next window is required to define the boundaries within the image where the particles will be measured, where particles that are not within or touching the red box are discarded by the measuring program. The particles which have been selected for measurement by the program are displayed in the box with blue to confirm that no particles have been truncated by the border of the image. Finally the particle diameters were measured, and to ensure the particles are measured as separate entities, a circle is generated in the centre of the measured particle.

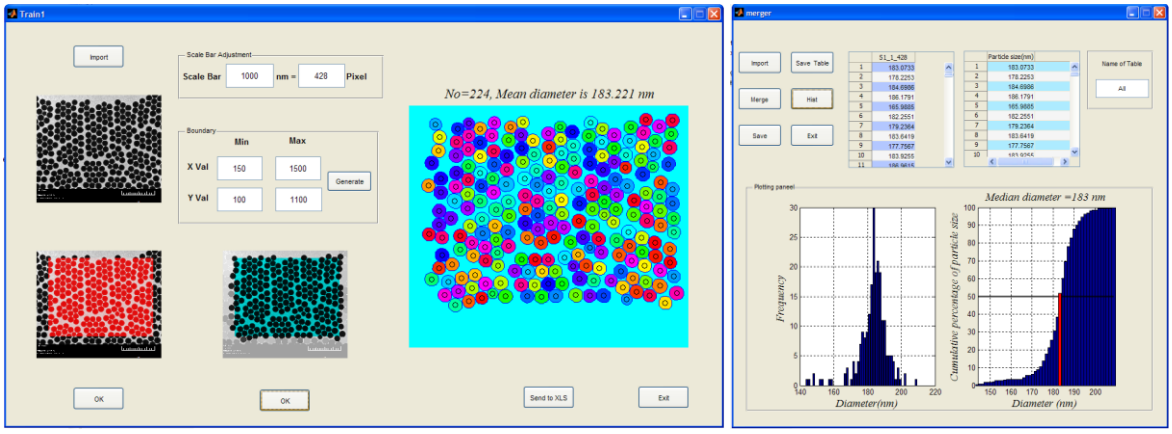

Figure 3.18: An example of the image processing software used to determine the size of the silica particles.

The data produced using this technique is then correlated to the diameter of the particles, including the mean, median and mode diameters, and the particle size range and standard deviation. The scale bar is generated by correlating the number of pixels in the image with the scale bar generated by the TEM.

3.3.3 Results and Discussion

After the measured diameters of the particles resulting from the 21 experiments were fed into the ANN network, an artificial model of the particle size with regards to temperature, ammonia and water was generated. The ANN model constructed three sets of 3-dimentional maps in which the response of two variables were plotted against one another, and between the three maps the interactions of each variable is plotted against all other variables. Information can be deciphered from these maps by observing the direction and gradient of the response slope. The direction provides information on the general trend of the parameter with regards to the particle size, while the gradient of the response describes the strength of the changing parameters influence on particle size.

Changes in the direction or gradient of the response in one plane (sections observed either horizontally or vertically of the colour charts) can give information on one variable while the other two parameters remain constant, while changes across the 3D shape of the response can offer information on the interactions occurring between the parameters. The colour charts produced can help to give a clearer indication of these changes, where quicker colour changes in one plane indicate a steeper slope, or repeated colours identify local maxima and minima in particle size.

The modelled data showed a 99% confidence in fitting, and the degree of influence of each variable was carried out using Garson method.[39] The model demonstrates the highest influence on particle size was attributed to temperature, followed by the ammonia content, and finally water.

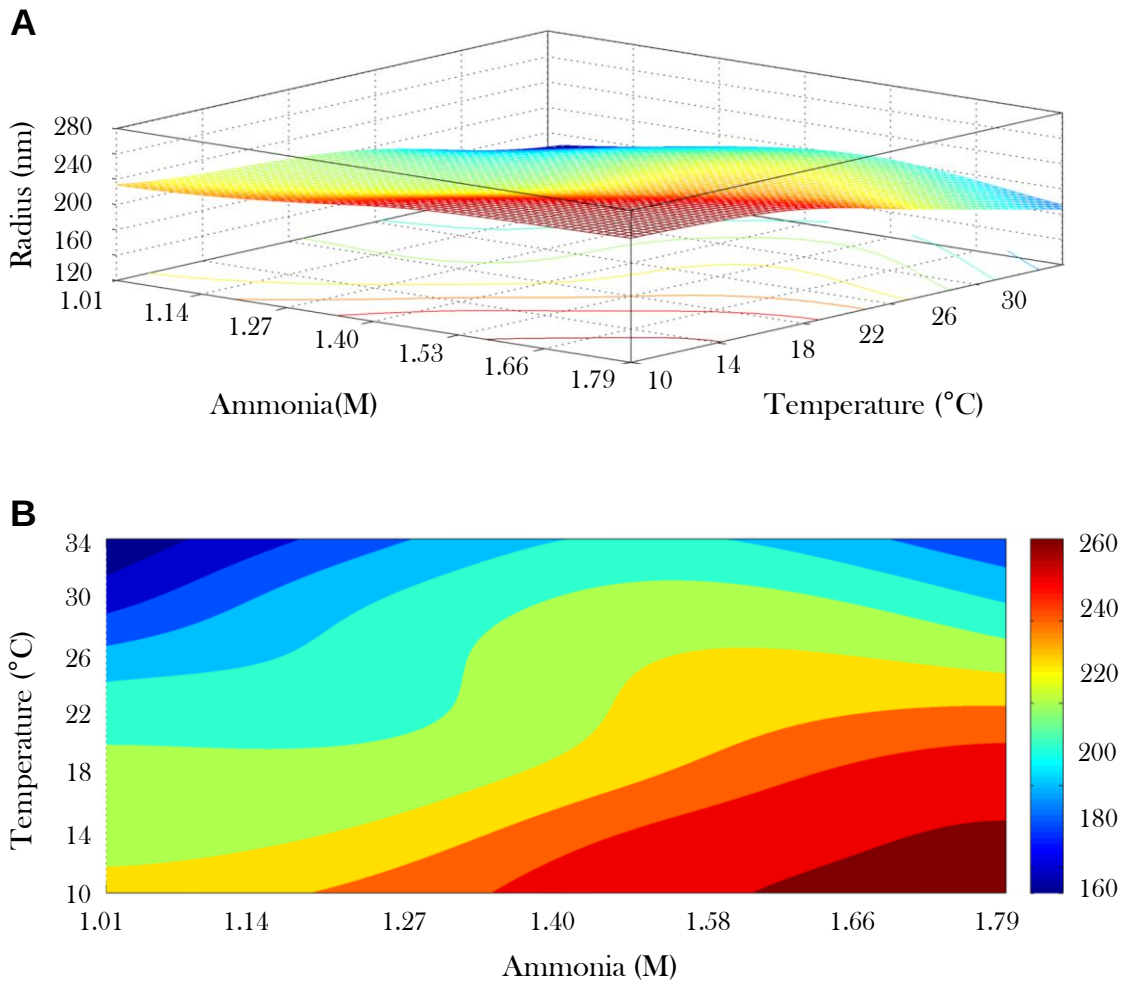

Figure 3.19: The silica particle size response compared with the variables temperature and ammonia concentration.

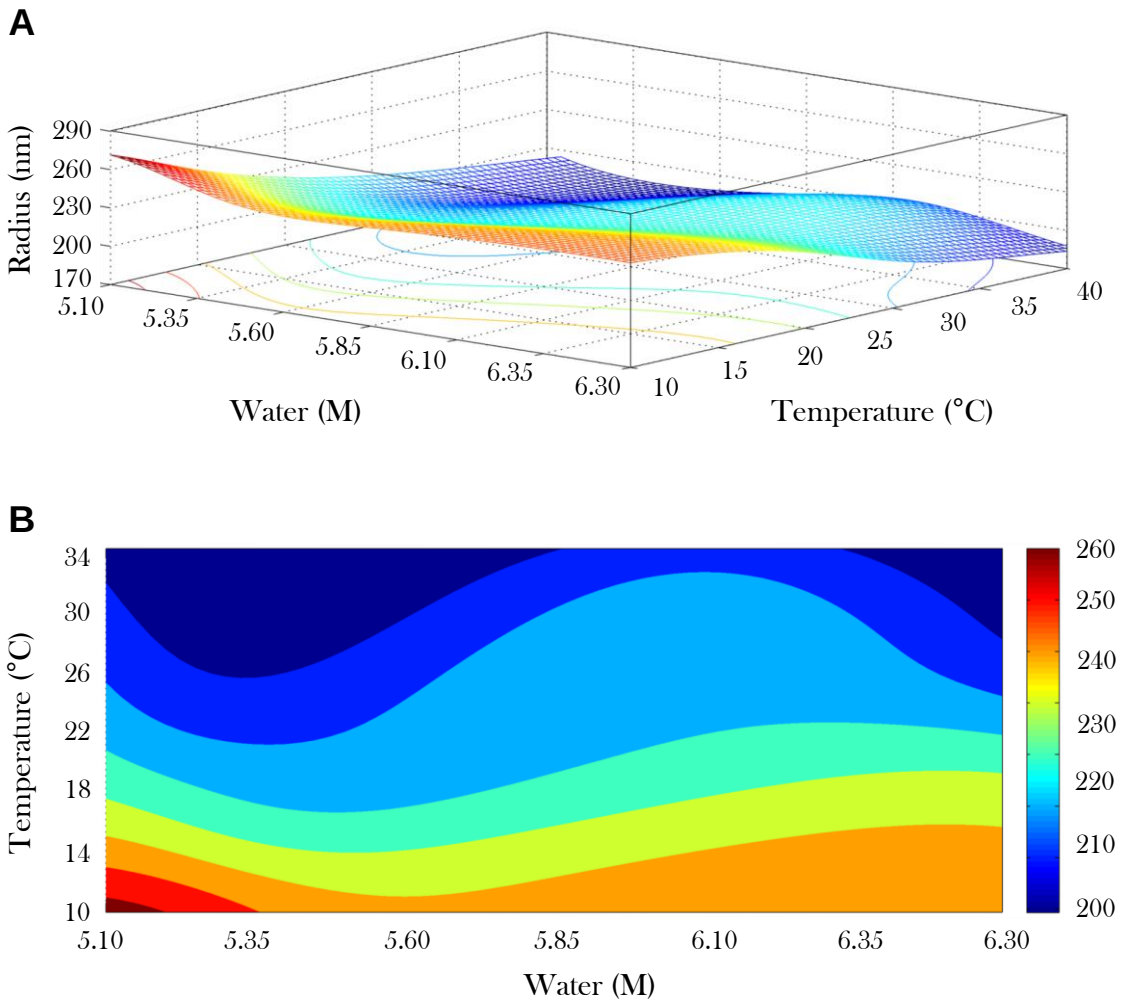

Figure 3.20: The silica particle size response compared with the variables temperature and water concentration.

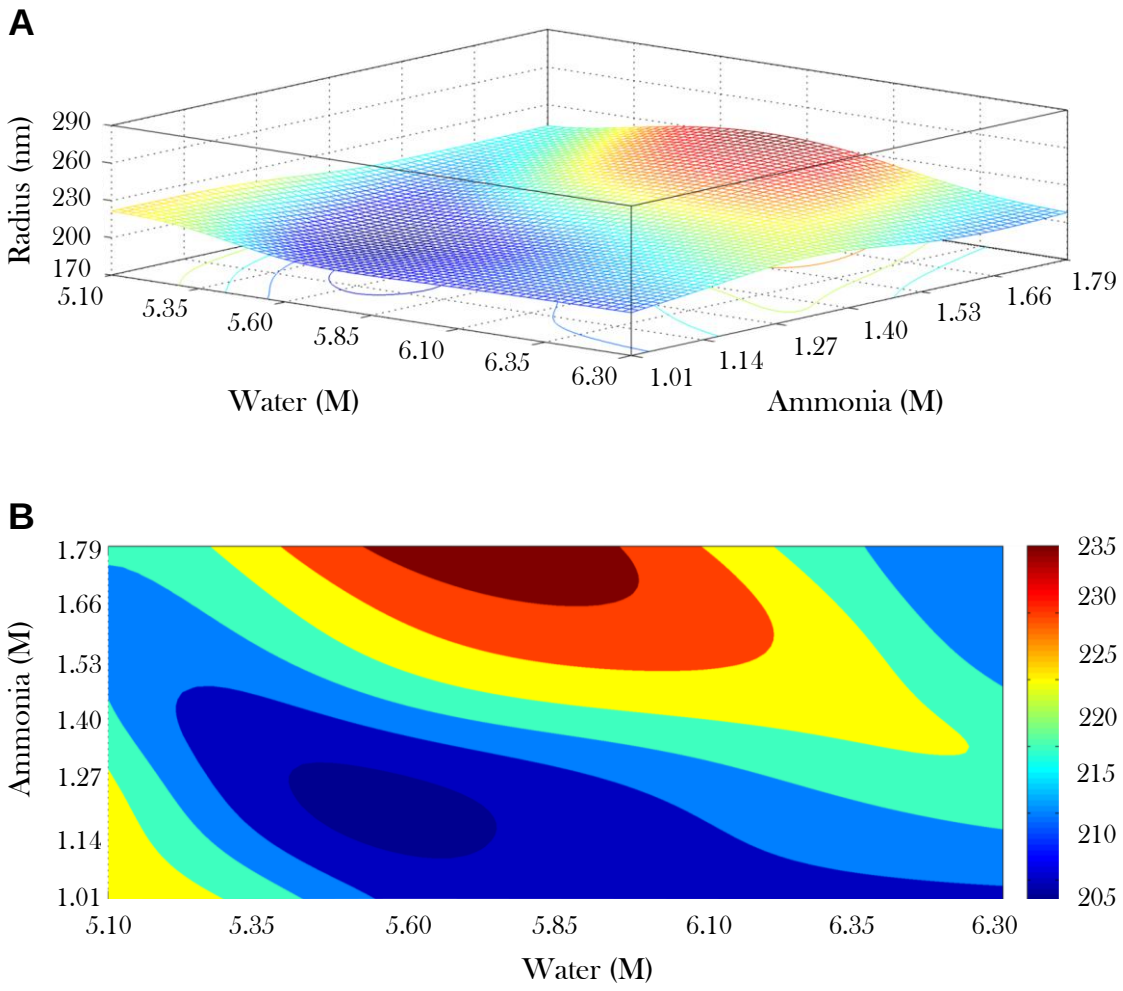

Figure 3.21: The silica particle size response compared with the variables ammonia concentration and water concentration.

3.3.3.1 Effect of Temperature on the Solid Core

Looking at the effects of temperature in Figure 3.19and Figure 3.20, there is always a gradual decrease in particle size as the temperature increases. Despite changes in the gradient of the response (looking at vertical sections moving from left to right of Figure 3.19B and Figure 3.20B), the general trend of the effect of temperature remains the same, with an inverse relationship between temperature and particles size.

Observing the effects between temperature and ammonia in Figure 3.19, it is interesting to see that at the medium ammonia concentration (~1.3 M) changes in temperature between 20 to 30 ºC seem to be less influential on the particle size. In contrast, at high ammonia concentration the temperature becomes much more influential to the particle size, and the trend in particle size is more linear, allowing for better size prediction.

When comparing the effects of temperature at different water concentrations, the particle size is a little more unpredictable. At low water concentrations, the influence of temperature on particle size is very strong, whereas at medium water concentrations temperature becomes less influential.

This demonstrates that although there is always a decrease in particle size as temperature increases, the behaviour of the response of temperature varies significantly depending on the other parameters. Consequently, the particle size cannot simply be predicted based on an inverse linear relationship between temperature and particle size. However, at either a high concentration of ammonia, or a low concentration of water, the effects of temperature are both prominent and slightly more predictable.

3.3.3.2 Effect of Ammonia on the Solid Core

The ANN model describes the influence of ammonia in Figure 3.19 and Figure 3.21 where the results display the general trend of ammonia to be proportional to the size of the particles, yet with a lesser influence when compared with the effect of temperature. When the effect of ammonia is compared to temperature in Figure 3.19, and this time the horizontal sections are analysed to represent a constant temperature, although the gradient of the response is not always constant it demonstrates a proportional relationship, where the particle size increases with concentration.

When analysing the influence of ammonia on the response map with water (Figure 3.21), the relationship is not as straight forward and different trends arise. Between the intermediate water concentrations ranging from 5.70 to 6.20 M, ammonia demonstrates a continuous increase in particle size as the concentrations is increased, however, at almost every other water concentration the response of ammonia results in dips and troughs in particle size, with no apparent trend occurring. This suggests that there must be some interaction occurring between the water and ammonia, which in turn affects the outcome of the particle size. This may indicate a point below which there are too few hydroxide ions being produced to facilitate the hydrolysis reaction at a fast rate, resulting in larger particles. In contrast, at the highest water concentration, an opposite trend occurs where a decrease in the ammonia concentration results in a dip in particle size. However, if the case of hydroxide availability was the only factor, then at a high constant of water, increases in ammonia should produce increased particle size, but as seen in Figure 3.21 the particle size dips before levelling out.

These results demonstrate that to obtain the strongest effects and greatest tunability from varying ammonia, the concentration of water must be considered, with a constant concentration of water at 5.80 M allowing for a more predictable outcome.

3.3.3.3 Effect of Water on the Solid Core

When looking at the response of water it is difficult to make a conclusion on its general trends, as it seems that both variations in temperature and ammonia concentration can result in a unique response shape and gradient. When comparing the effect of water against temperature (Figure 3.20) the particle size does not vary greatly which can be seen as a relatively flat gradient, with only one or two colour changes occurring at any constant temperature (seen as a horizontal section in Figure 3.20B). However there is no defined trend occurring, with size maxima and minima seen as dips and rises in the map. At lower temperatures the maxima and minima only span over a small size range, meaning that changes in water concentration would not result in significantly large differences in particle size. In comparison, at high temperatures the maxima and minima difference is amplified, therefore an increase in water concentration would result in a range of sizes that would appear to follow no trend.

When comparing the response of water against ammonia concentration, it becomes clear that there are not obvious trends, and that these two parameters interfere with each other parameter, which in turn influences the size of the particles. No matter what concentration the ammonia parameter is held at, the influence of water towards particle size is always fluctuating, making it very difficult to define any trends which could help in particle size

prediction. This demonstrates that the effect of water cannot be considered independently from the ammonia concentration.

From these results, it can be seen that the effect of temperature is a parameter that has the most linear relationship with particle size, making this parameter the best option for controlling the particle size in a predictable manner. This is then followed by ammonia, which although is less predictable, will typically follow the general trend of increased particle size with an increase in ammonia concentration. Lastly, water is a parameter that appears to have no single and predictable trend with regards to particle size, making this parameter one that is best kept constant when endeavouring to fabricate particles of a desired size. The effect of the solvent was unable to be investigated due to the complexity and computational power involved in a 4-varibale model in comparison to a 3 variable model.

3.3.3.4 Comparison of ANN with Single Variable Data

In this next section, ANN results produced from a single plane of the size response (where two of the three variables are kept constant) enables the comparison of the ANN particle size prediction against the single variable results of the previous sections, where one variable is changing while two of the other variables remain at either 25 ºC, ammonia concentration at 1.27 M, and water concentration at 5.66 M.

When comparing the size predictions generated from the ANN model with the data produced from the previous section, it can be seen that results are in good agreement with one another. Although the exact shape of the response with regards to the various parameters are not entirely consistent, the general trends are similar. Additionally, the size of the particles

that are predicted by the ANN are in the same range as the particles measured from the single variable experiments.

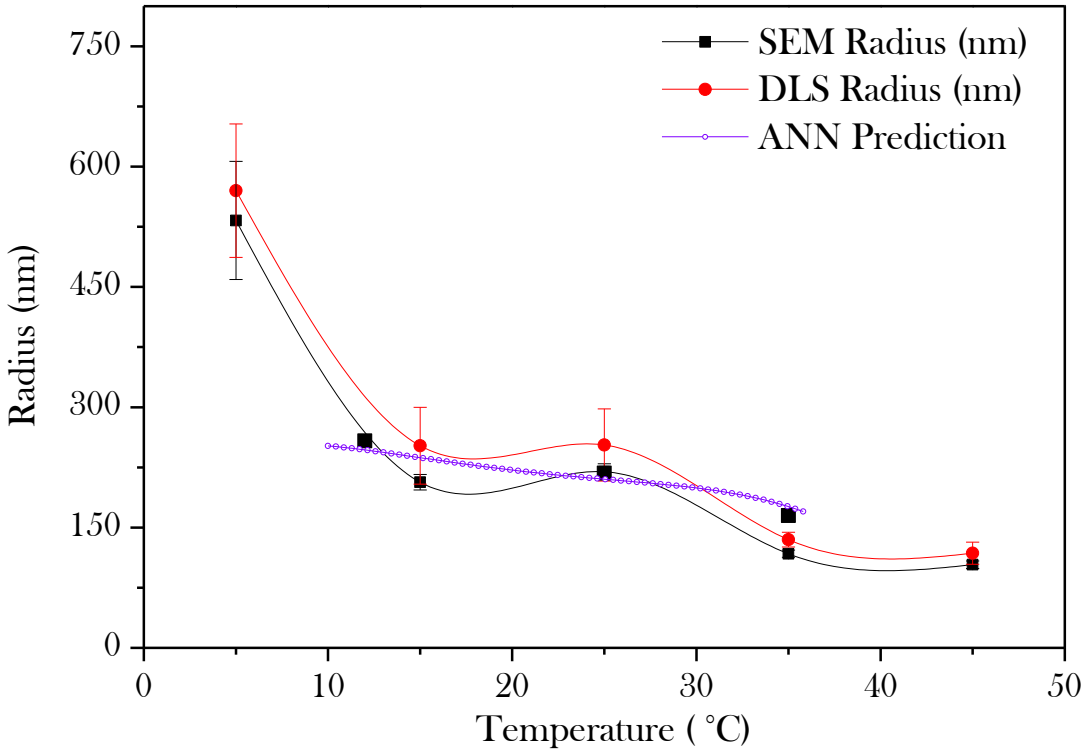

Figure 3.22: A comparison of the temperature effect between the particle sizes observed using single variable experiments and the size predicted from the ANN.

For the effect of temperature, the ANN generated the same general trend as the single variable experiment where there was a decrease in particle size as the temperature increased, however the results from the single variable experiments demonstrated a larger size range than the ANN predictions over the same temperature spectrum (Figure 3.22). The particles at 35 ºC in the previous sections were measured to be 117 nm, while the ANN model predicted a much large particle size of 176 nm. In addition, the particles that were produced at 15 ºC were also overestimated, from 206 nm in the previous section to 231 nm for the ANN result. Conversely, the intermediate particles which were fabricated at 25 ºC showed only a minor

difference in sizes from 219 nm to 210 nm for SEM and ANN, respectively. This suggests that although the ANN model may be very accurate at predicting particle size with regards to temperature in a small temperature range, at the more extreme temperatures the ANN model becomes less accurate and there is more chance of error. Furthermore, the ANN data looks more like an average trend line, and may suggest that ANN lacks accuracy in accounting for the local maxima and minima which seem to have occurred during the single variable experiment.

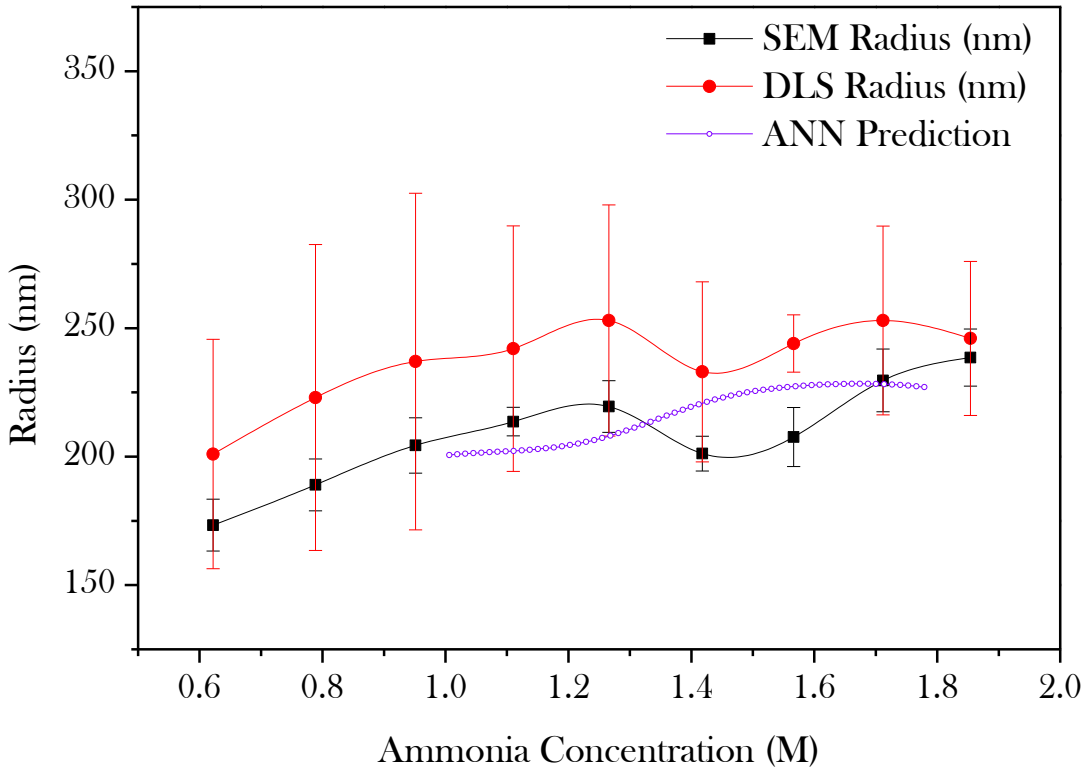

Figure 3.23: A comparison of the ammonia effect between the particle sizes observed using single variable experiments and the size predicted from the ANN.

In the single variable experiments where the ammonia concentration was altered, there was a gradual increase in size with an increase in concentration, but with a small dip in the slope at 1.4 M. In comparison, the ANN values estimated radii very close to what was

obtained in the single variable experiments, with the ANN results lying both above and below the single variable radii at various different points. However the slopes of the relationship curve was slightly different, with a slight hump at the same position where the single variable experiments demonstrated a slight dip. Nevertheless, when trend lines are fitted for both the single variable and ANN results it can be seen that the results correspond very closely for both the size values and the influence of the parameter (gradient).

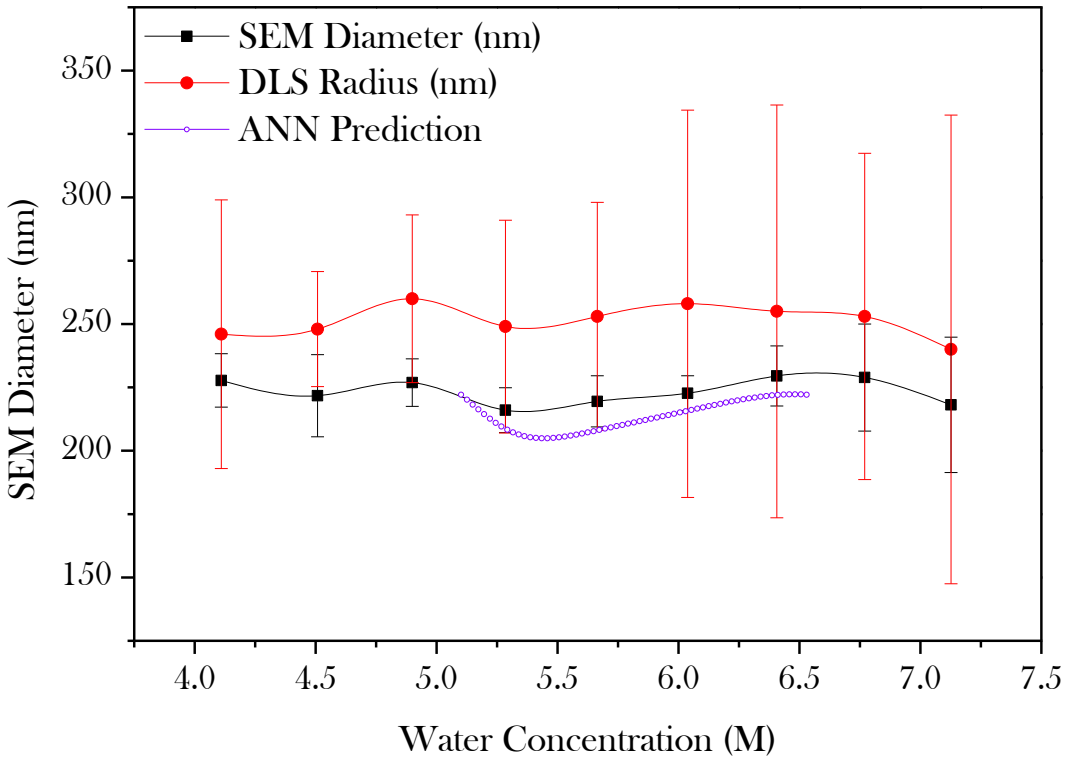

Figure 3.24: A comparison of the water effect between the particle sizes observed using single variable experiments and the size predicted from the ANN.

When comparing the ANN behaviour of water with the single-variant experiments, although there is not apparent relationship between concentration and particle size, there is a close correlation between the results, with an initial minimum which occurred in both the experimental and ANN at a water concentration of around 5.5 M. Furthermore, the gradual

increase in particle size from 5.5 – 6.5 M is in very strong agreement for both the previous data and ANN, with gradient of the slope almost identical.

3.3.4 Summary

Although numerous studies into Stöber based methods of silica synthesis have been undertaken,[7,8,18-21] the complex and unpredictable effects of the experimental parameters cannot be fully investigated through single variable techniques. However, through the fabrication of silica nanoparticles using experimental conditions dictated by the Doehlert design, a 3-dimentional virtual map of particle size with regards to the three experimental parameters temperature, ammonia and water concentration has been generated using an ANN. This approach allows for the observation of such things as; the general relationship between the particle size and the parameter, the amount of influence the parameter has on the particle size, and identifying if the parameters are mutually exclusive from one another or if they interact to further affect the particle size in unpredictable ways.

It was found that temperature had the largest influence on particles size and despite changes in the other parameters, its general effect remained the same, indicating little interference between the way in which temperature affects particle size and the way that the other parameters influence particle size. On the other hand, the effects on ammonia and water have demonstrated to disrupt one another's influence on particle size, which indicates that these parameters display dynamic interactions. Since the dissociation of ammonia is dependent on the amount of water, it is difficult to decouple their individual effects of the final particle size. These intra-parameter interferences can make particle size prediction very difficult unless both parameters are considered, therefore the 3D maps produced in ANNs are

essential for accurately predicting particle size when ammonia and water concentration are varied simultaneously.

We have also demonstrated that the model is capable of predicting particle size based on the parameters. Conversely, the model can be used to divulge the parameters required for a pre-specified particle size. Through the use of ANNs, the required number of experiments necessary for understanding the complex interactions and influences that the parameters temperature, ammonia and water have on the outcome of the silica sphere size and distribution can drastically reduce.

3.4 Conclusion

The individual effect of solvent, temperature, ammonia and water concentration on the size of the particles have been investigated using single variable experiments in order to identify general trends in areas where good particle growth was seen. This was then followed by multivariable investigations in which the experimental parameters of temperature, ammonia and water concentration were simultaneously altered, and the results were modelled using an ANN. This generated multiple 3-dimentional maps where the parameters were related to the size of the particles, allowing for the comparison of the parameter effects and interactions with one another. By employing both technique there is a better understanding of the dynamic effects of the experimental parameters, allowing for better prediction of particle size based on their parameters, or identifying the parameters required to manufacturing particles of a desired size.

3.5 References

1 Choi, H. S. *et al.* Renal clearance of quantum dots. *Nature biotechnology* **25**, 1165-1170, (2007).

2 Buzea, C., Pacheco, I. I. & Robbie, K. Nanomaterials and nanoparticles: sources and toxicity. *Biointerphases* **2**, (2007).

3 Itoh, T., Asahi, T. & Masuhara, H. Femtosecond light scattering spectroscopy of single gold nanoparticles. *Applied physics letters* **79**, 1667, (2001).

4 Johnston, A. P. R., Cortez, C., Angelatos, A. S. & Caruso, F. Layer-by-layer engineered capsules and their applications. *Current Opinion in Colloid & Interface Science* **11**, 203-209, (2006).

5 Wang, Y., Angelatos, A. S. & Caruso, F. Template Synthesis of Nanostructured Materials via Layer-by-Layer Assembly†. *Chemistry of Materials* **20**, 848-858, (2007).

6 Caruso, F. Hollow Capsule Processing through Colloidal Templating and Self-Assembly. *Chemistry - A European Journal* **6**, 413-419, (2000).

7 Stöber, W., Fink, A. & Bohn, E. Controlled growth of monodisperse silica spheres in the micron size range. *Journal of Colloid and Interface Science* **26**, 62-69, (1968).

8 Giesche, H. Synthesis of monodispersed silica powders I. Particle properties and reaction kinetics. *Journal of the European Ceramic Society* **14**, 189-204, (1994).

9 La Mer, V. K. *Industrial & Engineering Chemistry Research* **46**, 1270-1277, (1952).

10 La Mer, V. K. & Dinegar, R. H. *Journal of American Ceramic Society* **72**, 4847, (1950).

11 Capek, I. *Nanocomposite Structures and Dispersions: Science and Nanotechnology--fundamental Principles and Colloidal Particles*. Vol. 23 (Elsevier Science, 2006).

12 Reiss, H. The growth of uniform colloidal dispersions. *The Journal of Chemical Physics* **19**, 482, (1951).

13 Green, D., Jayasundara, S., Lam, Y. F. & Harris, M. Chemical reaction kinetics leading to the first Stober silica nanoparticles–NMR and SAXS investigation. *Journal of non-crystalline solids* **315**, 166-179, (2003).

14 Iler, R. *The Chemistry of Silica: Solubility, Polymerization, Colloid and Surface Properties and Biochemical of Silica*. (John Wiley & Sons, New York, NY, 1979).

15 Perry, C. C. & Keeling-Tucker, T. Biosilicification: the role of the organic matrix in structure control. *Journal of Biological Inorganic Chemistry* **5**, 537-550, (2000).

16 Icopini, G. A., Brantley, S. L. & Heaney, P. J. Kinetics of silica oligomerization and nanocolloid formation as a function of pH and ionic strength at 25 C. *Geochimica et cosmochimica acta* **69**, 293-303, (2005).

17 Brinker, C. J., Keefer, K. D., Schaefer, D. W. & Ashley, C. S. Sol-gel transition in simple silicates. *Journal of non-crystalline solids* **48**, 47-64, (1982).

18 Tan, C. G., Bowen, B. D. & Epstein, N. Production of monodisperse colloidal silica spheres: Effect of temperature. *Journal of Colloid and Interface Science* **118**, 290-293, (1987).

19 Wang, H. C., Wu, C. Y., Chung, C. C., Lai, M. H. & Chung, T. W. Analysis of parameters and interaction between parameters in preparation of uniform silicon dioxide nanoparticles using response surface methodology. *Industrial & Engineering Chemistry Research* **45**, 8043-8048, (2006).

20 Wang, X.-D. *et al.* Preparation of spherical silica particles by Stöber process with high concentration of tetra-ethyl-orthosilicate. *Journal of Colloid and Interface Science* **341**, 23-29, (2010).

21 Satoh, T., Akitaya, M., Konno, M. & Saito, S. Particle size distributions produced by hydrolysis and condensation of tetraethylorthosilicate. *Journal of chemical engineering of Japan* **30**, 759-762, (1997).

22 Green, D. L. *et al.* Size, volume fraction, and nucleation of Stober silica nanoparticles. *Journal of Colloid and Interface Science* **266**, 346-358, (2003).

23 Matsoukas, T. & Gulari, E. Dynamics of growth of silica particles from ammonia-catalyzed hydrolysis of tetra-ethyl-orthosilicate. *Journal of Colloid and Interface Science* **124**, 252-261, (1988).

24 Matsoukas, T. & Gulari, E. Monomer-addition growth with a slow initiation step: A growth model for silica particles from alkoxides. *Journal of Colloid and Interface Science* **132**, 13-21, (1989).

25 Chen, S. L., Dong, P., Yang, G. H. & Yang, J. J. Kinetics of formation of monodisperse colloidal silica particles through the hydrolysis and condensation of tetraethylorthosilicate. *Industrial & Engineering Chemistry Research* **35**, 4487-4493, (1996).

26 Bogush, G. & Zukoski IV, C. Studies of the kinetics of the precipitation of uniform silica particles through the hydrolysis and condensation of silicon alkoxides. *Journal of Colloid and Interface Science* **142**, 1-18, (1991).

27 Van Blaaderen, A., Van Geest, J. & Vrij, A. Monodisperse colloidal silica spheres from tetraalkoxysilanes: Particle formation and growth mechanism. *Journal of Colloid and Interface Science* **154**, 481-501, (1992).

28 Byers, C. H., Harris, M. T. & Williams, D. F. Controlled microcrystalline growth studies by dynamic laser-light-scattering methods. *Industrial & Engineering Chemistry Research* **26**, 1916-1923, (1987).

29 Harris, M. T., Brunson, R. R. & Byers, C. H. The base-catalyzed hydrolysis and condensation reactions of dilute and concentrated TEOS solutions. *Journal of non-crystalline solids* **121**, 397-403, (1990).

30 Napierska, D. *et al.* Size-Dependent Cytotoxicity of Monodisperse Silica Nanoparticles in Human Endothelial Cells. *Small* **5**, 846-853, (2009).

31 Van Blaaderen, A. & Vrij, A. Synthesis and characterization of colloidal model particles made from organoalkoxysilanes. *ADVANCES IN CHEMISTRY SERIES* **234**, 83-83, (1994).

32 Box, G. E. P. & Behnken, D. Some new three level designs for the study of quantitative variables. *Technometrics* **2**, 455-475, (1960).

33 Doehlert, D. H. Uniform Shell Designs. *Journal of the Royal Statistical Society. Series C (Applied Statistics)* **19**, 231-239, (1970).

34 Ferreira, S. L. C., Dos Santos, W. N. L., Quintella, C. M., Neto, B. B. & Bosque-Sendra, J. M. Doehlert matrix: a chemometric tool for analytical chemistry—review. *Talanta* **63**, 1061-1067, (2004).

35 Leparoux, M., Loher, M., Schreuders, C. & Siegmann, S. Neural network modelling of the inductively coupled RF plasma synthesis of silicon nanoparticles. *Powder Technology* **185**, 109-115, (2008).

36 Federer, W. T. Experimental design. *Experimental design.*, (1955).

37 Box, G. E. P. & Wilson, K. B. On the experimental designs for exploring response surfaces. *Ann. Math. Stat.* **13**, 1-45, (1951).

38 Esmaielzadeh Kandjani, A. *et al.* The use of artificial neural network (ANN) for modeling optical properties of hydrothermally synthesized ZnO nanoparticles designed based on Doehlert method. *Journal of optoelectronics and adavnced materials* **12**, 380-385, (2010).

39 Garson, D. & Expert, A. Vol. 6 47-51 (1991).

CHAPTER 4

COMPARISON OF TEMPLATING METHODS FOR THE SYNTHESIS OF POLYMERIC NANOCAPSULES

Since the control of size and monodispersity in drug delivery vehicles is imperative, templating approaches in capsule fabrication are becoming increasingly popular. The Layer-by-Layer approach has been used in countless studies, however, a lesser known templating approach utilising SC/MS template particles has also proven successful in establishing nano-sized polymeric capsules. Until now these two templating approaches have yet to be compared in a single comprehensive study to determine which is more advantageous for developing nanocapsules for drug delivery (DD) applications. The following chapter not only compares the nanocapsules fabricated using these two templating approaches, but also investigates the polymeric materials chitosan, poly(allylamine hydrochloride), and poly(sodium 4-styrene sulphonate) and their effects on the drug loading capability, cellular uptake and cytotoxic efficiency. It was found that the combination of the SC/MS fabrication approach with chitosan acting as the polymeric material produced nanocapsules with the most desirable properties for drug delivery applications.

4.1 Introduction

In past years there have been copious methods developed to fabricate various types of polymeric nanocapsules to be employed as drug delivery vehicles. These including emulsion techniques,[1,2] the use of high pressure sieves,[3] spray drying,[4-6] and nanoprecipitation,[7-9] with many more sub-classes within these methods.[10,11] Although these approaches produce suitable capsules for many industrial applications, they tend to lack the finer size control and narrow homogeneity required for use as drug delivery vehicles.[10,12,13] Furthermore, in techniques where the drug loading occurs during capsule synthesis, the experimental conditions can be harsh, and are not easily altered to the required conditions of the drug; therefore only robust drugs that are in accordance with these conditions can be incorporated.[10] Alternatively, the use of a template particle onto which a polymer layer is deposited, followed by subsequent removal of the template matrix, ensures the superior control over the size and homogeneity of the nanocapsules.

The most largely used template approach is the Layer-by-Layer (LbL) technique which was first adapted to the fabrication of capsules by Möhwald and Caruso *et al* in 1998, and involves the sequential layering of polymers onto a sacrificial template surface.[14-20] Another lesser used and more recently developed templating method for nanocapsule fabrication is the SC/MS template approach, developed by Wang *et al* in 2008,[21] in which polymeric material is infiltrated and cross-linked in a porous template shell. Although both these methods require a secondary stage of template dissolution, the templates allow for extremely well defined capsules with improved monodispersity and capsule wall uniformity. Furthermore, as the capsules developed from LbL and SC/MS methods are porous, drug

encapsulation can be done after capsule synthesis and in a variety of conditions, broadening the range of potentially encapsulated drugs, to include typically unstable drug of both hydrophobic and hydrophilic nature.

In LbL assembly, a smooth sacrificial particle, typically silica (similar to the particles optimised in chapter 3), can be used to sequentially deposit polymer layers onto the surface, followed by removal of the silica template to produce hollow polymer capsules.[14-20] The way in which the polymer material can be stabilized onto the surface of the template particles can be achieved through a variety of different approaches. These include using click chemistry to covalently bond each layer together,[22-24] hydrogen bonding to develop strong interactions between the hydrogen atoms of the polymer layers,[25,26] or by using electrostatic interactions which occur between oppositely charged polymer layers. Although the click chemistry and hydrogen bonding approaches are very successful, these approaches can be very complex. In contrast, the fabrication of capsules by layering oppositely charged polymers onto a template particle, and allowing the electrostatic interactions between the polymers to hold the capsule together, is relatively straight forward and cheap. Depending on the strength of the electrostatic interactions of the polyelectrolytes, this approach can be applied to any oppositely charged entities such as organic particles, inorganic particles, oligomers, multivalent ions, dyes, proteins, synthetic and natural polymers.[27] However, due to this LbL process depending on electrostatic or similar interactions,[28] the overall thickness of the polymer layer is limited to the extent of these forces, and therefore the types of polymers used and the thickness of their layers is restricted by their properties.[21] Furthermore, although possible through the exploitation of hydrogen bonding and click chemistry,[24,29] the LbL approach typically requires two polymers for the layering to occur, and hence, single

component polymer capsules can be difficult to achieve. Another drawback of the LbL process is that, although it has demonstrated to be very successful at producing micro sized capsules, there are very few reports of sub-micron capsules as aggregation becomes problematic.[30-33] Finally, one of the largest disadvantages of the LbL approach is that it is both labour-intensive and time-consuming, making it less suitable for large scale commercial applications.[19,21] Recently Zelikin *et al* has published an outstanding review on the LbL approach, highlighting some of these issues while critically looking at the approach.[34]

The employment of the SC/MS silica particles as templates for nanocapsules synthesis may offer significant advantages over the solid silica templates used in LbL techniques. Developed by Büchel *et al*,[35] SC/MS particles are solid core (SC) silica nanoparticles with an outer mesoporous shell (MS) that are fabricated in a two-step process. The first step involves the fabrication of solid silica cores using the method optimised in chapter 3, while the second step involves the growth of an outer silica shell that is riddled with mesopores. It is in the mesopores of the template shell that polymeric material can infiltrate using simple charge interactions, creating a network of overlapping polymer chains with a simple polymeric material that is subsequently cross-linked to form a robust capsule. This allows for single component capsules to be fabricated which have only been previously achieved through click chemistry and hydrogen bonding when using templates. The potential advantages of single component capsules over duel component capsules include more predicable behaviour of capsule degradation, its interaction with the body, or drug loading capacity. Both the SC/MS and Layer-by-Layer approaches to nanocapsule fabricating have been summarised in Figure 4.1 below.

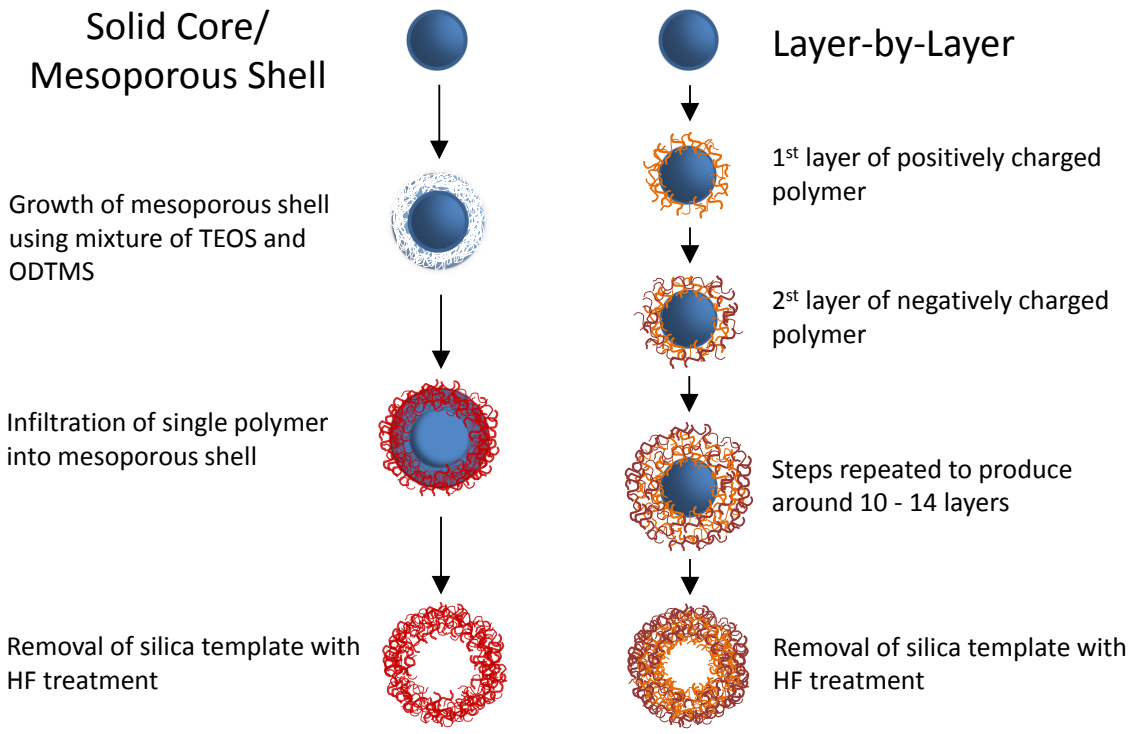

Figure 4.1: A schematic detailing the solid core/mesoporous shell and Layer-by-Layer methods of nanocapsule synthesis.

In comparison to the LbL method which has been employed in many studies over the past two decades, [14-20,34] the SC/MS method has only been reported in the literature once,[21] with the exclusion of the work carried out in the current thesis. In the previous study, Wang *et al* reported the successful fabrication of high monodispersity, single component poly(allylamine hydrochloride), (PAH); poly(L-glutamic acid), (PGA); and poly(L-lysine), (PLL), polymer nanocapsules using the SC/MS approach. Furthermore they achieved a sub-micron size range (270 nm – 400 nm) of nanocapsules which is not often achieved in LbL approaches.[34] However, this method has never been compared with the LbL technique in a single, comprehensive study.[21]

The type of polymeric materials employed in nanocapsule fabrication is also very important, especially as the polymeric material comes into direct contact with the body and the immune system when acting as a drug delivery system. Furthermore, not only can the polymer dictate the capsule's therapeutic drug loading ability, but it also affects its uptake into cells and its efficiency to induce cytotoxicity. The polymers poly(allylamine hydrochloride) (PAH), and poly(sodium 4-styrene sulphonate) (PSS) were chosen in the following investigations due to their extensive employment in previous LbL studies,[36-39] allowing for a comparison of the capsules fabricated herein with previous studies. Moreover, the two polymers both have strong electrostatic charges, with PAH acting as a cationic polymer due to the presence of amine functional groups and PSS acting as an anion owing to the presence of a sulphonate group, making them ideal for the layer-by-layer approach. Chitosan was chosen due to its proven biocompatible and biodegradable nature. With the chemical structure [Poly-(1,4) 2-amino-2-deoxy-β-D-glucan], chitosan is also a positively charged molecule, however it is not as cationic as PAH.[40]

4.1.1 Rationale

To our knowledge there have been no studies which have directly compared the Layer-by-Layer method of capsule fabrication against the lesser known SC/MS method. Furthermore, although the Layer-by-Layer approach has been extensively employed in the literature, the capsules fabricated are usually reported to be in the micron size range, with very few reports of capsules below 500 nm.[34] In the following chapter, nanocapsules of ca. 300 nm have been synthesised by employing both the SC/MS and LbL methods, and the polymers chitosan, PAH and PSS. The effects of capsule aggregation, polymer loading, drug loading, cellular uptake and cytotoxicity of all systems were compared in an effort to identify the most

advantageous fabrication method and polymer material for drug delivery applications which would warrant further investigation.

4.2 Experimental Section

4.2.1 Fabrication of the SC/MS silica template particles

The SC/MS silica template particles were fabricated through a two stage process. In the first stage, solid core (SC) silica nanoparticles of ca. 300 nm were fabricated based on the method optimised in chapter 3. This was achieved by the mixing of 1 mL of absolute ethanol, 135 µL of deionized (MilliQ) water, and 113 µL of ammonia solution (28 %) in a 1.5 mL eppendorf tube, and heating the mixture to 25 ºC. Next 75 µL of tetraethoxysilane (TEOS) was added to the solution which was then mixed for 4 seconds. The solution was then kept very still and held at 25 ºC for one hour while the particles formed.

In the second stage, an outer shell of ca. 40-50 nm with mesopores throughout is grown onto the solid core particles to produce the solid core/mesoporous shell (SC/MS) template. To achieve this, 65 µL of additional TEOS and 13 µL of n-octadecyltrimethoxysilane (ODTMS) was mixed in a fresh 1.5 mL eppendorf tube, and the content was slowly added, drop-by-drop, to the solid core solution over a period of 20 min at 25 °C under shaking conditions. After all the TEOS/OTMS solution was depleted, the particles were left to incubate for an additional hour under shaking conditions. Finally, the formed SC/MS particles were washed thrice with ethanol, and the powder was obtained by drying in an oven at 70 ºC, followed by a period of 6 h in a furnace at 550 ºC in air to remove the porogen ODTMS through calcination.

4.2.2 Fabrication of the solid silica template particles

The solid core silica template particles were fabricated in the same manner as the solid cores of the SC/MS particles. However, in order to keep the LbL template particles of roughly the same size as the SC/MS particles which not only have a solid core but also an outer shell, the smooth particles for LbL were fabricated to be as close to 350 nm as possible. To achieve this, of 1 mL of absolute ethanol, 135 µL of deionized (MilliQ) water, and 113 µL of ammonia solution (28 %) was again mixed in a 1.5 mL eppendof tube, and heating the solution to 22 °C as opposed to the 25 °C employed in the SC/MS synthesis. Again 75 µL of TEOS was added and mixed for 4 seconds before incubation for 1 h, however for the LbL template particles there is no additional stage of shell growth. After incubation the particles were washed thrice with ethanol, and dried at 70 ºC to obtain the particles in powder form.

The SC/MS and LbL silica templates were imaged by scanning and transmission electron microscopy (SEM and TEM). The particle size and distribution was determined using SEM where a minimum of 100 particles were measured for accuracy.

4.2.3 Fabrication of Chitosan and PAH Nanocapsules Using the SC/MS Templating Approach

The chitosan and (PAH) nanocapsules were both fabricated using (SC/MS) silica nanoparticles as templates, where the polymer is dissolved before being allowed to infuse into the pores of the outer template shell. Afterward, the infiltrated polymer, either chitosan or PAH, is cross-linked with glutaric dialdehyde to form a dense, interconnected network of material. Finally the template is removed to generate the SC/MS-chitosan or SC/MS-PAH capsule.

The polymer solutions were prepared separately, with the chitosan polymer stock solution containing 4 mg of low molecular weight chitosan that was dissolved in 1 mL of pH 7.2 phosphate buffer saline (PBS 0.02 M) along with 0.8% acetic acid. The PAH stock was prepared by dissolving 2.5 mg of PAH in 1 mL of pH 8.5 Borate buffer (0.025 M). For the processing of the SC/MS template particles prior to use, 5 mg of particles was weighed into a 1.5 mL eppendorf tube, and washed thoroughly with both ethanol and deionised water, before being redispersed in 450 µL of deionised water. The template particles were then mixed with either 1 mL of chitosan or PAH stock solution, and allowed to incubate together overnight on a rotary shaker.

After the appropriate polymer was allowed to infuse into the mesoporous shell of the SC/MS particles, any excess chitosan or PAH was removed by separating the SC/MS particles with infiltrated polymer through centrifugation (6 rpm for 5 minute), followed by discarding the supernatant. The remaining infiltrated particles were redispersed (without sonication) in 800 µL PBS before adding 20 µL of glutaric dialdehyde (25% w/v) to cross-link the polymeric material within the mesoporous shell. The solution was then incubated for a further 2 hours on a rotary shaker. The cross-linked SC/MS-chitosan or SC/MS-PAH particles were washed three times with deionized water, followed by removal of the SC/MS silica templates with hydrofluoric acid (2M) in an ammonium hydroxide buffer (8M). (Warning: hydrofluoric acid is highly corrosive, and extreme care should be taken while handling hydrofluoric acid). The capsules were washed repetitively with deionised water to remove all hydrofluoric acid, and the polymer nanocapsules obtained were stored in water.

4.2.4 Fabrication of PAH/PSS Nanocapsules Using the Layer-by-Layer Approach

PAH/PSS nanocapsules were fabricated using the layer-by-layer (LbL) technique, whereby solid silica template particles were incubated with alternating solutions of dissolved polymer. This enabled the build-up of layers of opposite charged PAH and PSS polymers onto the surface of the template. The PAH stock solutions was made with 2.5 mg mL^{-1} of PAH dissolved in borate buffer (0.025 M) and the pH was adjusted to 8.5 with 0.01M sodium hydroxide. For the PSS stock solution, 2.5 mg mL^{-1} of PSS polymer was dissolved in potassium hydrogen phosphate (0.01 M) and the pH adjusted to 6.5 with 0.1 M hydrochloric acid. After washing 10 mg of LbL template particles thrice each with ethanol and deionised water, the templates were allowed to incubate with the polymer solutions, starting with 2 mL of the positively charged PAH solution. After 30 minutes of incubation time the particles were centrifuged and the supernatant removed to discard any excess, un-adsorbed polymer. The particles were then washed once with pH 8.5 buffer solution which did not contain any dissolved polymer. After removing the pH 8.5 buffer solution, the same process was repeated with the PSS polymer layer, where 2 mL of PSS stock solution was added and allowed to incubate for 30 minutes. After incubation the particles were washed once with pH 6.5 buffer solution to remove any excess PSS. These steps were repeated multiple times until the particles were incubated with each polymer stock solution 5 times, ending in a final incubation with PSS.

Finally, half the solution was removed and washed after the 10^{th} incubation step with PSS, while the other half underwent an additional incubation with PAH stock solution. This lead to half the particles possessing a final layer of PSS (LbL-PSS), i.e. $(PAH/PSS)_5$, and half

the material possessed a final layer of PAH (LbL-PAH), i.e. $(PAH/PSS)_5PAH$. Both particles were then washed thrice with deionised water. The nanocapsules were obtained by the same hydrofluoric acid treatment to remove the silica template as used in the previous section. This was followed by centrifugation (7 rpm for 5 minute) and repetitive washing of the remaining and intact capsules with deionized water.

All the nanocapsules were imaged using TEM and the weight of polymeric material per capsule was obtained by by Thermogravimetric analysis (TGA) using Perkin Elmer Pyris 1 TGA instrument.

4.2.5 Curcumin Loading into the Chitosan Nanocapsules

The capsules were loaded with the lipophilic drug mixture of curcumin dissolved in oleic acid using a method similar to the previously demonstrated for the loading of lipophilic chemotherapeutic drugs doxorubicin and 5-fluorouracil into poly(methacrylic acid) capsules.[41] Briefly, the capsules were first dehydrated with ethanol to ensure no water was present in the capsule interior. The capsules were then incubated with a curcumin/oleic acid solution (10 µg curcumin per mL of oleic acid), and the oil mixture was allowed to infiltrate through the porous walls of the capsules for 12 hours. Following incubation, the capsules were washed with hexane to remove any non-infiltrated curcumin/oleic acid and any residual hexane was allowed to evaporate. A portion of the capsules were then used to determine the drug loading capacity by redispersing in ethanol to release the internalised curcumin mixture, followed by quantifying the amount of curcumin released by making standard curves using a Cary 50 Bio UV-Vis spectrophotometer at the absorbance maxima of curcumin at 430 nm.

4.2.6 Cellular Uptake and Cytotoxicity of Curcumin-loaded Nanocapsules

MCF-7 cells were employed to study cytotoxicity and the cellular uptake of the four different types of polymeric capsules. The human breast cancer cell line (MCF-7) was obtained from American Type Culture collection and maintained in DMEM medium (Life technologies) supplemented with 10% Foetal bovine serum (Thermofisher Scientific). The culture was maintained at 5 % CO2 in a humidified incubator at 37°C.

For cellular uptake studies, 50,000 cells were seeded on a glass coverslip overnight, followed by exposure to 2 x 10^9 capsules in 2 ml media, and incubated for 24 hours. The coverslips were washed with phosphate buffer saline (PBS) and fixed with paraformaldehyde (3.7%) for 10 minutes. The coverslips were then washed again with PBS and mounted onto fresh slides along with Prolong Gold Antifade medium containing DAPI. Imaging of the coverslips was done using confocal microscope (CLSM; Nikon Confocal Microscope). As glutaraldehyde was used to cross-link both the SC/MS-chitosan and SC/MS-PAH capsules, these particles were highly fluorescent and therefore immuno-labelling was not required, however the LbL capsules did not fluoresce. For this reason all confocal images were taken with capsules that were infiltrated with curcumin which fluoresces at 490 nm.

To study the cytotoxic efficiency of the four types of capsules, 20,000 cells were exposed to increasing concentrations of pristine (curcumin free) and loaded (curcumin-infiltrated) capsules. The concentration of capsules ranged from 1 x 10^7 – 125 x 10^7 capsules per well and were incubated for 24 hours in 96-well plates under appropriate growth conditions as explained in the previous section. The cell viability was measured using a soluble tetrazolium-based colorimetric assay (Promega MTS CellTiter 96® aqueous kit) and

the absorbance measured at 490 nm using a microplate reader (Perkin Elmer, USA). To compare against the cytotoxicity of uncapsulated, free curcumin, increasing concentrations of curcumin dispersed in water was also tested. Each treatment was performed in triplicate and the data average was taken, with standard error of mean shown as error bars.

4.3 Results and Discussion

In the following section, four different nanocapsules have been synthesised and tested for their therapeutic efficiency as drug delivery systems. Two of the capsule types were fabricated using the solid core/mesoporous shell (SC/MS) method, where one set was single component, cross-linked chitosan capsules (denoted as SC/MS-chitosan), and the other set was single component, cross-linked PAH capsules (denoted as SC/MS-PAH). The next two capsule types were fabricated using the Layer-by-Layer (LbL) approach, where both capsules were composed of a combination of poly(allylamine hydrochloride) and poly(sodium 4-styrene sulphonate), or PAH/PSS, however the capsules were terminated on either a PSS layer (LbL-PSS), or a PAH layer (LbL-PAH).

4.3.1 Template characterisation

After fabrication of the SC/MS and LbL template particles through the hydrolysis and condensation of TEOS which was optimised in chapter 3, their size and distribution was determined using SEM. (For the SC/MS templates, the size and distribution was measured both before and after growth of the mesoporous shell, while the LbL template particles only needed to be measured once, because the LbL templates didn't contain a mesoporous shell).

The solid core of the SC/MS particles were found to be 290 ± 24 nm in diameter, with an outer mesoporous shell of 46 ± 7 nm in thickness. When combined, the overall size of the SC/MS particles came to 382 ± 38 nm. After the calcination and removal of porogen ODTMS, the mesopores were measured with BET surface analysis and found to be 3.68 nm in diameter. In contrast, the LbL templates were fabricated to 348 ± 28 nm, and due to the lack of pores on the surface of the particles as can be seen in Figure 4.2D, BET was not required.

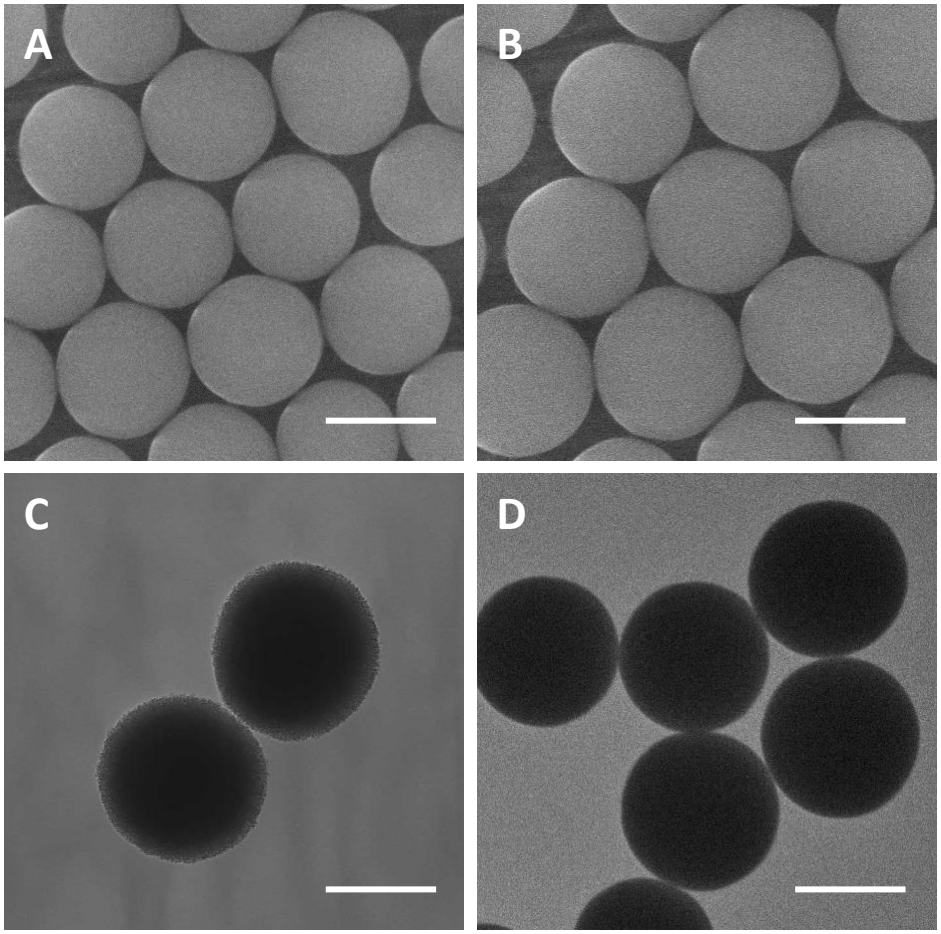

Figure 4.2: SEM (A and B) and TEM (C and D) images of the template particles, where (A) is the solid core particles of the SC/MS template, (C) is the solid core with mesoporous shell of the SC/MS templates, and (B and D)) are solid core silica particles of the LbL templates.

4.3.2 Characterisation of the Nanocapsules

TEM imaging was performed on the fabricated nanocapsules after removal of the SC/MS silica template and is displayed in Figure 4.3. The main difference that can be seen from the images is the amount of aggregation occurring, with capsules made via the LbL method showing more aggregation that those made using the SC/MS technique. Although capsules fabricated via the layer by layer method have been shown to have good monodispersity in previous literature, these capsules are usually in the micron range, with very few successful capsules reported below 500 nm.[34] At sub-micron ranges aggregation it thought to becomes more problematic as a result of stronger interparticle. Unlike the SC/MS approach where the bulk of the polymeric material resides within the mesoporous silica shell, the polymeric material is entirely on the surface in the LbL approach, providing more opportunity for interparticle interactions. This may indicate that although LbL capsules can be very successfully fabricated in the micron range, when approaching the sub-micron range, monodispersed and uniform capsules are very difficult to achieve.

At further observation, the chitosan and PAH capsules fabricated by the SC/MS approach appear relatively thicker, with a more robust and uniform shell, in comparison with the capsules made using the LbL technique. However, to confirm and quantify the weight of polymeric material present, either infiltrated into or absorbed onto the template particles, thermogravimetric analysis (TGA) was performed. Shown in Table 4.1, TGA demonstrated that the PAH and chitosan capsules made using the SC/MS method showed the largest and second largest amount of polymer loading, respectively. In contrast, both capsules made using the LbL approach demonstrated a lower amount of polymer absorbing onto the template

surface. The difference in the amount of polymer loading between these methods is not unexpected due to the extensive differences in the mode of polymer material attachment.

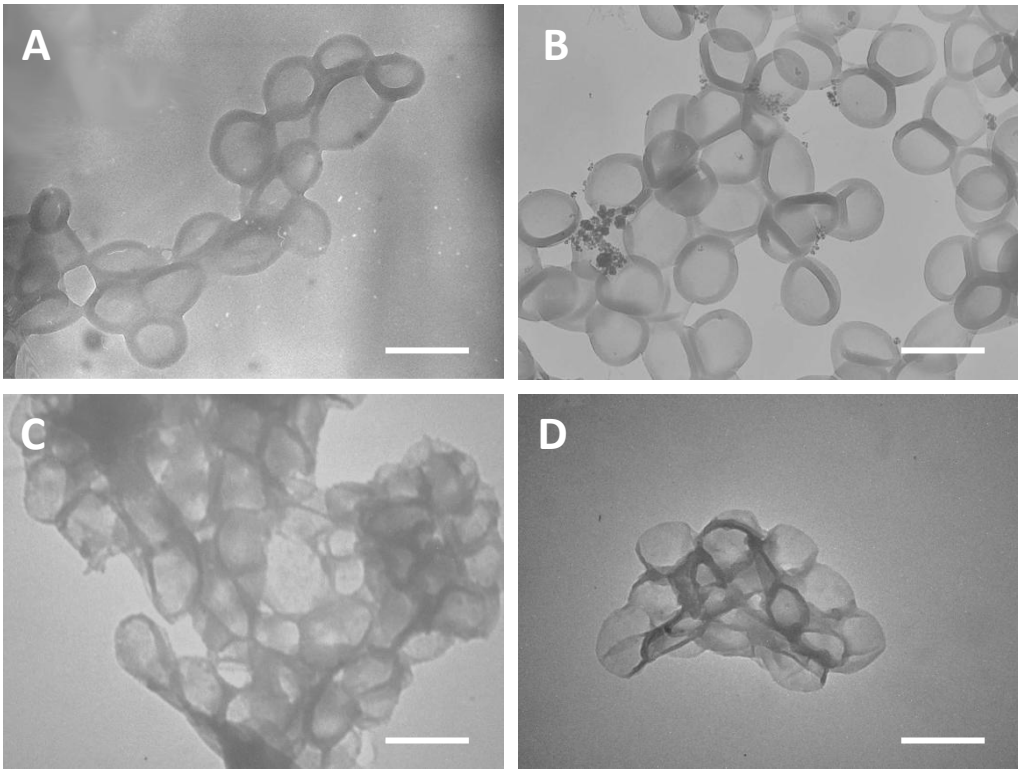

Figure 4.3: TEM images of the fabricated nanocapsules (A) SC/MS-chitosan, (B) SC/MS-PAH, (C) LbL-PSS, and (D) LbL-PAH. All scales bars correspond to 500 nm.

Capsule	% Weight at 110 °C	% Weight at 600 °C	% Weight Loss	Weight of Polymer (mg/g template)
SC/MS-Chitosan	87.94	79.92	8.03	87.26
SC/MS-PAH	90.50	81.19	9.31	102.60
LbL-PSS	89.30	83.15	6.15	65.53
LbL-PAH	92.55	86.60	5.95	63.28

Table 4.1: Thermogravimetic analysis data of the capsule weight

The polymer material in the SC/MS method drives itself into the oppositely charged pores riddled throughout the outer shell of the template. In this method the polymer loading

step is only preformed once, yet through electrostatic attraction between the negatively charged silica and the positively charged polymer (either chitosan or PAH) a substantial amount of polymer embeds itself within the pores of the template shell, as well as a small amount onto the particle surface. Within these walls some of the pores containing individual polymer chains come into contact with one another, and during the cross-linking stage these chains are bonded together to give additional strength to the structure and reducing any desorption of polymeric material.

Unlike the SC/MS method, the layer-by-layer method takes advantage of oppositely charged polymers. The polymers absorb onto a smooth template particle, immediately reducing their loading ability to the surface of the particle rather than the high surface area of a mesoporous shell. Once there is a build-up of one charge on the surface due to the polymer, no more of that polymer will absorb. Through multiple steps of alternating between differently charged polymers, a build-up of many layers is achieved. Unfortunately for this method to achieve the same capsule wall thickness achieved by the SC/MS approach, many incubation and washing steps need to be performed, which are very time consuming and laborious. For instance, if each polymer layer deposition step during LbL process typically leads to ~2 nm thick layer,[14,17,42] it will require 15-30 LbL steps to obtain capsules of the same thickness as obtained by the SC/MS method in a single step. The LbL capsules presented here underwent 10 and 11 polymer layers, yet remained much thinner than the capsules fabricated in one step via SC/MS templates.

The difference between the modes of polymer adhesion between these techniques can help to explain the significant variation in the polymer loadings. Although in some drug

delivery applications where polymeric nanocapsules are employed, a thin walled vessel may be required, it is usually the robust yet porous vehicles which are essential. It is more often required that the vehicles possess thick capsule walls to prevent rupture or degradation, and consequently, preventing premature loss of encapsulated drug during transportation. Therefore, capsules synthesised through the SC/MS template approach already demonstrate greater promise over the LbL approach in fabricating robust and thick walled capsules due to reduced aggregation and an increased amount of polymeric loaded in a single step. Furthermore, as the capsules made via SC/MS also undergo a stage of polymeric cross-linking, the formed bonds induce additional strength to the capsule structure that is not present in those made via non-crosslinked LbL methods.

4.3.3 Quantification of Curcumin Loading

An important property of a drug delivery system is the amount of drug that can be loaded per carrier. As such, the drug loading capacity of the capsules was investigated, and the influence of the fabrication method and the polymeric material was compared. This was achieved by loading of a hydrophobic anti-cancerous drug curcumin into the capsules, and the weight per capsule quantified. To compare this and other characteristics between capsule types, the number of capsules present in the following investigations was kept constant. This method of quantification has been outlined in the Appendix and was calculated based on the assumption that each template particle resulted in a capsule. Due to this assumption it should be noted that there is potential for significant error, however as this method was the only available means of quantification, we believe this assumption is acceptable.

Curcumin was used as a model lipophilic drug due to its well-established anti-cancerous properties, while oleic acid was employed as the oil phase as it has been FDA-approved. Another reason why curcumin was chosen as a model drug was that curcumin is well-known to degrade in an aqueous environment,[43] and therefore curcumin stabilized in a hydrophobic oleic acid phase within the cavity of the capsules provides a unique opportunity to study its drug efficiency during its stable and active form.

Briefly, curcumin was first dissolved in oleic acid which acts as the oil phase, the nanocapsules were then allowed to incubate and be infused with a curcumin/oleic acid mixture overnight. After infiltration, all un-encapsulated mixture was removed through multiple hexane washes, before the remaining (encapsulated) curcumin/oleic acid mixture was dehydrated from the capsules with ethanol and detected using UV-vis spectroscopy. The curcumin detected was quantified against the standard curve displayed in (Figure 4.4).

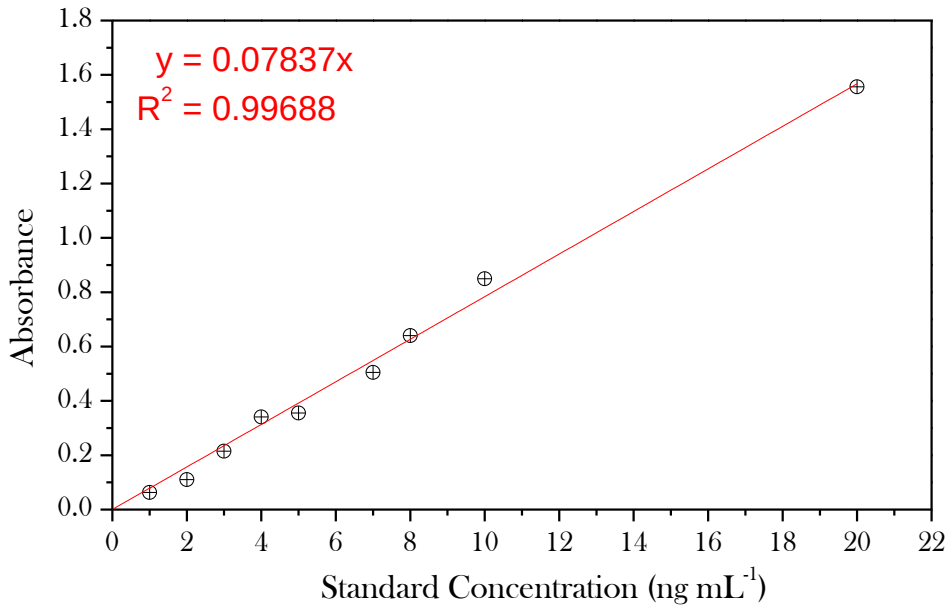

Figure 4.4: The linear absorbance curve plotted from standard curcumin concentrations.

From the viewpoint of drug loading capability, it can be seen in Figure 4.5 that there appears to be no obvious advantage in using either the SC/MS or the LbL method, with the SC/MS method demonstrating both the highest and lowest loading capacity per capsule (depending on the polymer), while the LbL approach displays an intermediate capacity. The SC/MS-chitosan capsules demonstrate the greatest drug encapsulation, followed closely by the LbL-PSS capsules, and then to a lesser extent LbL-PAH and SC/MS-PAH, respectively. It is likely that the loading is dependent on several factors which include the structural characteristic of the capsules such as the capsule size and wall thickness, in addition to the polymer material employed which may exhibit differences in drug binding.

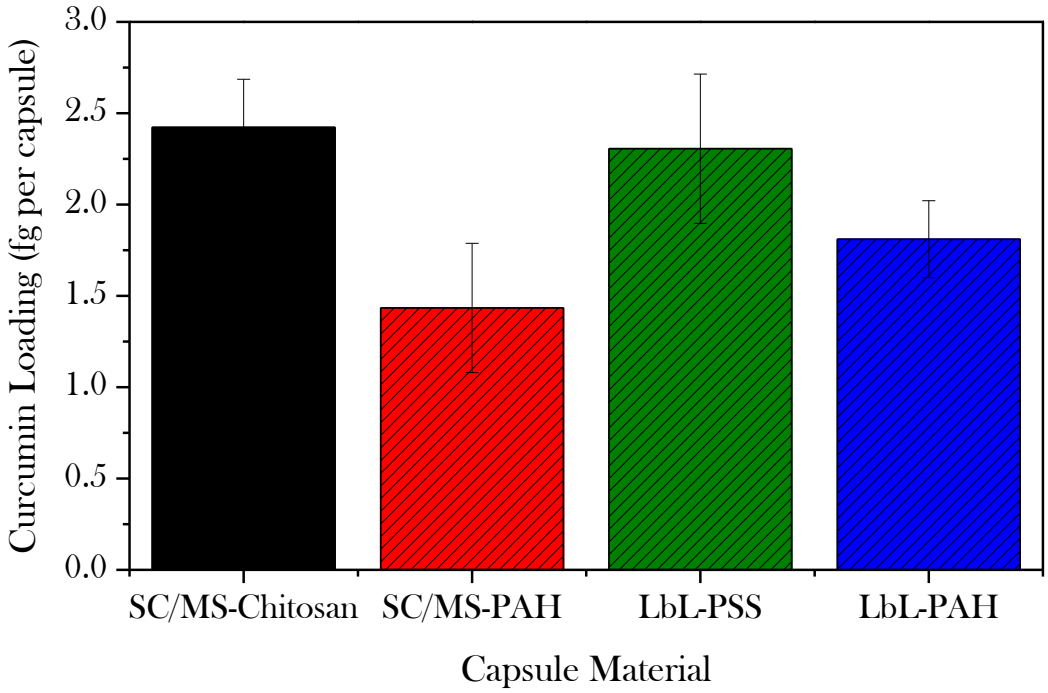

Figure 4.5: The curcumin loading capacity of the different capsules types.

4.3.4 Cellular Uptake of Curcumin-Loaded Nanocapsules

The four different capsules fabricated through two dissimilar methods and comprising of three different polymers, were tested for both their cellular uptake and cytotoxic behaviour to evaluate their ability as drug delivery vehicles against MCF-7 breast cancer cells. To ensure cellular uptake was occurring, curcumin-loaded capsules were incubated with the MCF-7 cells overnight, followed by confocal imaging, with the results displayed in Figure 4.6. Curcumin-loaded capsules were chosen for confocal images as curcumin is fluorescent, negating the need to add fluorescent tags to the capsules.

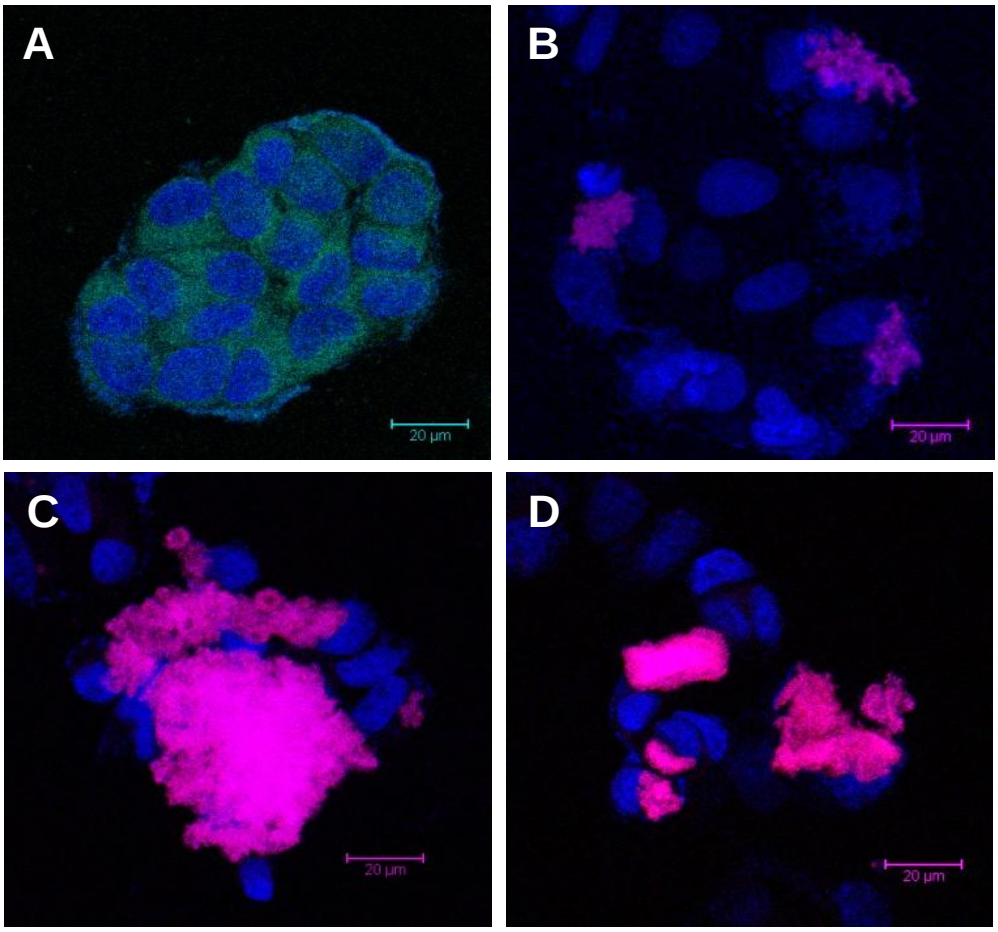

Figure 4.6: Confocal images of MCF-7 breast cancer cells incubated for 24 hours with (A) SC/MS-chitosan, (B) SC/MS-PAH, (C) LbL-PSS, and (D) LbL-PAH.

Although the most fluorescence is occurring in both confocal images with the LbL capsules (Figure 4.6, C and D), the capsules do not appear to have infiltrated the cells. Instead, the high intensity of the fluorescence is caused by the aggregation of the capsules above and around the cells. When looking at the LbL-PSS capsules, they have undergone the largest amount of aggregation, and although it is difficult to confirm that very little engulfment has occurred, the size of one of the aggregated masses is so large (~50 μm) that is would likely deter any take up by the smaller cells (~15 μm).

In contrast, the SC/MS capsules are not nearly as aggregated, and more cell uptake can be observed. Looking at Figure 4.6A, it is clearly evident that the SC/MS-chitosan capsules are being taken up by the cells the most readily, with fluorescence clearly visible from the cytoplasm within the cells. It is likely that the cells are able to engulf the capsules through endocytosis.[44] This would also have been aided by the reduced amount of aggregation by the particles, preventing them from agglomerating into masses above which the cells would be unable to internalise. Furthermore, chitosan is a positively charged material which would assist in the uptake across the negatively charged cellular membrane.

The SC/MS-PAH capsules appear to be the next most engulfed capsules. Although these capsules do not demonstrate a large amount of fluorescence, this is in part due to the lower amount of curcumin per carrier. From the fluorescence which is occurring, it appears to be originating from within the cells. Like the SC/MS-chitosan capsules, SC/MS-PAH has also refrained from undergoing large amounts of aggregations, allowing for better engulfment by the cells.

4.3.5 Cytotoxicity of Curcumin-loaded Nanocapsules

The cytotoxicity of the pristine (empty) and curcumin-loaded capsules was determined against MCF-7 breast cancer cells by incubating the cells with increasing concentrations of capsules and observing the cell viability as a percentage after 24 hours. Using the number of capsules present at each concentration, along with the calculated amount of drug present per capsule, the dosage of curcumin per cell was also calculated to allow for a clear comparison of the cytotoxic efficiency with regard to capsule type. The effect of the capsule fabrication method and polymer material was investigated, and the most effective capsule type was identified.

Pristine capsules of each type, in which no curcumin was loaded, were tested to determine their cytotoxicity. It is very important that the capsules do not induce toxicity independently due to a number of reasons. One reason is that the control over cytotoxicity should reside in the drug itself or its dosage, as these properties can be tuned to each application. Another reason is that any cytotoxicity that occurs from pristine capsules will affect the cells in a different manner, where the mode of cytotoxicity will be dissimilar to that of the drug and possibly result in unexpected behaviour. Knowing the approximate number of capsules per concentration, and using the value of the number of cells seeded per well (2×10^4), the results have been displayed with reference to capsules per cell (Figure 4.7A).

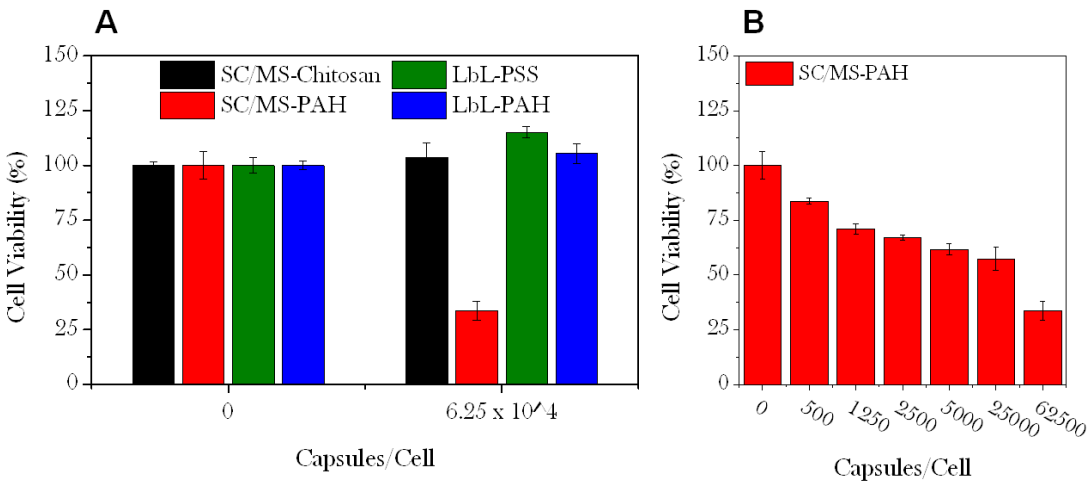

Figure 4.7: The cytotoxicity profile before any loading with curcumin of (A) the four types of pristine capsules at the highest capsule concentration, and (B) the cytotoxic profile of SC/MS-PAH capsules as the capsule concentration increased.

From the results seen in Figure 4.7A it is evident that all the capsules except the cross-linked SC/MS-PAH capsules are not toxic before curcumin loading. For brevity, only the highest concentrations of the pristine capsules which showed low toxicity have been shown in Figure 4.7A, while the toxicity profile for the SC/MS-PAH capsules is displayed in further detail in Figure 4.7B . Even at very high concentrations there is no detectable cell death for the SC/MS-chitosan and both LbL capsules, which ensures that any cell death occurring after curcumin loading is a direct result of the drug. The only pristine capsules that have demonstrated a significant amount of cytotoxicity before any drug has been introduced is the SC/MS-PAH capsules, with less than 40 % cell viability at the highest concentration. Displayed as red bars in Figure 4.7B, it can be seen that the cell viability readily decreases with an increase in pristine SC/MS-PAH capsules.

Despite the high toxicity of the SC/MS-PAH capsules before curcumin loading, it is clear from the high cell viability of the SC/MS-chitosan capsule that the toxicity is not a result

of the SC/MS method. Additionally, PAH is only toxic when in its cross-linked form. This is evident as both LbL capsule types also contain PAH, yet no toxicity was seen. Consequently, the significant toxicity of the SC/MS-PAH capsules before drug loading makes these capsules immediately less attractive as potential drug delivery vehicles.

The cytotoxicity profile of the curcumin-loaded capsules, displayed in Figure 4.8, shows the required number of each type of capsule per cell to induce cell death. From these results it can be seen that the SC/MS-chitosan capsules are the most cytotoxic, requiring the lowest number of capsules per cell to induce cell death, followed by LbL-PAH. Interestingly the LbL-PSS capsules are more toxic than the SC/MS-PAH at lower concentrations, while at higher concentrations this is reversed.

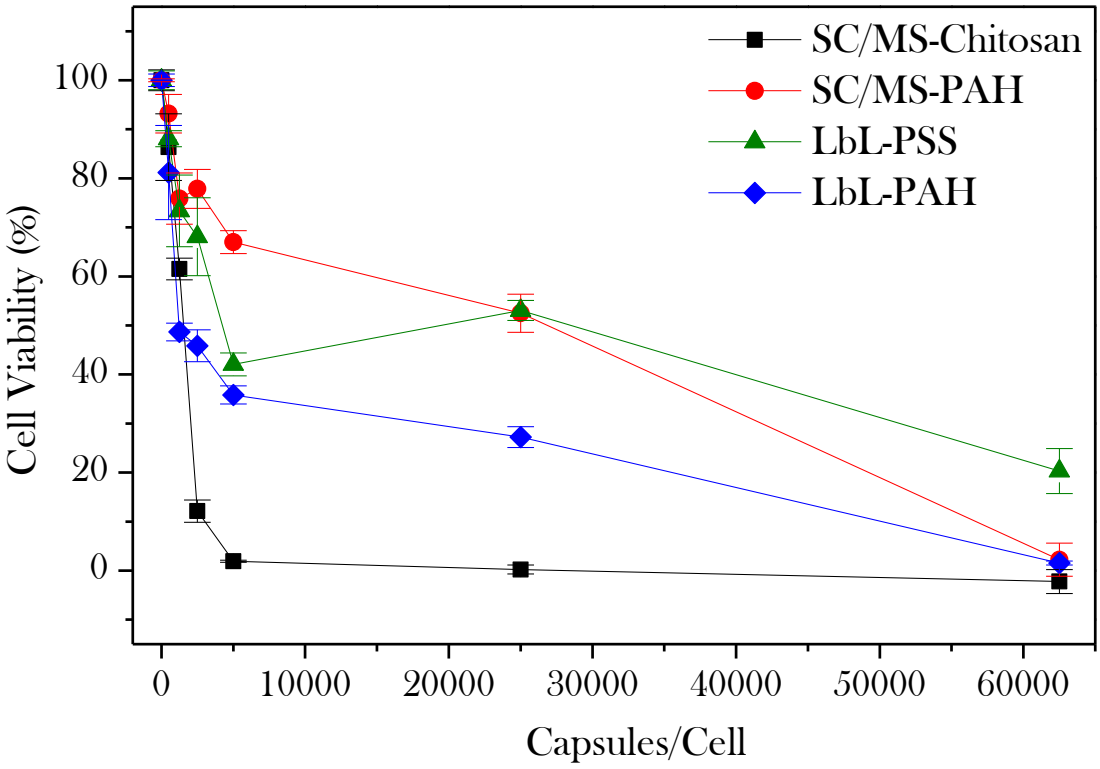

Figure 4.8: Profile of the number of capsules required per cell to induce cytotoxicity against MCF-7 breast cancer cells.

From these results alone, there is no apparent advantage over the method of capsule fabrication that is used. At certain concentrations the SC/MS method demonstrates both the best and worst cytotoxicity. Instead it is a combination of the SC/MS approach along with chitosan acting as the carrier material which demonstrates the greatest cytotoxicity. This was not unexpected due to the combination of higher curcumin loading, low particle aggregation, positive polymer nature, and the greatest cellular uptake observed. Although all these properties contribute to the increase cytotoxicity seen by SC/MS-chitosan, it is unclear which factor is most influential.

When observing the other capsules (SC/MS-PAH, LbL-PSS, LbL-PAH), there is no obvious trend between their cytotoxicity and cellular uptake, aggregation, or capsule charge. Nor is the cytotoxicity simply a reflection of curcumin loading per capsules. The drug loading of the LbL-PSS capsules is almost identical to that of SC/MS-chitosan, yet the cytotoxicity is much less. Furthermore, the curcumin loading of LbL-PSS is 28 % higher than that of the LbL-PAH capsules, yet the LbL-PAH capsules induce more toxicity.

From the results in Figure 4.8 alone it is difficult to determine if the cytotoxicity is simply a result of cellular uptake. This is because the cytotoxicity will be dramatically affected by both the cellular uptake and the curcumin loading per capsule simultaneously, and as the loading is inconsistent between capsule types, it will be very difficult to interpret these two effects separately. This suggests the cytotoxicity is a result of a complex combination of properties. However, by using the calculations of the curcumin loading per capsules and the number of capsules at each concentration, the dose of curcumin that was present per cell could be plotted against the viability, allowing for a clearer comparison of the cytotoxic efficiency

of the different capsules and their chemical-physical effects regardless of the variation in curcumin loading.

Only when the cell viability is plotted against the curcumin dose (Figure 4.9) it can be seen that the SC/MS template approach demonstrates a significant advantage over the LbL approach. The SC/MS-chitosan capsules are the most efficient at inducing cytotoxicity as they require the lowest dosage of 12 pg of curcumin per cell to induce 100 % cell death, followed next by SC/MS-PAH capsules which required 90 pg of curcumin. Although the LbL-PSS capsules never induced 100 % cell death, speculating from the graph it can be estimated that these capsules would have to deliver approximately 180 pg to each cell for >90 % cell death, while the LbL-PAH capsules require a dosage of 120 pg to each cell. Therefore, although the SC/MS-PAH capsules require more particles per cell to induce death, this is only a result of their decreased curcumin loading, and that they are actually more efficient at inducing cytotoxicity as the overall dosage of curcumin required is lower than that required by LbL capsules. As the drug loading is no longer a factor, the higher efficiency of the SC/MS capsules is likely due to the lower amount of aggregation that occurs when using the SC/MS templates which effects the amount of cellular uptake that occurs.

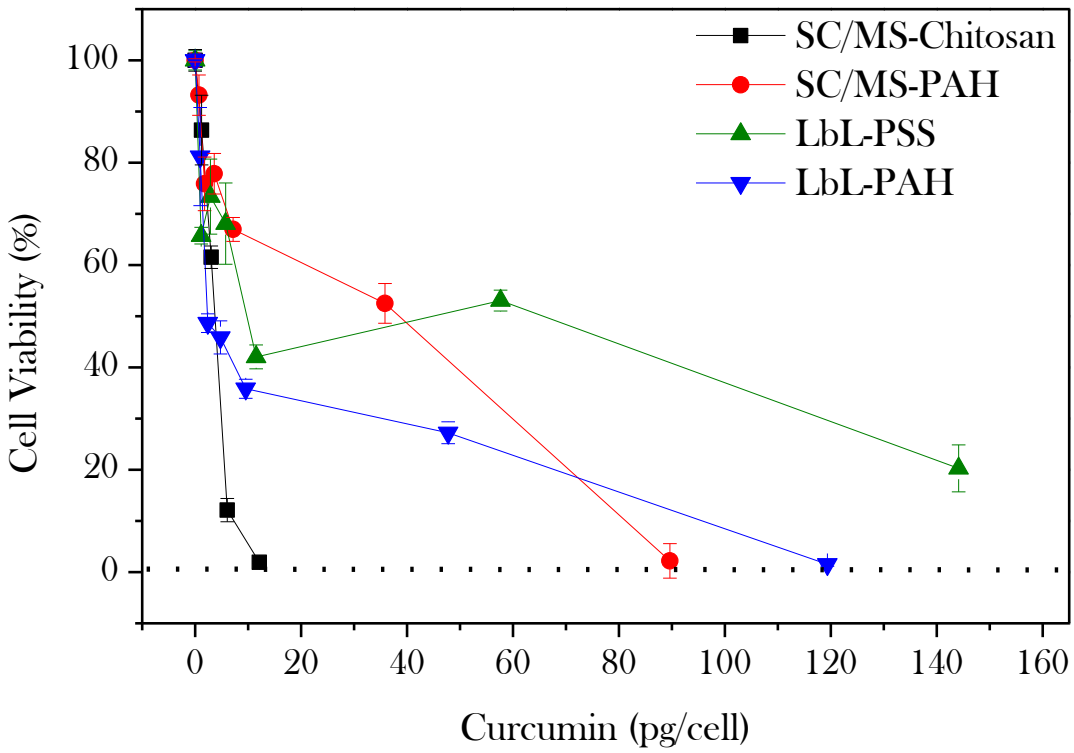

Figure 4.9: The cytotoxic efficiency of the different capsule types.

Interestingly, the dosage required per cell by the LbL capsules are both over an order of magnitude more than the amount required for the SC/MS-chitosan capsules. From these results along with the confocal images, it becomes increasingly probable that at higher concentrations there is a very limited amount of cellular uptake of the capsules bar the SC/MS-chitosan capsules. This is also supported by the behaviour of toxicity as the capsule concentrations increase. Looking back at Figure 4.8, at low capsule concentrations (<5,000) both LbL capsules are relatively toxic, and dropping the cell viability down to 40 % very quickly. At this same concentration the SC/MS-PAH capsules have only dropped the cell viability to 70 %. In contrast, as the capsule concentrations increase (>25,000), although the SC/MS-PAH capsules continue to show a steady increase in toxicity, indicating proportional cellular uptake occurring, the LbL capsules begin to lose their effectiveness at inducing

toxicity as the concentration increases, suggesting that less uptake is occurring. This type of behaviour indicates that unlike the SC/MS-chitosan and SC/MS-PAH which has not demonstrated a large amount of aggregation, the LbL capsules aggregate once the capsule concentration increases above a point, so that the amount of cellular uptake is very limited.

To compare the cytotoxic efficiency of encapsulated curcumin against un-encapsulated, free curcumin, the curcumin powder was dissolved in media and added to the cells at similar concentrations to those where toxicity was seen. Both fresh curcumin and curcumin incubated in media overnight were tested to increase the accuracy of the results. The overnight curcumin was used to simulate the curcumin within the capsules that had been incubated for 12 hours during the drug infiltration stage. However, as curcumin is known to degrade very quickly in aqueous environments,[43] fresh curcumin was also used to simulate the un-degraded curcumin that would have been present in the capsules.

Seen in Figure 4.10, both the overnight and fresh free curcumin are much less efficient at inducing cytotoxicity than the encapsulated curcumin. It is believed that the lower efficiency of un-encapsulated curcumin may be due to an increase in drug degradation which would occur on exposure to the biological environment, instantly reducing its cytotoxic properties. In addition, as the curcumin is administered as free molecules, it would diffuse throughout the cell media. This would generate an even but low concentration of drug in the media, and as this molecule is taken up by the cell through diffusion, the local concentration may not be great enough for much internalization. In contrast, encapsulation of curcumin prevents drug degradation which results in a higher toxic effect, as well as potentially more curcumin internalisation due to capsule-facilitated endocytotic uptake. Similarly, it has been

previously demonstrated that loading drugs within nanocarriers significantly enhances its efficiency by allowing higher uptake of drug carrier system over free drug molecules.[21] Since it is well known that curcumin and several other chemotherapeutic drugs are unstable in aqueous environments,[45-47] nano-encapsulation of such drug molecules provides a significant opportunity to achieve higher efficiency of existing chemotherapeutic drugs.

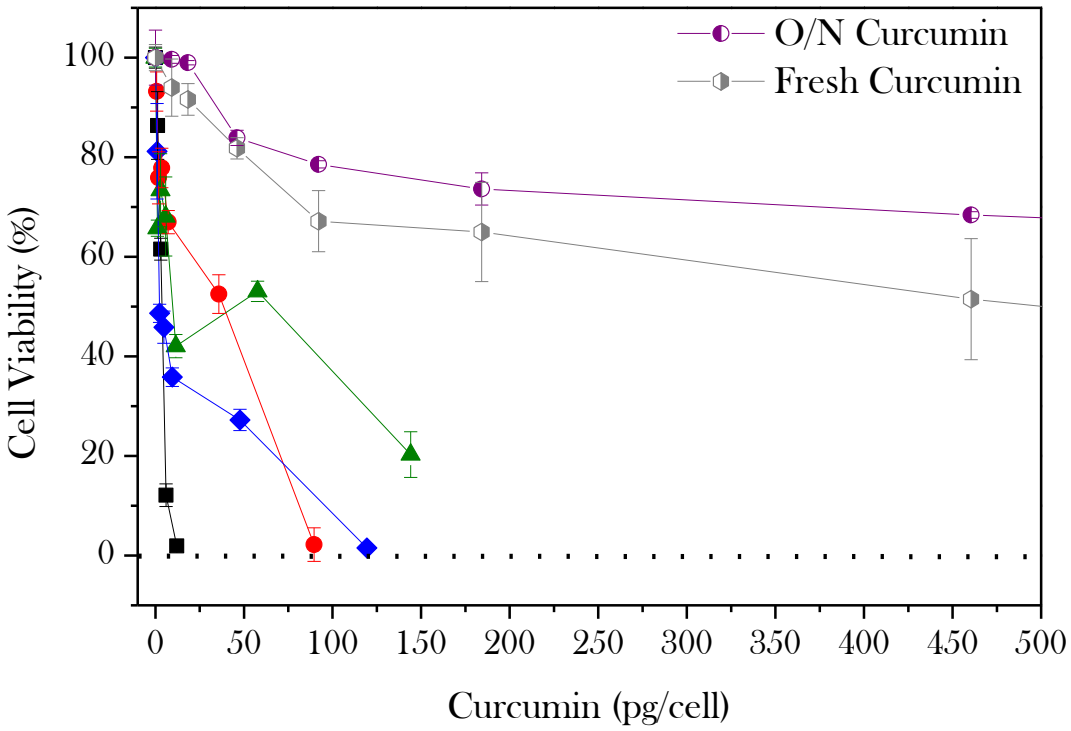

Figure 4.10: A comparison of the cytotoxicity of the free curcumin and the various curcumin-loaded capsules.

4.4 Conclusion

This chapter demonstrates that the SC/MS method paired with the polymer chitosan establishes a capsule system of superior properties, optimal for the application in drug delivery. Although the LbL approach for capsule synthesis has been employed in countless

studies over the last two decades,[14-20] there are few reports on its use at the nanoscale.[30,32-34] Furthermore, to the author's knowledge there are currently no reports comparing the extensively used LbL method with the lesser used SC/MS method for capsule synthesis. Throughout this chapter the SC/MS and LbL methods have been compared, where it was found that employing the SC/MS approach for nanocapsule fabrication allows for an easier method of fabrication, with capsules that demonstrate improved capsule wall thickness and less aggregation when compared to the more laborious LbL approach. Furthermore, the increased aggregation occurring as a result of the LbL approach was found to be the influencing factor in the cytotoxic efficiency of the sub-micron capsules. When comparing the polymeric material used, chitosan demonstrated to be the most suitable due to its biocompatibility, high drug loading capacity, and its polysaccharide nature which encourages more cellular uptake. These properties combined establish a nanocapsule system which demonstrates the optimum cytotoxic efficiency and the greatest potential in drug delivery applications.

4.5 References

1 Moinard-Checot, D., Chevalier, Y., Briançon, S., Fessi, H. & Guinebretière, S. Nanoparticles for drug delivery: Review of the formulation and process difficulties illustrated by the emulsion-diffusion process. *Journal of nanoscience and nanotechnology* **6**, 9-10 (2006).

2 Tiarks, F., Landfester, K. & Antonietti, M. Preparation of polymeric nanocapsules by miniemulsion polymerization. *Langmuir* **17**, 908-918 (2001).

3 Lee, M. Y., Min, S. G., Bourgeois, S. & Choi, M. J. Development of a novel nanocapsule formulation by emulsion-diffusion combined with high hydrostatic pressure. *Journal of microencapsulation* **26**, 122-129 (2009).

4 Randolph, T. W., Randolph, A. D., Mebes, M. & Yeung, S. Sub-Micrometer-Sized Biodegradable Particles of Poly (L-Lactic Acid) via the Gas Antisolvent Spray Precipitation Process. *Biotechnology progress* **9**, 429-435 (1993).

5 Ré, M. Microencapsulation by spray drying. *Drying technology* **16**, 1195-1236 (1998).

6 Vehring, R. Pharmaceutical particle engineering via spray drying. *Pharmaceutical research* **25**, 999-1022 (2008).

7 Calvo, P., Vila-Jato, J. L. & Alonso, M. J. Evaluation of cationic polymer-coated nanocapsules as ocular drug carriers. *International Journal of Pharmaceutics* **153**, 41-50 (1997).

8 Radtchenko, I. L. *et al.* Assembly of alternated multivalent ion/polyelectrolyte layers on colloidal particles. Stability of the multilayers and encapsulation of macromolecules into polyelectrolyte capsules. *Journal of Colloid and Interface Science* **230**, 272-280 (2000).

9 Stella, B. *et al.* Encapsulation of gemcitabine lipophilic derivatives into polycyanoacrylate nanospheres and nanocapsules. *International Journal of Pharmaceutics* **344**, 71-77 (2007).

10 Mora-Huertas, C. E., Fessi, H. & Elaissari, A. Polymer-based nanocapsules for drug delivery. *International Journal of Pharmaceutics* **385**, 113-142 (2010).

11 Soppimath, K. S., Aminabhavi, T. M., Kulkarni, A. R. & Rudzinski, W. E. Biodegradable polymeric nanoparticles as drug delivery devices. *Journal of Controlled Release* **70**, 1-20 (2001).

12 Fernández-Nieves, A. *et al.* Optically anisotropic colloids of controllable shape. *Advanced Materials* **17**, 680-684 (2005).

13 Hsu, P., Poulin, P. & Weitz, D. Rotational diffusion of monodisperse liquid crystal droplets. *Journal of Colloid and Interface Science* **200**, 182-184 (1998).

14 Donath, E., Sukhorukov, G. B., Caruso, F., Davis, S. A. & Möhwald, H. Novel Hollow Polymer Shells by Colloid-Templated Assembly of Polyelectrolytes. *Angewandte Chemie International Edition* **37**, 2201-2205 (1998).

15 Caruso, F., Caruso, R. A. & Möhwald, H. Nanoengineering of Inorganic and Hybrid Hollow Spheres by Colloidal Templating. *Science* **282**, 1111-1114 (1998).

16 Caruso, F. Hollow Capsule Processing through Colloidal Templating and Self-Assembly. *Chemistry - A European Journal* **6**, 413-419 (2000).

17 Peyratout, C. S. & Dähne, L. Tailor-Made Polyelectrolyte Microcapsules: From Multilayers to Smart Containers. *Angewandte Chemie International Edition* **43**, 3762-3783 (2004).

18 Quinn, J. F., Johnston, A. P. R., Such, G. K., Zelikin, A. N. & Caruso, F. Next generation, sequentially assembled ultrathin films: beyond electrostatics. *Chemical Society Reviews* **36** (2007).

19 Sablon, K. Single-component polymer nanocapsules for drug delivery application. *Nanoscale Research Letters* **3**, 265-267 (2008).

20 Wang, Y., Angelatos, A. S. & Caruso, F. Template Synthesis of Nanostructured Materials via Layer-by-Layer Assembly†. *Chemistry of Materials* **20**, 848-858 (2007).

21 Wang, Y., Bansal, V., Zelikin, A. N. & Caruso, F. Templated Synthesis of Single-Component Polymer Capsules and Their Application in Drug Delivery. *Nano Letters* **8**, 1741-1745 (2008).

22 Liang, K. *et al.* Charge-Shifting Click Capsules with Dual-Responsive Cargo Release Mechanisms. *Advanced Materials* **23**, H273-H277 (2011).

23 Ochs, C. J., Such, G. K., Städler, B. & Caruso, F. Low-Fouling, Biofunctionalized, and Biodegradable Click Capsules. *Biomacromolecules* **9**, 3389-3396 (2008).

24 Such, G. K., Tjipto, E., Postma, A., Johnston, A. P. R. & Caruso, F. Ultrathin, Responsive Polymer Click Capsules. *Nano Letters* **7**, 1706-1710 (2007).

25 Ochs, C. J., Such, G. K., Yan, Y., van Koeverden, M. P. & Caruso, F. Biodegradable Click Capsules with Engineered Drug-Loaded Multilayers. *ACS Nano* **4**, 1653-1663 (2010).

26 Zhang, Y., Guan, Y., Yang, S., Xu, J. & Han, C. C. Fabrication of Hollow Capsules Based on Hydrogen Bonding. *Advanced Materials* **15**, 832-835 (2003).

27 Sukhorukov, G., Fery, A. & Möhwald, H. Intelligent micro-and nanocapsules. *Progress in Polymer Science* **30**, 885-897 (2005).

28 Decher, G. & Hong, J.-D. Buildup of ultrathin multilayer films by a self-assembly process, 1 consecutive adsorption of anionic and cationic bipolar amphiphiles on charged surfaces. *Makromolekulare Chemie. Macromolecular Symposia* **46**, 321-327 (1991).

29 Johnston, A. P. R., Read, E. S. & Caruso, F. DNA Multilayer Films on Planar and Colloidal Supports: Sequential Assembly of Like-Charged Polyelectrolytes. *Nano Letters* **5**, 953-956 (2005).

30 Gittins, D. I. & Caruso, F. Multilayered Polymer Nanocapsules Derived from Gold Nanoparticle Templates. *Advanced Materials* **12**, 1947-1949 (2000).

31 Lamprecht, A. & Benoit, J.-P. Etoposide nanocarriers suppress glioma cell growth by intracellular drug delivery and simultaneous P-glycoprotein inhibition. *Journal of Controlled Release* **112**, 208-213 (2006).

32 Gittins, D. I. & Caruso, F. Tailoring the Polyelectrolyte Coating of Metal Nanoparticles. *The Journal of Physical Chemistry B* **105**, 6846-6852 (2001).

33 Schneider, G. & Decher, G. From Functional Core/Shell Nanoparticles Prepared via Layer-by-Layer Deposition to Empty Nanospheres. *Nano Letters* **4**, 1833-1839 (2004).

34 Städler, B., Price, A. D. & Zelikin, A. N. A Critical Look at Multilayered Polymer Capsules in Biomedicine: Drug Carriers, Artificial Organelles, and Cell Mimics. *Advanced Functional Materials* **21**, 14-28 (2011).

35 Büchel, B., Klaus, K. U., Akihiko, M. & Kazuo, T. A Novel Pathway for Synthesis of Submicrometer-Size Solid Core/Mesoporous Shell Silica Spheres. *Advanced Materials* **10**, 1036-1038 (1998).

36 Caruso, F., Trau, D., Möhwald, H. & Renneberg, R. Enzyme encapsulation in layer-by-layer engineered polymer multilayer capsules. *Langmuir* **16**, 1485-1488 (2000).

37 Schmitt, J. *et al.* Internal structure of layer-by-layer adsorbed polyelectrolyte films: a neutron and X-ray reflectivity study. *Macromolecules* **26**, 7058-7063 (1993).

38 Sukhorukov, G. B. *et al.* Layer-by-layer self assembly of polyelectrolytes on colloidal particles. *Colloids and Surfaces A: physicochemical and engineering aspects* **137**, 253-266 (1998).

39 Voigt, A. *et al.* Membrane filtration for microencapsulation and microcapsules fabrication by layer-by-layer polyelectrolyte adsorption. *Industrial & engineering chemistry research* **38**, 4037-4043 (1999).

40 Ilium, L. Chitosan and its use as a pharmaceutical excipient. *Pharmaceutical research* **15**, 1326-1331 (1998).

41 Sivakumar, S. *et al.* Degradable, Surfactant-Free, Monodisperse Polymer-Encapsulated Emulsions as Anticancer Drug Carriers. *Advanced Materials* **21**, 1820-1824 (2009).

42 Caruso, F., Caruso, R. A. & Mohwald, H. Production of Hollow Microspheres from Nanostructured Composite Particles. *Chemistry of Materials* **11**, 3309-3314 (1999).

43 Mehta, K., Pantazis, P., McQueen, T. & Aggarwal, B. B. Antiproliferative effect of curcumin (diferuloylmethane) against human breast tumor cell lines. *Anticancer Drugs* **8**, 470–481 (1997).

44 Shukla, R. *et al.* Biocompatibility of gold nanoparticles and their endocytotic fate inside the cellular compartment: a microscopic overview. *Langmuir* **21**, 10644-10654 (2005).

45 Oetari, S., Sudibyo, M., Commandeur, J. N. M., Samhoedi, R. & Vermeulen, N. P. E. Effects of curcumin on cytochrome P450 and glutathione S-transferase activities in rat liver. *Biochemical Pharmacology* **51**, 39-45 (1996).

46 Pandey, R., Sharma, S. & Khuller, G. K. Chemotherapeutic Efficacy of Nanoparticle Encapsulated Antitubercular Drugs. *Drug Delivery* **13**, 287-294 (2006).

47 Wang, Y.-J. *et al.* Stability of curcumin in buffer solutions and characterization of its degradation products. *Journal of Pharmaceutical and Biomedical Analysis* **15**, 1867-1876 (1997).

4.6 Appendix

4.6.1 Quantifying of the number of capsules

For an effective comparison of the fabricated capsules and their properties, ie drug loading, cytotoxicity etc, the number of capsules had to be known. However, due to the difficulty in determining the number of capsules fabricated through optical or counting methods, we based our calculations on the number of template particles, with the assumption that each template particle resulted in a capsule.

Due to the optical properties of silica, the particle number could not be determined by atomic absorption spectroscopy or a particle counter. Therefore a similar approach to many cell counting techniques was employed, whereby the number of particles were counted in a smaller sample size and then multiplied. A known mass of the largest available spheres (490 nm) was dispersed in water and diluted down multiple times. Next 0.5 µL was drop cast onto an SEM stub and the number of particles present in the droplet were counted. Due to the extremely large number of particle and the time consuming process of particle counting, only the large sized solid cores were counted by this method.

It was assumed that the density of silica within the particles, regardless of their diameter, was the same. Using this information, and knowing the number of 490 nm spheres present in 1 mg of silica powder, the relative number of particles per mg of silica power of the LbL and SC/MS template particles could be calculated using their diameter. However, this method of calculation could only be used before the addition of a mesoporous shell required in the SC/MS template. Therefore, before the mesoporous shell was grown on the SC/MS

particles, the number of solid core (SC) particles was calculated, and the change in weight that occurred due to the addition of the mesoporous shell (measured before and after shell growth) had to be taken into account and used to recalculate the number of particles.

Due to the assumption that each template particle resulted in a capsules, it is important to note the potential error that could have occurred. However, due to the inability to count the capsules in any other manner we found this process of particle calculation to be satisfactory. Furthermore, to decrease the potential error during the sample counting of the large particles, over 1000 particles were counted.

CHAPTER 5

SC/MS TEMPLATED SYNTHESIS OF CHITOSAN NANOCAPSULES FOR DRUG DELIVERY APPLICATIONS

Amphiphilic nanoparticulate carriers have gained intense interest as potential drug delivery vehicles for a myriad of biomedical applications. However, many current development methods lack control and consistency in the structural characteristics of the drug delivery vehicles. This chapter focuses on the successful production of homogeneous chitosan nanocapsules with tunable properties such as controlled capsule size, shell thickness and porosity. Through a facile template-mediated approach using SC/MS silica nanoparticles with variable core size, mesoporous shell thickness and porosity, chitosan nanocapsules with replicated structural properties have been developed. The anti-cancer drug curcumin was used to act as a model drug-in-oil substance to demonstrate the drug-encapsulation efficiency and cell toxicity as a function of capsule size, thickness and porosity. The cell toxicity of the nanocapsules was also determined in an *in vitro* study with P815 Mouse cells, whereby the chitosan capsules on their own showed low toxicity, which increased drastically with curcumin loaded capsules. This study provides a detailed investigation into a novel method of chitosan nanocapsule synthesis, as well as the effect of the synthesis parameters on the drug-loading and cellular toxicity of these capsules.

5.1 Introduction

Chitosan [Poly-(1,4) 2-amino-2-deoxy-β-D-glucan] is a biopolymer that has shown immense promise as a preferred carrier system due to its broad range of proven biomedical applications (the chemical structure is shown in Figure 5.1) .[1,2] Unlike most polypeptides which are typically immunogenic, chitosan is a polysaccharide and demonstrates low immunogenicity, low toxicity, and good mechanical properties.[3] Furthermore, chitosan can be broken down in the body by lysozymes to harmless *N*-acetyl glucosamine making the biodegradable material highly desirable in forming carrier vehicles for drug delivery.[4] Due to the advantages of chitosan nanocapsules, further investigation into these particles has been made to increase their potential as drug delivery vehicles.

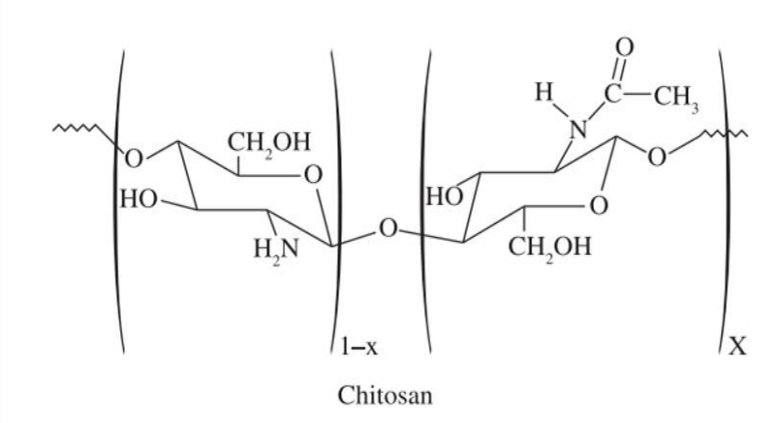

Figure 5.1. The chemical structures of chitosan[5]

Different approaches have been undertaken in the past to prepare chitosan-based nanoparticulate systems, including chitosan nanosphere and bead fabrication by way of emulsion cross-linking,[6-8] spray-drying,[9-11] coacervation/precipitation,[12] ionic gelation,[13-15] the emulsion-droplet coalescence method,[16] the reverse micellar method,[17] and the sieving method.[18] Although these particles represent very promising drug delivery platforms, most of

these methods produce solid chitosan particles, thereby restricting their drug loading capacity to the carrier system and neglecting to protect the drug from degradation by the external environment. Moreover, it is extremely difficult to control the polydispersity of the chitosan particles synthesized via these routes, thus limiting their ability to control the drug payload during administration.

Demonstrated in the previous chapter, the use of a solid core/mesoporous shell silica template into which chitosan is deposited, followed by subsequent removal of the template matrix, can result in a chitosan nanocapsule with superior drug delivery properties. The combination of the SC/MS method and chitosan acting as the polymer material demonstrated significant drug loading and cytotoxic efficiency over other templating method and polymers tested, exhibiting good monodispersity, a high loading capacity of a drug-in-oil mixture, low cytotoxicity before drug infiltration, and efficient cytotoxicity after drug is incorporated into the capsules.

The choice of polymer material is not the only factor in determining a nanocapsule's therapeutic capabilities. A range of structural properties, such as the nanocapsule size, shape, wall thickness and porosity may play an important yet complex role in determining the therapeutic efficiency of the particle. These properties can affect the drug loading capacity, the cellular uptake and cytotoxic efficiency against cells.[19-22] By altering these structural features, their individual effects can be investigated, and the properties that are most influential can be identified.

5.1.1 Rationale

The structural characteristics of a drug delivery system can define its application and affect its functionality. In this chapter it is demonstrated for the first time that, by tuning relevant features of the sacrificial SC/MS template, chitosan nanocapsules of controllable size, wall thickness and porosity can be fabricated. The approach presented here combines the versatility of solid core particles with the high loading capacity of mesoporous shells to prepare nearly monodispersed chitosan capsules of three different diameters (220, 270 and 440 nm), three different wall thickness (28, 45 and 56 nm), and three different pore sizes (inversely corresponding to template pore diameter of 2.9, 3.68 and 4.85 nm). This led to seven structurally different chitosan capsules, amongst which one capsule type was common with the intermediate features of 270 nm for capsule size, 45 nm wall thickness and 3.68 nm template pore size. To understand the role of different structural properties (size, wall thickness and porosity) of the chitosan nanocapsules in drug delivery, these capsules were further infiltrated with curcumin, a hydrophobic anticancer drug, naturally found in the yellow curry spice turmeric,[23] and the effect of these seven different types of curcumin-loaded chitosan nanocapsules on the cell viability of mouse mastocytoma cells was studied.

And finally, although nanocapsular systems have been heavily studied,[24-34] it is not entirely clear which amongst the various structural properties plays the dictating role in determining their therapeutic efficiency. It is the aim of this study to decouple the effects of the size, shell thickness and porosity of nanocapsular polymer vehicles to enable researchers in identifying the most influential structural feature of nanocapsule-based drug delivery systems.

5.2 Experimental Section

In this chapter we have fabricated seven structurally different SC/MS template particles. This was achieved by fabricating three different sized solid silica cores based on the method optimised in Chapter 3, followed by a secondary stage of synthesis where a mesoporous shell of various thickness and porosity was grown onto each of the cores. By employing these SC/MS silica particles as sacrificial templates into which chitosan polymer was infused and cross-linked, several structurally diverse chitosan nanocapsules were fabricated (Figure 5.2).

5.2.1 Preparation of Solid Silica Particles

Based on the modified Stöber method[35] used in chapter 3, the solid core (SC) silica spheres were prepared in appropriate amounts of ethanol, deionized water (MilliQ) and ammonia solution (28%) as per Table 5.1 and the solutions were mixed well before heating to the required temperature. After the solution temperature had stabilised, 75 µL of tetraethoxysilane (TEOS) was added and the solution was mixed for 4 seconds. The solutions were then kept very still and held at their appropriate temperatures while the reaction took place over a 1 hour period.

Template Type	Ethanol (µL)	Water (µL)	Ammonia (µL)	Temperature (°C)	Core Size (nm)
$TempC_1$	1000	135	100	30	170 ± 12
TempC	1000	135	113	25	290 ± 24
$TempC_2$	1000	135	133	18	490 ± 14

Table 5.1: The experimental conditions for the synthesis of the three size solid cores of the SC/MS silica template particles.

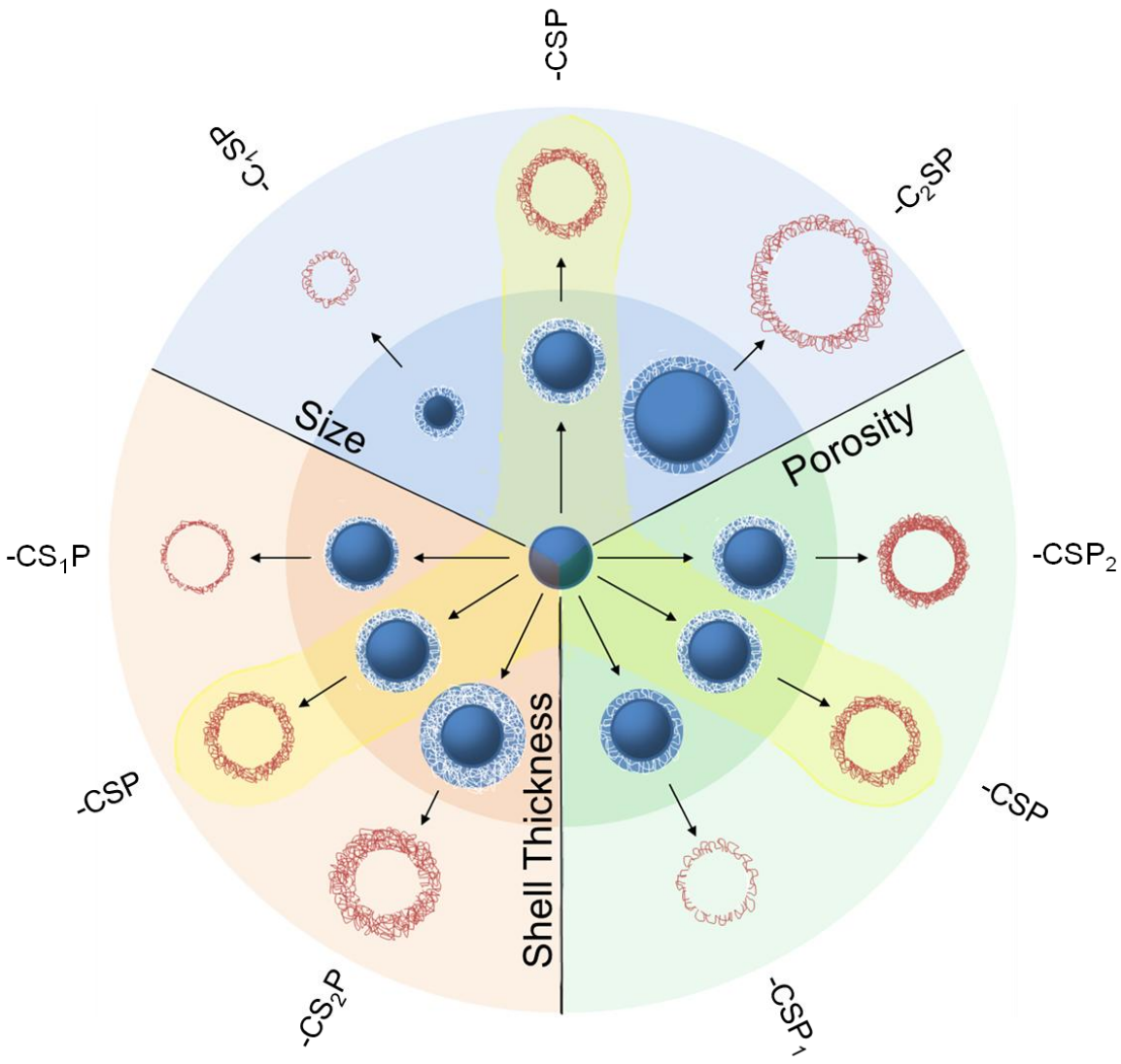

Figure 5.2: Schematic representation of the solid core/ mesoporous shell (SC/MS) approach employed to fabricate seven different types of chitosan nanocapsules with different structural features, with one common type of SC/MS template in each category (highlighted by an arching triangle).

5.2.2 Preparation of SC/MS Silica Templates

To grow the mesoporous shell (MS) of specified thickness and porosity on the solid cores, solutions containing mixtures of TEOS and n-octadecyltrimethoxysilane (ODTMS) were slowly added to the solutions from the previous step containing solid core silica particles

over a period of 20 min at 25 °C under shaking conditions (Table 5.2 for the TEOS and OTMS volumes).

Template Type	TEOS (µL)	ODTMS (µL)	Shell Thickness (nm)
TempCSP	65	13	46 ± 7
TempC_1SP	125	25	49 ± 16
TempC_2SP	5	1	42 ± 13
TempCS_1P	25	5	31 ± 21
TempCS_2P	135	27	55 ± 12
TempCSP_1	70	7	42 ± 9
TempCSP_2	50	25	48 ± 14

Table 5.2: The experimental conditions for the synthesis of the mesoporous shells of the SC/MS silica template particles.

Note that there are significant variations in the total volume of the TEOS/OTMS solutions, as well as the ratios of TEOS:ODTMS that have been used. The solutions were then incubated under shaking at 25 °C for 1 hour, followed by centrifugation and washed three times with ethanol to obtain the precipitated powder. This powder was heated to 550 °C for 6 h to remove the porogen ODTMS through calcination, this resulted in the SC/MS silica particle templates.

The obtained SC/MS templates were characterised by scanning and transmission electron microscopy (SEM and TEM). The surface area and pore diameter of the SC/MS templates were measured using the (BET) technique.[36]

5.2.3 Preparation of Chitosan Nanocapsules

The chitosan capsules were fabricated using the same method employed in chapter 4. Briefly, the capsules were prepared by dispersing 5 mg SC/MS template particles in 450 µL of deionised water, followed by overnight incubation after adding 1 mL aqueous solution containing 4 mg low molecular weight chitosan (Sigma Aldrich – dissolved using 0.8% acetic acid) in pH 7.2 phosphate buffer saline (PBS). Following overnight incubation, the chitosan-infiltrated SC/MS particles were obtained by centrifugation, and redispersed in 800 µL PBS and 50 µL glutaric dialdehyde for 2 hours to cross-link the chitosan within the mesoporous shell of SC/MS particles. After washing three times with deionized water, the SC/MS silica template was removed by hydrofluoric acid (2M) treatment in an ammonium hydroxide buffer (8M), followed by centrifugation and repetitive washing with deionised water (Warning: hydrofluoric acid is highly corrosive, and extreme care should be taken while handling hydrofluoric acid). The chitosan nanocapsules thus obtained were analysed using TEM, and the thickness of the capsule wall was determined from TEM images of ultramicrotomed sections of capsules embedded within epoxy resin. The degree of chitosan loaded within the mesoporous shell of SC/MS silica template was determined by thermogravimetric analysis (TGA) using Perkin Elmer Pyris 1 TGA instrument.

5.2.4 Loading and Quantification of Curcumin in Chitosan Nanocapsules

Following the synthesis of seven different types (different sizes, wall thicknesses and porosities) of chitosan nanocapsules, these capsules were dehydrated in ethanol and dispersed in curcumin/oleic acid mixture (10 µg curcumin per mL of oleic acid) to allow infiltration of the oil phase through the porous walls of chitosan nanocapsules and filling the capsules over a

period of 12 hours on a rotary shaker. Following incubation, curcumin-loaded chitosan nanocapsules were obtained by centrifugation and washed thrice with hexane to remove any non-infiltrated curcumin/oleic acid. These curcumin-filled chitosan capsules were found to make stable dispersions on addition to water and biological buffers. The high solubility of curcumin in absolute ethanol was exploited to determine the curcumin loading within different type of chitosan nanocapsules by exposing the drug-infiltrated capsules to absolute ethanol after their precipitation. This resulted in the release of all the curcumin internalized within chitosan capsules to the supernatant, which was further quantified by making standard curves using a Cary 50 Bio UV-Vis spectrophotometer at absorbance maxima of curcumin at 430 nm.

5.2.5 Cellular Uptake and Cytotoxicity of Curcumin-loaded Chitosan Nanocapsules

P815 mouse mastocytoma cells (obtained from Manassas, VA, USA) were used to study both the uptake and the toxicity of the chitosan nanocapsules. The cells were cultured in RPMI-1640 media (Sigma) containing 10% FBS and supplemented with gentamycin, glucose, pyruvate, 2-mecaptoethanol and L-glutamine. The cells were maintained in a humidified incubator at 37 °C and 5% CO_2. For cell uptake studies, 10^5 P815 cells were exposed to 10^8 chitosan capsules for 24 h, followed by cell harvesting, washing three times with PBS, and seeding onto glass slides for imaging by confocal laser scanning microscopy (CLSM; Nikon A1 Confocal Microscope). As the glutaraldehyde cross-linking step during chitosan nanocapsules makes them highly fluorescent, fluorescent dye labelling was not required for CLSM studies.

To determine the efficiency of curcumin-infiltrated chitosan capsules on cell mortality of P815 mouse mastocytoma cells, 10^5 cells were exposed to different numbers (final concentration ranging from 10^5 to 10^8 capsules per treatment) of seven different types of capsules for 24 h in 96-well plates under appropriate growth conditions as explained in the previous section. This was followed by determination of cellular viability using a soluble tetrazolium-based colorimetric assay (Promega MTS CellTiter 96® aqueous kit) and measuring the absorbance at 490 nm using a microplate reader (Perkin Elmer, USA). The same experiments were performed on pristine chitosan capsules, which served as a control. Since pristine capsules did not show significant cytotoxicity, for brevity, only the mean cytotoxicity of seven different types of pristine chitosan capsules used in this study has been shown. The cytotoxicity studies of curcumin dispersed in water was also performed for comparison. Each treatment was performed in quadruplicate and repeated three times, which means that the data presented here is an average of 12 experiments, with standard error of mean shown as error bars.

5.3 Results and Discussion

Several modifications were made to the protocol, including variations in the reaction temperature, as well as ammonia, porogen and TEOS concentration during particle synthesis to achieve SC/MS silica particles of different solid core sizes (TempC_1SP, TempCSP and TempC_2SP); mesoporous shell thicknesses (TempCS_1P, TempCSP and TempCS_2P); and porosities (TempCSP_1, TempCSP and TempCSP_2) (Figure 5.3), wherein variable 'C' corresponds to different core diameters, 'S' corresponds to shell thicknesses and 'P' corresponds to different porosity levels. To compare the structural variations and their effects

between templates and the resulting capsules, TempCSP particles were used as a common control in the three sections of size, shell thickness and porosity. Furthermore, TempCSP is the same SC/MS template used in chapter 4, allowing comparisons between the results of the previous and current chapters.

The synthesised SC/MS particles were then employed to fabricate chitosan nanocapsules with comparable structural characteristics with their corresponding templates, with variations in capsule size ($CapC_1SP$, Cap CSP, and $CapC_2SP$), capsule wall thickness ($CapCS_1P$, CapCSP, and $CapCS_2P$), and capsule wall porosity/density ($CapCSP_1$, CapCSP, and $CapCSP_2$).

5.3.1 Capsules with Different Diameters

The size of a drug delivery vehicle can have a dramatic effect on the clinical application of particles due to major influences in their drug loading capabilities, retention time in the body, and the efficiency in cellular uptake.[19,20,37] Consequently, by controlling the size of a drug delivery vehicle it is possible to tune these characteristics for a particular application rather than have the application dictated by the capabilities (and limitations) of a drug vehicle of a single size. In this section, we showed that chitosan nanocapsules of different diameter can be fabricated by controlling the size of the template particles from which they are formed, and in doing so, demonstrate the variation in their potential to act as drug delivery vehicles.

The chitosan nanocapsules were fabricated using SC/MS silica particles as template, however, before the growth of a mesoporous shell on these template particles, solid core particles were first fabricated based on the method used and optimised throughout Chapter 3.

At the time that these experiments were carried out the smallest and largest silica spheres that were successfully achieved with high monodispersitiy were 170 nm and 490 nm in diameter. These were achieved by altering the reaction temperature and the ammonia concentration during particle synthesis. As discussed in Chapter 3, the particle size is inversely related to the reaction temperature, and to a lesser extent directly related to the ammonia concentration. An intermediate solid core silica sphere of 290 nm was also grown using intermediate temperature and ammonia parameters. The three particles of increasing core size from 170, 290 and 490 nm will be referred to as $TempC_1$, TempC and$TempC_2$ for brevity, and are displayed in Figure 5.3 A-C.

After synthesis of the near monodispersed solid silica cores, these particles were used to develop three SC/MS template by growing a secondary, mesoporous shell on the surface. To better compare the effect of their core size on the resulting capsules, the mesoporous shells were all grown to ~45 nm in thickness (see Table 5.3). However, as the surface area of the particles varied significantly from 25.9 m^2g^{-1} (for the particles with the smallest diameter) to 8.5 m^2g^{-1} (for the largest particles), the amount of TEOS/TMS mixture added had to be in accordance with this change (see Table 5.2) After the growth of the mesoporous shells, the surface area of the particles then rose to 300.0, 252.6 and 164.2 m^2g^{-1} from the smallest to largest SC/MS templates, respectively (see Table 5.3). The solid core particles of three different diameters with ~45 nm mesoporous shell were now of total diameter 268 ± 14 nm ($TempC_1SP$), 382 ± 19 nm (TempCSP) and 574 ± 12 nm ($TempC_2SP$), with the SEM images shown in Figure 5.3 D-F.

Template	Description	Core Size (nm)	MP Shell Thickness (nm)	Surface Area (m^2 g^{-1})	Pore Size in Shell (nm)	Pore Volume (mL g^{-1})
	Solid Cores					
$TempC_1$	Small diameter	170 ± 12	-	25.86	-	-
TempC	Medium Diameter	290 ± 24	-	14.37	-	-
$TempC_2$	Large Diameter	490 ± 14	-	8.50	-	-
	Solid Cores, Mesoporous Shell					
$TempC_1SP$	Medium Diameter, Medium Shell Thickness, Medium Pores Size	290 ± 24	46 ± 7	252.6	3.68	0.27
TempCSP	Small diameter, Medium Shell Thickness, Medium Pore size	170 ± 12	49 ± 16	300.0	5.12	0.44
$TempC_2SP$	Large Diameter, Medium Shell Thickness, Medium Pore Size	490 ± 14	42 ± 13	164.2	3.30	0.16

Table 5.3: A summary of the structural characteristics of i) the solid cores (before mesoporous shell growth) of the SC/MS templates, and ii) the SC/MS templates.

The SC/MS silica templates with three significantly different sized cores were then employed in the aim to fabricate chitosan nanocapsules with similar capsule wall thickness and porosity, but with a hollow inner cavity that would closely compare to the diameter of the solid cores of their corresponding templates. The chitosan capsules were fabricated by incubating aqueous chitosan solution with the appropriate SC/MS silica template, followed by polymer cross-linking using glutaraldehyde and subsequent removal of the silica template. Illustrated in Figure 5.3 G-I are the TEM images of chitosan nanocapsules of different diameters synthesized using the SC/MS silica templates shown in Figure 5.3 D-F, respectively. By utilizing templates of increasing diameter, the resulting size of the capsules can be controlled accordingly. It can be seen from Figure 5.3 G-I that the total diameter of the chitosan capsules, including wall thickness, increased to ca. 220 nm, 270 nm and 440 nm with respect to the increase in template size of 268 nm, 380 nm and 574 nm, respectively. This

correlation is further displayed in Figure 5.4, which demonstrated the relative increase in the capsule size. The capsules are in good accordance with the templates and demonstrated 15–30 % shrinkage when imaged in the TEM. However, a large amount of shrinkage would only occur upon drying before TEM imaging.

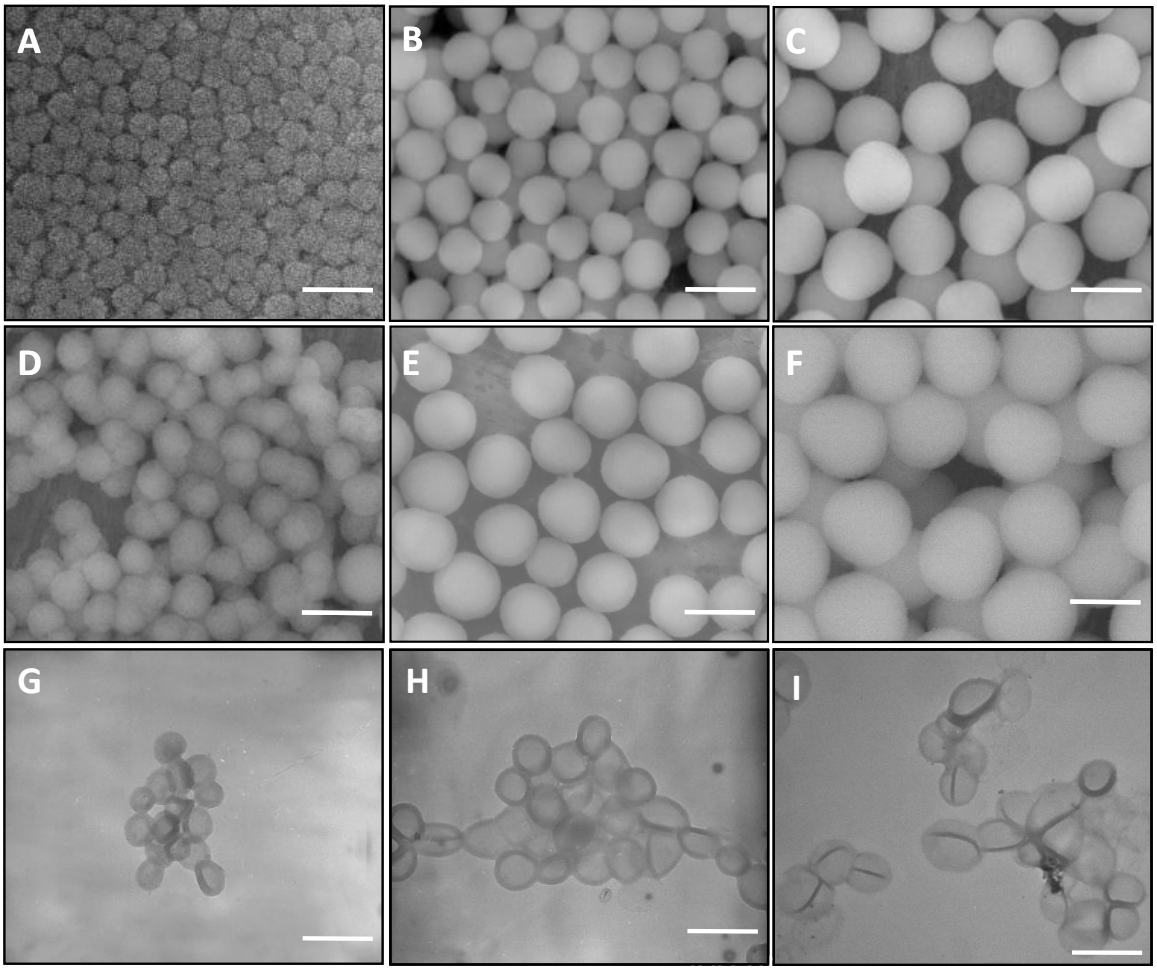

Figure 5.3: SEM images of different sizes of solid silica cores (A-C), corresponding to (A) TempC_1, (B) TempC, and (C) TempC_2. These solid cores where then employed to fabricate the solid core/mesoporous shell (SC/MS) silica templates (D-F), which correspond to (D) TempC_1SP, (E) TempCSP and (F) TempC_2SP, respectively. (G-I) TEM images of chitosan nanocapsules of three different sizes (G) CapC_1SP, (H) CapCSP and (I) CapC_2SP, synthesized using (D-F) as templates, respectively. Scale bars correspond to 500 nm.

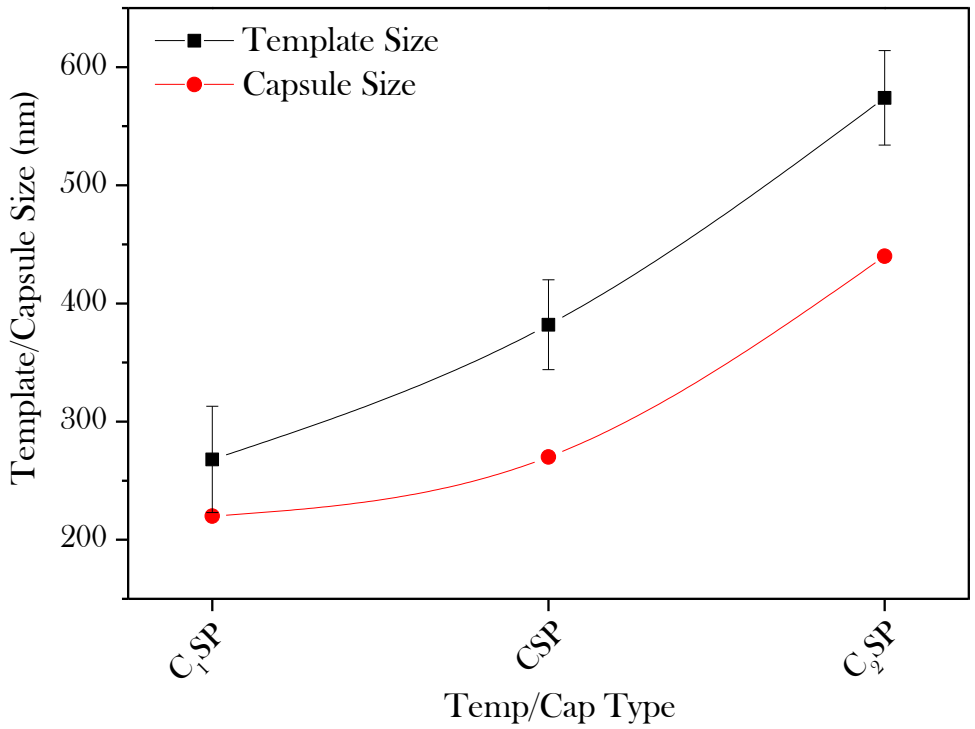

Figure 5.4: The correlation between the size of the SC/MS template particles and the size of the capsules fabricated from the respective template.

Following the synthesis of these chitosan nanocapsules with significantly different diameters, their drug loading capabilities were investigated to determine what effect the size of the nanocapsules has. One of the major advantages of using capsular systems is the ability to separate the encapsulated material from the surrounding environment. This enables an oil phase to be incorporated into a hydrophilic environment through its encapsulation into a partically amphiphilic capsule, bypassing the difficulties that can arise when trying to introduce an oil phase into an aqueous phase.

Even though chitosan is known to act as a hydrophilic biopolymer due to its amine groups, it can also accommodate hydrophobic components within its partially hydrophobic centre, and this advantageous ability of introducing oil in water was demonstrated. By

incubating the chitosan nanocapsules in a curcumin/oleic acid mixture the drug/oil was allowed to permeate through the semi-porous walls of the capsules before the system was transferred to hydrophilic phosphate buffer (pH 7.2). This technique has been previously used to investigate the drug/oil encapsulation in other nanocapsular systems using a technique reported by *Sivakumar* et al.[38]

Curcumin was used as a model anticancer drug because recent studies have established that not only does it inhibit the growth of a number of human cancer cell lines, it is also a potent anti-oxidant and it possesses anti-proliferative activities against tumor cells *in vitro*. Furthermore, as shown in chapter 4, curcumin has limited applicability due to its instability in the aqueous environment,[39] but encapsulation of curcumin within the capsules prevents the degradation of the compound and enables the investigation of its toxicity during its active form.

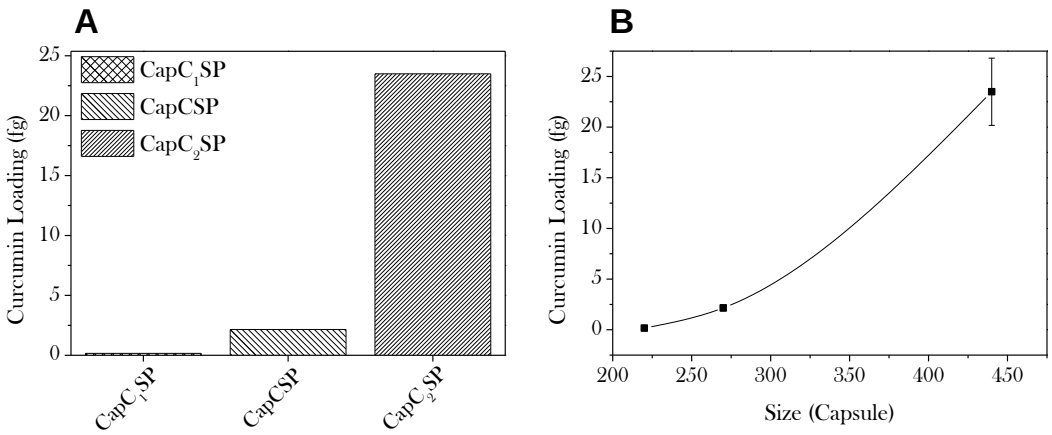

Figure 5.5: A representation to the loading of curcumin per capsule with regards to the A) capsule type, and B) capsule size.

After dehydration of the internalised drug/oil solution, the drug loading was quantified using UV-vis spectroscopy. As expected, the capsules of different sizes demonstrated

significant disparity in curcumin loading capacities (Figure 5.5) ranging from 0.16 fg per capsule of 220 nm ($CapC_1SP$) to 2.15 fg and 23.49 fg, for 270 nm (CapCSP) and 440 nm capsules ($CapC_2SP$), respectively. This indicates that the largest and the medium sized capsules can be loaded with ca. 145 and 13 times more curcumin, respectively, than the smallest capsules. It also demonstrates that the dosage of drug can be controlled based on the initial template employed for capsule fabrication. It should be noted that; if the volume capacity of these capsules of three different sizes is considered, their volumes should be in the ratio of 1:2:8 for smaller, medium and large size capsules. The disparity between the theoretical volume capacity of the capsule cavity (1:2:8) and the actual capsule drug loading ability (1:13:145) strongly indicates that, in addition to the curcumin infiltrated in capsule cavity, a significant amount of curcumin must also be loading into the capsule wall.

These results demonstrate that SC/MS templates can be employed to successfully fabricate chitosan nanocapsules of three different diameters which, exhibit a variation in curcumin drug loading ability over a large dosage range. Furthermore, the drug loading capability of these nanocapsules can be tuned through the use of differently sized SC/MS template particles.

5.3.2 Capsules with Different Wall Thickness

After discovering that there may have been a significant amount of drug loading occurring into the capsule wall, an investigation into the relationship between the thickness of the capsule wall and the drug loading capabilities was carried out. It is extremely important that the effects of the wall thickness are well understood as any additional drug loading due to the thickness in the capsule wall will have repercussions on their uses in clinical applications.

Referring back to the SC/MS template particles, it was determined that the thickness of the mesoporous shell surrounding the solid core silica spheres could be controlled by altering the amount of TEOS/TMS mixture that was added to the particles. This in turn was expected to alter the wall thickness in the resulting chitosan capsules. In order to investigate the effect that the thickness of the mesoporous shells of the SC/MS template has on the resulting chitosan capsules, it was required that all other variables were kept as constant as possible. To minimise the number of variables, the same medium size solid core developed in the previous section (Temp C of diameter 290 nm) was employed here to grow SC/MS particles with three dissimilar mesoporous shell thickness, see Figure 5.6. By using the same SC/MS particles TempCSP from previous section it is also possible to compare these results with results from the other sections.

Through exposure to varying volumes of TEOS/TMS mixture while keeping a constant TEOS:TMS ratio of 5 (Table 5.2), mesoporous shells of three different thicknesses were grown around the same medium size solid core (290 nm diameter). Measured from TEM images in Figure 5.6, the mesoporous shell thickness increases with an increase in the volume of TEOS/TMS mixture, creating SC/MS particles of identically-sized solid cores with increasingly different mesoporous shell thicknesses of 31 nm (TempCS_1P), 46 nm (TempCSP as in section 5.3.1), and 55 nm (TempCS_2P), see Figure 5.7.

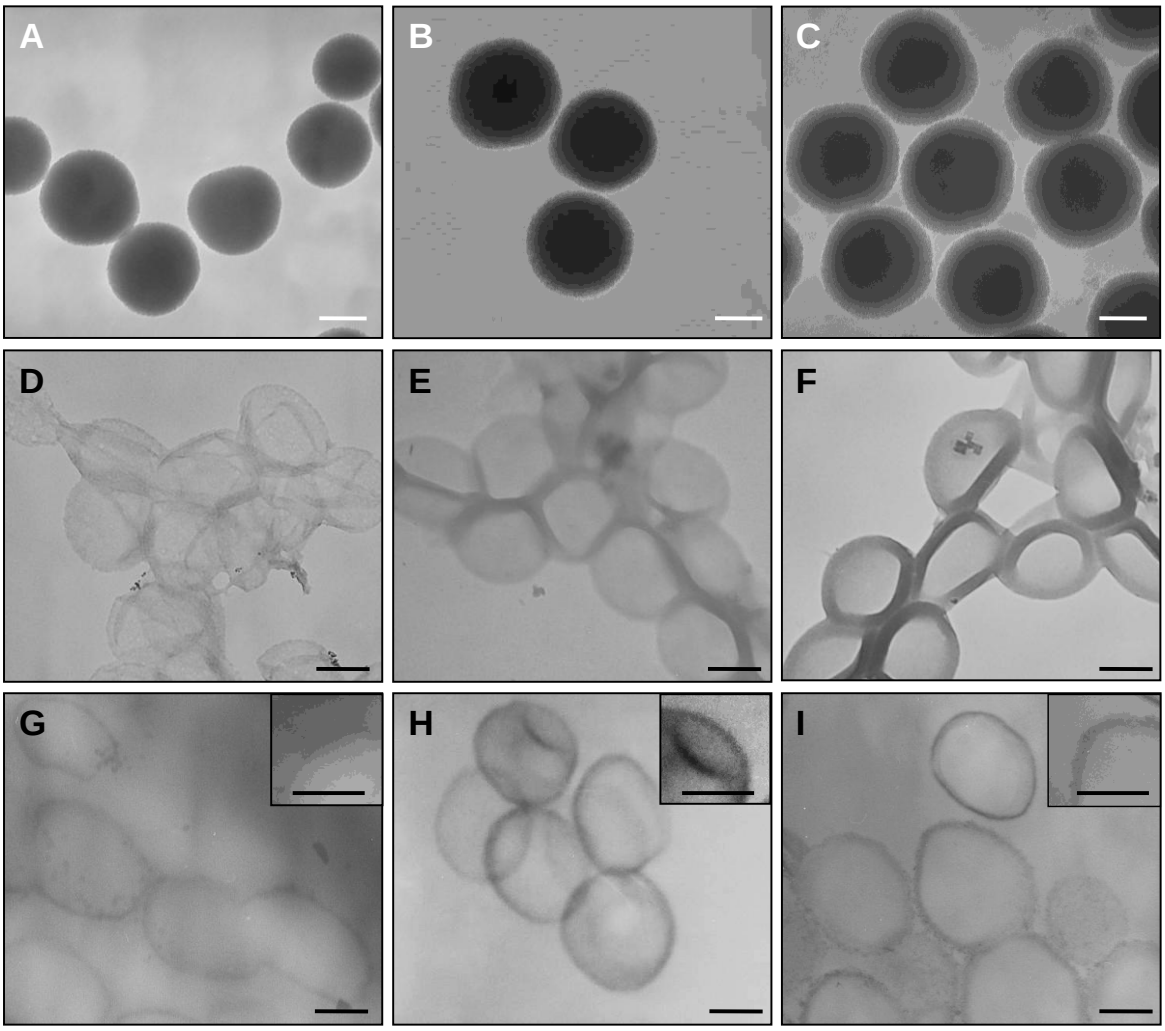

Figure 5.6 TEM images of (A-C) SC/MS silica templates of the same core diameter of 290 nm but different mesoporous shell thickness viz. (A) 31 nm, (B) 45 nm, and (C) 55 nm. (D-F) Chitosan nanocapsules of three different wall thickness (D) CapCS$_1$P, (E) CapCSP and (F) CapCS$_2$P, synthesized using SC/MS templates shown in A-C, respectively. (G-I) show TEM images of ultramicrotomed chitosan nanocapsules shown in D-F, respectively. Scale bars correspond to 200 nm.

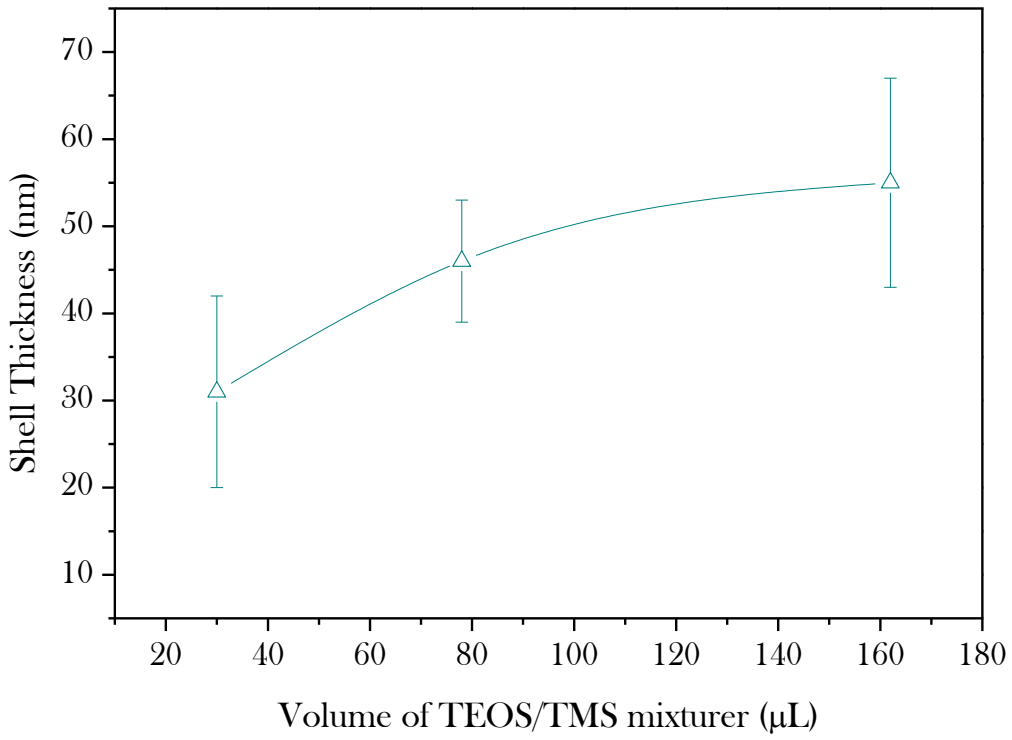

Figure 5.7: The variation in the thickness of the mesoporous shell of the SC/MS template particles when exposed to different volumes of the TEOS/TMS mixture during synthesis.

To ensure that there were more potential sites in the template shell where the chitosan could infuse, BET analysis of the pore size and volume was carried out. As can be seen in Figure 5.8A, the pore diameter remains relatively constant at ca. 3 nm, however as the mesoporous shell is increased in thickness the pore volume increases proportionally as shown in Figure 5.8B. These SC/MS particles of the same core size but with varying mesoporous shell thickness were then used to fabricate three types of chitosan nanocapsules, of which it was expected to have a corresponding increase in capsule wall thickness.

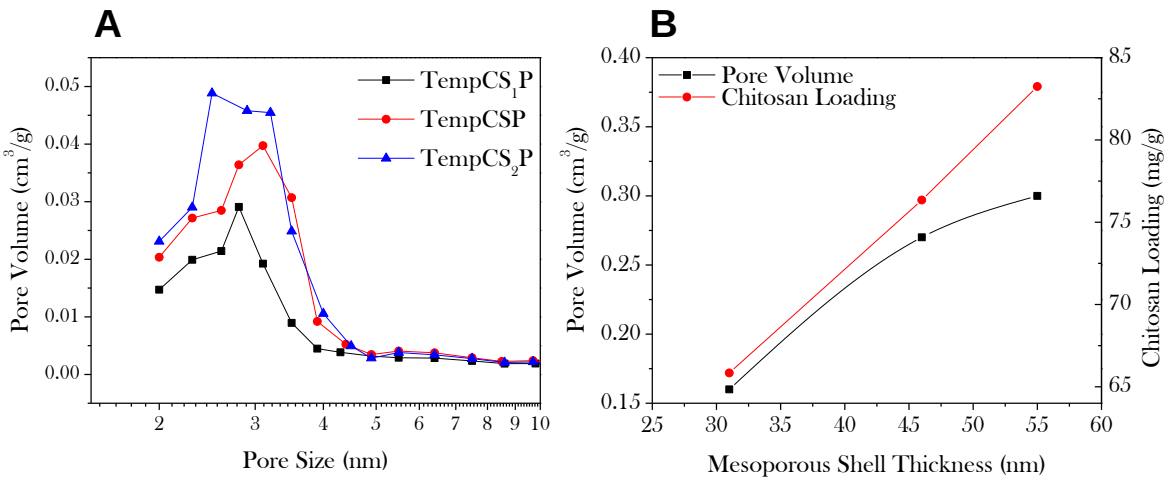

Figure 5.8: A) BET-BJH pore distribution with regards to the templates with various shell thickness. B) A representation of the relationship between the mesoporous shell thickness of the template and the pore volume and chitosan loading.

The mass of chitosan that was infused into the templates $TempCS_1P$, TempCSP, and $TempCS_2P$ was determined by TGA, where the change in weight from the template + chitosan, and the template after chitosan has burned off, was measured. The TGA determined that the amount of chitosan present per capsule was proportional to the thickness in the corresponding templates (Figure 5.8B), with the weight of chitosan polymer loading increasing from 65.84, 76.35 to 83.25 mg per gram of silica template with shell thicknesses of 31, 46 and 55 nm ($TempCS_1P$, TempCSP, and $TempCS_2P$) respectively.

After TGA was performed, the template particles were removed though selective etching to produce the chitosan capsules $CapCS_1P$, CapCSP and $CapCS_2P$. TEM images of these capsules were taken in an effort to observe the increase in capsule wall thickness (Figure 5.7D-F), however, due to extensive shrinkage upon TEM sample preparation and drying, it became very difficult to accurately determine the thickness of the walls. To overcome this obstacle, ultramicrotomed slices of the three chitosan capsules were obtained and TEM

images of thin sections were taken. As can be seen in Figure 5.7G-I there is a noteworthy increase in the thickness of the capsules wall with regards to the increase in the mesoporous shells of the corresponding templates. By measuring the thickness by this approach, we could estimate the relative increase in capsule wall thickness from ca. 28 nm to 45 nm to 56 nm. Furthermore, these images confirm the structural integrity of the capsules and show that a uniform shell is formed around the fabricated capsules.

Similar to the previous section, the loading capacity of curcumin/oleic acid into the capsules with different wall thickness was again investigated using UV-vis spectroscopy at a wavelength of 430 nm. In the case of capsule wall thickness, the loading was found to be proportional, with the drug encapsulation increasing from 0.74, 2.16 and 6.87 fg/capsule for the thinnest to thickest walls, respectively. This further supports the notion that significant amounts of curcumin is being loaded into the cavity wall because if the curcumin was primarily in the capsule cavity, the amount of curcumin observed here should have been very similar. Although the curcium loading range is not as broad as in the previous section where the capsule size was varied, the curcumin loading was still found to be proportional to the wall thickness. It can be seen in Figure 5.9(B) that there is a direct link between the drug encapsulation and the thickness of the shell of the template that has been used to fabricate the capsules.

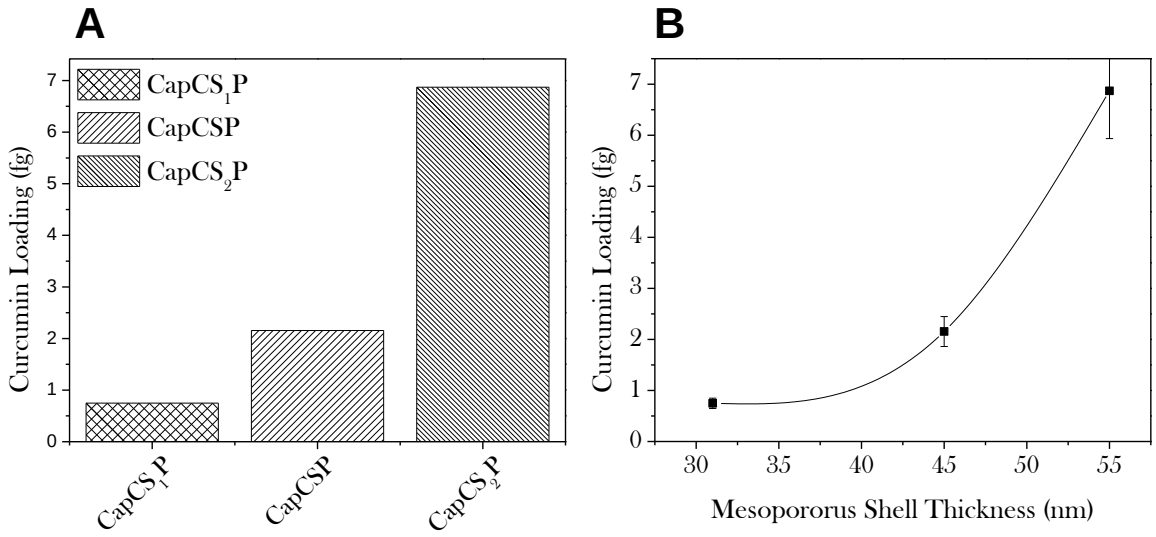

Figure 5.9: A representation of the curcumin loading with regards to A) the shell thickness of the template particles B) the three capsule types which have different capsule wall thickness.

This trend between shell thickness and drug loading suggests that while employing nanocapsules for drug delivery applications, it is highly important to consider drug loading both within the capsule cavity and its polymeric shell, which is often neglected, and this parameter has been shown to be controllable, allowing for further control of the drug dosage. Furthermore, this parameter offers a potential secondary site to include more than one chemotherapeutic agent using a single drug-delivery platform, wherein a hydrophilic or a hydrophobic drug may be conjugated to the capsule wall and another lipophilic drug may be loaded within the capsule cavity in a controllable manner.

5.3.3 Capsules with Different Shell Porosity

In a third set of separate experiments, the degree of porosity in the mesoporous shell of the SC/MS templates was an additional parameter which could be controlled and therefore exploited for the synthesis of more structurally unique capsules. Again, the same medium

solid core (TempC of diameter 290 nm) was employed; however the ratio of the porogen (TMS) to the silica precursor (TEOS) was varied from 0.1 to 0.5 (See Table 5.2) during mesoporous shell growth to produce the templates $TempCSP_1$, TempCSP, and $TempCSP_2$. This led to fabrication of templates with the same core size (290 nm) and similar mesoporous shell thickness (~45 nm), but with variations in the average pore diameter, and in turn the pore volume of the mesoporous shell. (Please note that the template TempCSP is the same template for the previous two sections, and was made with an intermediate ratio of 0.2 TMS to TEOS). TEM images for templates with different porosity levels have not been shown for brevity, as the pores are too small to distinguish and as such the TEM images for such templates appear identical. Instead, the variation in porosity levels of the silica templates was confirmed by BET surface area measurements, as shown in Figure 5.10. In comparison to the previous section where pore volume increases while the average pore size remained relatively constant (Figure 5.8A), here we see that both the pore volume and the average pore size increase in almost a linear fashion in regards to the changes in the ODTMS:TEOS ratio. From these results it is reasonable to expect an increase in chitosan loading, and therefore denser chitosan capsules which should show the higher curcumin loading in the order of $TempCSP_2$>TempCSP>$TempCSP_1$.

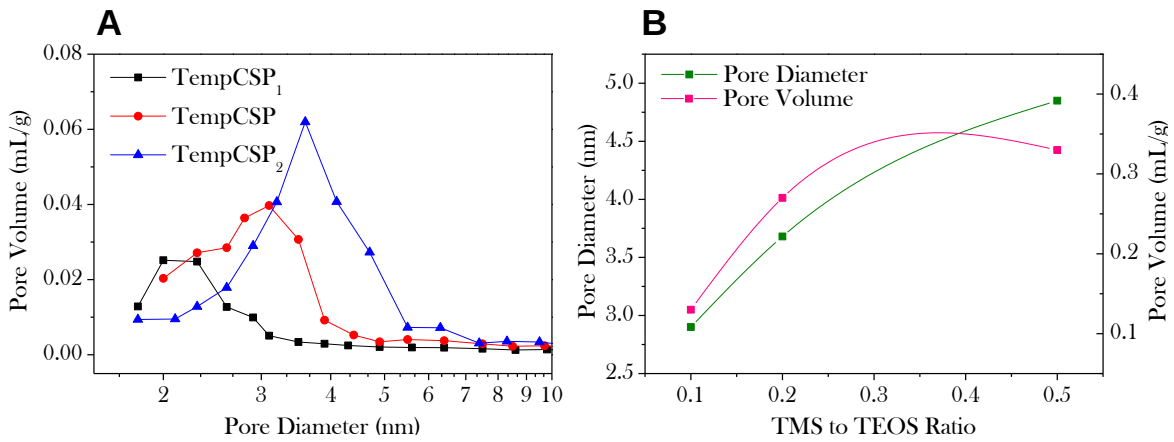

Figure 5.10: A) shows the BET-BJH pore size distribution of the SC/MS templates with varying porosity, and B) describes the changes in pore diameter and pore volume with respect to the TMS to TEOS ratio.

These SC/MS template particles which have demonstrated to have the same core and shell diameter but different shell pore diameters ($TempCSP_1$, TempCSP and $TempCSP_2$) were employed for a further set of structurally unique chitosan capsules with different levels of porosity. As the pore diameter effects the pore volume of the templates, the potential amounts of polymer infiltrated into the template for capsule fabrication can be controlled, and as the chitosan capsules were created using a templating process, the porosity of capsules is expected to be inversely proportional to the porosity of the SC/MS silica templates. Capsules prepared using templates with larger pores would allow more chitosan molecules to adsorb, thus generating capsule walls of the same thickness but increased chitosan density (Figure 5.3).

After template removal, the capsules $CapCSP_1$, CapCSP, and $CapCSP_2$ were produced and are displayed in Figure 5.11. Visually it seems that the capsules are becoming denser, with more chitosan material present across the capsules $CapCSP_1$, CapCSP, and $CapCSP_2$,

respectively. However, to more conclusively demonstrate that more chitosan material was present in the various templates shells before template removal, TGA analysis was carried out and the difference in weight was correlated to the amount of chitosan loading.

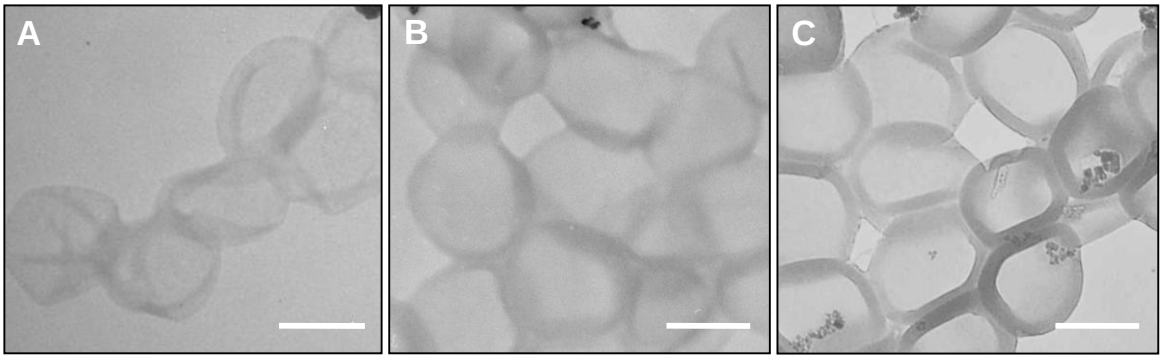

Figure 5.11: TEM images of chitosan nanocapsules of different porosity levels (A) $CapCSP_1$, (B) CapCSP and (C) $CapCSP_2$, synthesized using SC/MS templates $TempCSP_1$, TempCSP and $TempCSP_2$, respectively. Scale bars correspond to 200 nm.

TGA analysis revealed that as the pore volume of the mesoporous shell template increases from 0.13 to 0.27 and 0.33 mL g^{-1}, the weight of chitosan infiltrated within the template rose from 47.11, 76.35 to 81.26 mg per gram of silica template, respectively (Figure 5.12B). This supports the notion that different levels of porosity have been achieved in chitosan nanocapsules as the use of a mesoporous template produces inverse capsule. This is also further supported from the comparison of TEM images shown in Figure 5.11 where chitosan capsules with lowest loading (highest porosity) have significantly more folds and creases (Figure 5.11A) in comparison to other capsules, while the ones with lowest porosity (Figure 5.11C) appears well-formed and structurally rigid.

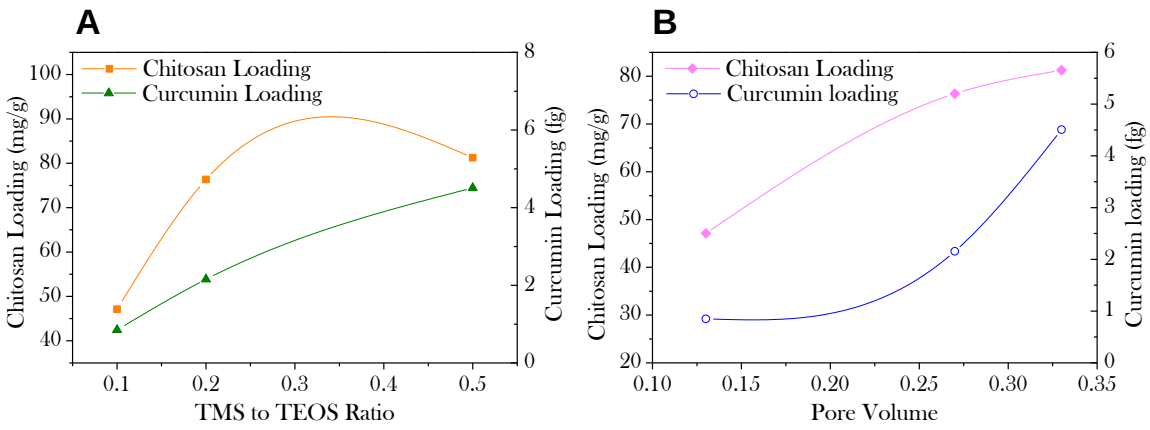

Figure 5.12: A representation of the chitosan and curcumin loading in regards to A) the TMS to TEOS ratio used, and B) the pore volume of the templates.

The amount of chitosan present in the SC/MS template particles has also demonstrated an effect on the curcumin drug loading capacity, with a close correlation between the pore volume and the chitosan loading. This indicates that there is at least some drug binding occurring onto the chitosan material as the capsules $CapCSP_1$, CapCSP and $CapCSP_2$ possess very few structural and functional differences from one another, meanwhile their drug loading capability are quite dissimilar, ranging from 0.851 to 4.507 fg per capsule. It is also plausible that the capsules with the denser wall ($CapCSP_2$) have a greater ability in retaining the encapsulated drug due to lower porosity, whereas the other capsules could undergo a small amount of leakage.

This controllable property of porosity is highly advantageous as it might allow for tunable diffusion and release kinetics of an incorporated drug, with denser capsules taking much longer to break down, allowing enough stability to reach a target site before drug delivery. Similar to a controllable capsule wall thickness, the controllability in the density of

the capsule wall also offers the potential of dosage control of a secondary drug if conjugated to the polymer material before capsule synthesis.

5.3.4 Cellular Uptake and Cytotoxicity of Curcumin-loaded Chitosan Nanocapsules

All types of chitosan nanocapsules which have been described throughout this chapter which possess the various structural characteristics of capsule size, capsule wall thickness and porosity, have been investigated and their chemotherapeutic cytotoxicity and efficiency against P815 mouse mastocytoma cells (leukemia cell line) was determined. As stated in the previous chapter, for comparative investigations the number of capsules between capsules of different type was kept constant, and the method of quantifying the number of capsules is outlined in Appendix 5.6.2. Although this method of quantification was exposed to potential error, it was the only possible method for comparison between capsule types, and therefore was deemed acceptable. Before the cytotoxicity studies were undertaken, the uptake of the chitosan capsules by P815 mouse mastocytoma cells was first determined. Confocal microscopy confirmed that there was a significant uptake of chitosan nanocapsules into the cells which can be seen as the fluorescent signal in Figure 5.13.

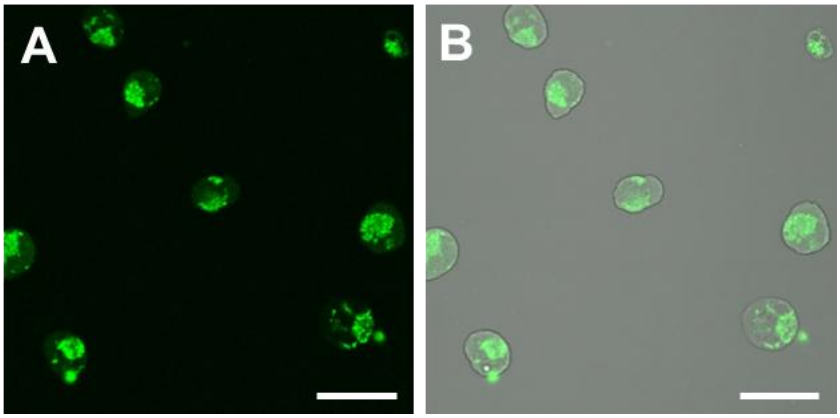

Figure 5.13: (A) Fluorescent and (B) an overlay of fluorescent and phase contrast image, showing cellular uptake of chitosan nanocapsules by P815 mast cells, as obtained by confocal microscopy. Scale bars correspond to 20 µm.

After capsule internalization into a cell, the enzymes present in lysosomes are known to be able to breakdown the cross-linked chitosan capsule wall to release the drug inside to cause a measurable and unique cytotoxic effect, therefore all the different types of chitosan capsules (CapCSP, $CapC_1SP$, $CapC_2SP$, $CapCS_1P$, $CapCS_2P$, $CapCSP_1$ and $CapCSP_2$) were tested through the incubation of i) pristine, chitosan only capsules, and ii) curcumin-loaded chitosan capsules over a 24 hour period, and the percentage of live cells that remained after treatment were counted.

On exposure to the pristine curcumin-free chitosan capsules, it was found that the capsules were highly biocompatible, showing negligible cytotoxicity with more than 95% cell viability on exposure to 750 capsules per cell, which slightly reduced to more than 85% on exposure to 1000 capsules per cell (Figure 5.14). Conversely, all types of curcumin-loaded capsules caused 95-100% cell death on exposure to less than 1000 capsules. The following investigations found that the minimum number of capsules required to cause >95 % cell death varied with the type of capsule used, wherein capsule size was found to show the most influential effect on toxicity, followed by porosity and wall thickness.

The cytotoxicity data displayed in Figure 5.14 corresponds to number of capsules per cell and therefore can be used to compare the ability of a single capsule of different type towards causing cytotoxicity, while later Figure 5.15 compares the chemotherapeutic efficiency of a particular capsule type with regards to amounts of curcumin available to cells during exposure to different type of capsules.

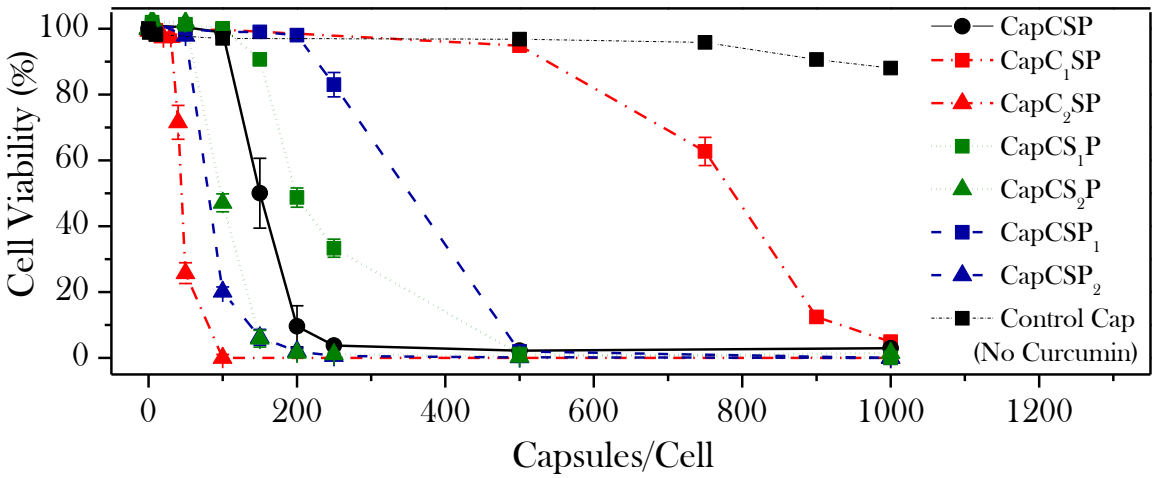

Figure 5.14: Comparison of the cytotoxicity profile of P815 mouse leukemic mast cells on exposure to equivalent numbers of different types of chitosan capsules per cell

Figure 5.15 suggests that if chemotherapeutic drugs are administered based on the lowest number of capsules required to cause cytotoxicity, in the order of decreasing cytotoxicity potential, the largest capsule ($CapC_2SP$) outperform all other capsule types, where smallest capsule ($CapC_1SP$) show lowest cytotoxicity potential and all other capsule types show intermediate effect in the order $CapCSP_2$> $CapCS_2P$> CapCSP> $CapCS_1P$> $CapCSP_1$. For instance, comparison of capsule size revealed that while exposure of only 100 largest size capsules ($CapC_2SP$) per cell is required to cause 100 % cell death, it will require a ten-fold higher number of smallest size capsules per cell to cause similar cytotoxicity. This is not surprising considering that a large capsule will have significantly higher amount of curcumin loading in comparison with a small capsule (23.49 and 0.16 fg per capsules, respectively). This is also the case with capsules that have a different wall thickness and wall density, with the cytotoxic potency increasing with an increase in capsule wall thickness or wall density, which in both cases also corresponds to an increase in curcumin loading.

Although these results give us a good idea of how the capsules will behave in clinical applications, these results reflect more on the drug loading capacities per capsules rather than the efficiency of the capsules. To compare their overall efficacy and to determine which capsule parameters display the greatest promise for drug delivery vehicles, the cell viability has been represented as a function of curcumin dosage, irrespective of the number of capsules required.

When comparing the overall efficiency of these nanocapsule systems (Figure 5.15), it becomes evident that the capsules with the smallest diameter are likely to be most efficient for therapeutic applications. This is notable because the overall amount of curcumin present in a dose of small capsules to achieve full cell death, regardless of the number required, is significantly lower (0.163 pg) than that required in a dose of largest

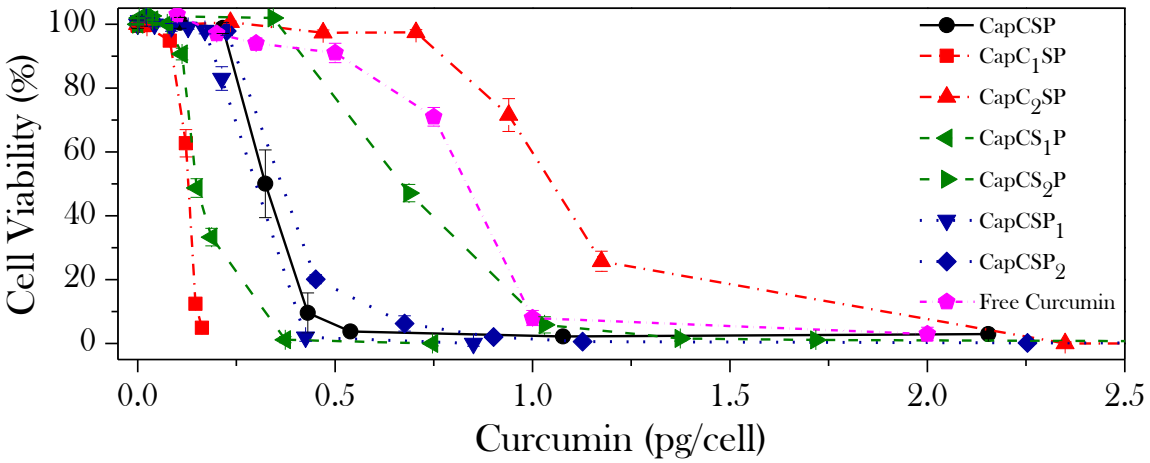

Figure 5.15: A depiction of the cytotoxicity efficiency of different types of capsules with regards to the amount of curcumin present in the specific capsule type

capsules (2.349 pg). This indicates that only 7% of the drug is required to achieve similar cytotoxic effects if smaller size capsules are used for drug delivery applications.

Interestingly, if one compares the efficiency of free curcumin molecules with that of smallest capsules loaded with curcumin, the latter requires one-sixth of the curcumin to achieve 95-100% cell death. In fact, most of the curcumin-loaded nanocapsular systems showed higher cytotoxic efficiency over free curcumin. This was as expected as it has been demonstrated in the previous chapter 4 that the free curcumin is not as efficient as encapsulated curcumin due to its degradation in the aqueous environment.

The next most influential factor (after capsule size) in controlling chemotherapeutic efficiency was found to be the thickness of the capsule wall, as is evident from Figure 5.15, wherein thinner capsules ($CapCS_1P$) were found to outperform capsules of medium thickness (CapCSP) and capsules with thickest walls ($CapCS_2P$), respectively. In comparison with the capsule size and wall thickness, the porosity of the capsule was found to have minimal effect on the chemotherapeutic efficiency of curcumin loaded within the capsules of different porosities, wherein the capsules of different porosities ($CapCSP_1$, CapCSP and $CapCSP_2$) showed very similar chemotherapeutic efficiencies (Figure 5.15).

From the above discussion, it is clearly evident that all the three factors *viz.* size, wall thickness and wall porosity contribute towards controlling the drug delivery profile of loaded curcumin. However, to further confirm that the size of the drug delivery vehicles is indeed the most influential factor to enable higher chemotherapeutic efficiency, and where variations in the shell thickness and porosity have minimal influence when the size is constant, a histogram in the order of their decreasing chemotherapeutic efficiency was plotted. The histogram (Figure 5.16) clearly shows that when these parameters are plotted in the order of their decreasing chemotherapeutic efficiency (as derived from Figure 5.15), the only trend that is

consistent is that of capsule diameter. Both the shell thickness and pore diameter show no linear relationship with the decrease in efficiency as the plot moves to the right. This suggests that amongst different structural characteristics of a nanocapsule-based drug carrier system, size of the nanocapsules is likely to play the most important role in dictating the chemotherapeutic efficiency of such systems.

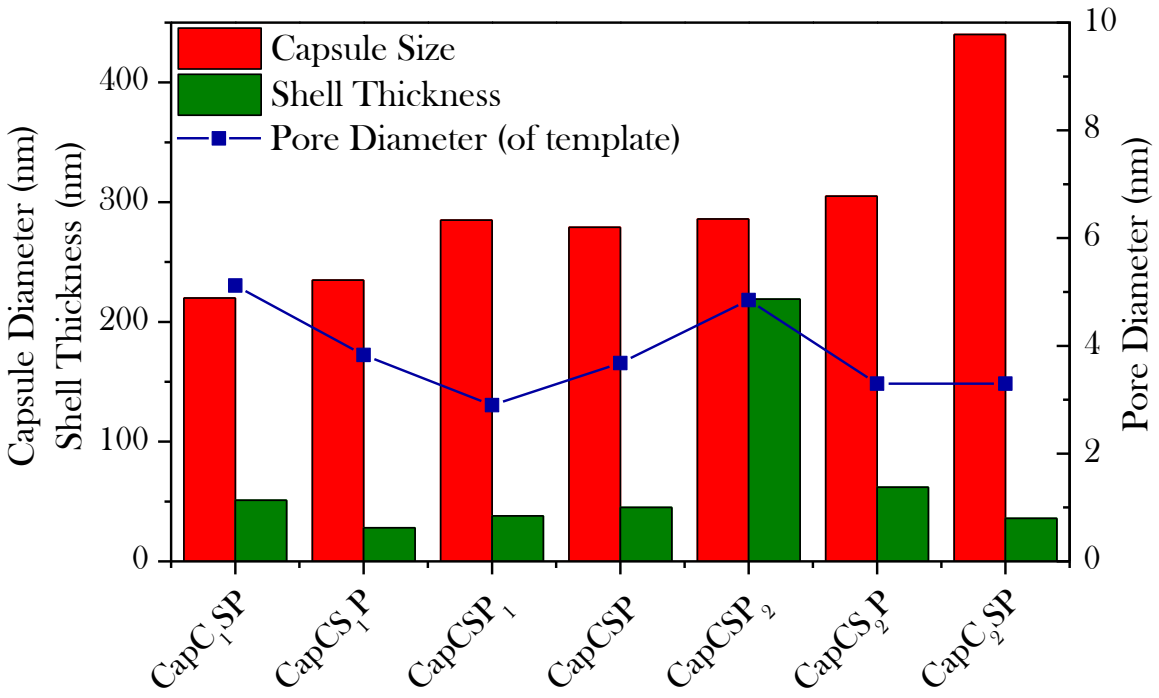

Figure 5.16: **Experimental conditions for the synthesis of meosporous shell of SC/MS silica template particles.**

5.4 Conclusion

It has been demonstrated for the first time that the structural characteristics of chitosan nanocapsules such as capsule size, wall thickness and wall porosity can be fine-tuned in a facile manner by simply controlling the structural characteristics of the SC/MS template particles without varying the chemical characteristics of the capsules. Studies into the effect of

size on a capsule's drug loading and cell toxicity characteristics have been previously investigated.[19,40] However, to the author's knowledge there are currently no reports in which the three interconnected characteristics of capsule size, wall thickness and porosity have been investigated in a single, comprehensive study. The loading of seven types of chitosan capsules possessing different structural features (e.g. nanocapsule diameters ranging from ca. 220 to 440 nm, nanocapsule shell thickness ranging from ca. 31 to 55 nm, and pore diameter varying from 2.9 to 5.1 nm) with curcumin, a lipophilic anticancer drug, enabled us to correlate the effect of these structural features of chitosan nanocapsules with their anticancerous efficiency. These investigations revealed that by controlling the structural characteristics of chitosan nanocapsule, the amount of curcumin loading within these capsules can be controlled between ca. 0.2 to 23.5 fg per capsule. The pristine chitosan nanocapsules were found to be biocompatible and interestingly, the capsules with the smallest diameter (220 nm) were found to be six times more efficient for cancer therapy in comparison with equivalent amount of free curcumin. This suggests that encapsulation of water-intolerant drug molecules such as curcumin within chitosan capsules provides a significant opportunity to achieve higher efficiency of existing chemotherapeutic drugs. Most importantly, this study establishes an important finding in the field of nanocapsule-based drug delivery systems that although several structural characteristics of a nanocapsule might be responsible in influencing their efficiency as a chemotherapeutic carrier, size of the nanocapsules is likely to play the most important role in dictating the chemotherapeutic efficiency of such systems. This finding will generate new exciting opportunities for designing drug delivery vehicles for a range of therapeutic applications.

5.5 References

1 Khor, E. & Lim, L. Y. Implantable applications of chitin and chitosan. *Biomaterials* **24**, 2339-2349, (2003).

2 Ravi Kumar, M. N. V. A review of chitin and chitosan applications. *Reactive and Functional Polymers* **46**, 1-27, (2000).

3 Zeng, X. & Ruckenstein, E. Control of Pore Sizes in Macroporous Chitosan and Chitin Membranes. *Industrial & Engineering Chemistry Research* **35**, 4169-4175, (1996).

4 Gan, Q. & Wang, T. Chitosan nanoparticle as protein delivery carrier--Systematic examination of fabrication conditions for efficient loading and release. *Colloids and Surfaces B: Biointerfaces* **59**, 24-34, (2007).

5 Goy, R. C., Britto, D. d. & Assis, O. B. G. A review of the antimicrobial activity of chitosan. *Polímeros* **19**, 241-247, (2009).

6 Al-Helw, A. A., Al-Angary, A. A., Mahrous, G. M. & Al-Dardari, M. M. Preparation and evaluation of sustained release cross-linked chitosan microspheres containing phenobarbitone. *Journal of Microencapsulation* **15**, 373-382, (1998).

7 Kumbar, S. G. & Aminabhavi, T. M. Synthesis and characterization of modified chitosan microspheres: Effect of the grafting ratio on the controlled release of nifedipine through microspheres. *Journal of Applied Polymer Science* **89**, 2940-2949, (2003).

8 Kumbar, S. G., Kulkarni, A. R. & Aminabhavi, T. M. Crosslinked chitosan microspheres for encapsulation of diclofenac sodium: Effect of crosslinking agent. *Journal of Microencapsulation* **19**, 173-180, (2002).

9 Conti, B. *et al.* Microencapsulation of cetylpyridinium chloride with a bioadhesive polymer. *Proceedings of the Controlled Release Society*, 822-823, (1998).

10 Ganza-González, A., Anguiano-Igea, S., Otero-Espinar, F. J. & Blanco Méndez, J. Chitosan and chondroitin microspheres for oral-administration controlled release of metoclopramide. *European Journal of Pharmaceutics and Biopharmaceutics* **48**, 149-155, (1999).

11 He, P., Davis, S. S. & Illum, L. Chitosan microspheres prepared by spray drying. *International Journal of Pharmaceutics* **187**, 53-65, (1999).

12 Nishimura, K., Nishimura, S. & Seo, H. Macrophage activation with multi-porous beads prepared from partially deacetylated chitin. *Journal of Biomedical Materials Research* **20**, 1359-1372, (1986).

13 Aydin, Z. & Akbuğa, J. Chitosan beads for the delivery of salmon calcitonin: Preparation and release characteristics. *International Journal of Pharmaceutics* **131**, 101-103, (1996).

14 Sezer, A. D. & Akbuga, J. Controlled release of piroxicam from chitosan-beads. *International Journal of Pharmaceutics* **121**, 113-116, (1995).

15 Shu, X. Z. & Zhu, K. J. A novel approach to prepare tripolyphosphate/chitosan complex beads for controlled release drug delivery. *International Journal of Pharmaceutics* **201**, 51-58, (2000).

16 Tokumitsu, H., Ichikawa, H. & Fukumori, Y. Chitosan-gadopentetic acid complex nanoparticles for gadolinium neutron- capture therapy of cancer: Preparation by novel emulsion- droplet coalescence technique and characterization. *Pharmaceutical Research* **16**, 1830-1835, (1999).

17 Mitra, S., Gaur, U., Ghosh, P. C. & Maitra, A. N. Tumour targeted delivery of encapsulated dextran-doxorubicin conjugate using chitosan nanoparticles as carrier. *Journal of Controlled Release* **74**, 317-323, (2001).

18 Agnihotri, S. A. & Aminabhavi, T. M. Controlled release of clozapine through chitosan microparticles prepared by a novel method. *Journal of Controlled Release* **96**, 245-259, (2004).

19 Cortez, C. *et al.* Influence of Size, Surface, Cell Line, and Kinetic Properties on the Specific Binding of A33 Antigen-Targeted Multilayered Particles and Capsules to Colorectal Cancer Cells. *Acs Nano* **1**, 93-102, (2007).

20 Desai, M., Labhasetwar, V., Amidon, G. & Levy, R. Gastrointestinal Uptake of Biodegradable Microparticles: Effect of Particle Size. *Pharmaceutical Research* **13**, 1838-1845, (1996).

21 Elsner, N., Dubreuil, F. & Fery, A. Tuning of microcapsule adhesion by varying the capsule-wall thickness. *Physical Review E* **69**, 031802, (2004).

22 Sukhorukov, G. B. & Möhwald, H. Multifunctional cargo systems for biotechnology. *TRENDS in Biotechnology* **25**, 93-98, (2007).

23 Ammon, H. P. T. & Wahl, M. A. Pharmacology of Curcuma longa. *Planta Med.* **57**, 1-7, (1991).

24 Chen, Y., Lin, X., Park, H. & Greever, R. Study of artemisinin nanocapsules as anticancer drug delivery systems. *Nanomedicine: Nanotechnology, Biology and Medicine* **5**, 316-322, (2009).

25 Gregory, L., Elias, F., Huguette, P.-A., Annette, G. & Patrick, C. Polyisobutylcyanoacrylate nanocapsules containing an aqueous core as a novel colloidal carrier for the delivery of oligonucleotides. *Pharmaceutical Research* **17**, 707, (2000).

26 Guterres, S. S., Fessi, H., Barratt, G., Puisieux, F. & Devissaguet, J.-P. Poly(D,L-Lactide) Nanocapsules Containing Non-Steroidal Anti-Inflammatory Drugs: Gastrointestinal Tolerance Following Intravenous and Oral Administration. *Pharmaceutical Research* **12**, 1545-1547, (1995).

27 Krol, S. *et al.* Nanocapsules—A Novel Tool for Medicine and Science. *Frontiers of Multifunctional Integrated Nanosystems*, 439-446, (2005).

28 Lenaerts, V. *et al.* Nanocapsules with a reduced liver uptake: targeting of phthalocyanines to EMT-6 mouse mammary tumour in vivo. *European Journal of Pharmaceutics and Biopharmaceutics* **41**, 38-43, (1995).

29 Li, S., He, Y., Li, C. & Liu, X. In vitro release of protein from poly(butylcyanoacrylate) nanocapsules with an aqueous core. *Colloid & Polymer Science* **283**, 480-485, (2005).

30 Mora-Huertas, C. E., Fessi, H. & Elaissari, A. Polymer-based nanocapsules for drug delivery. *International Journal of Pharmaceutics* **385**, 113-142.

31 Sablon, K. Single-component polymer nanocapsules for drug delivery application. *Nanoscale Research Letters* **3**, 265-267, (2008).

32 Shu, S. *et al.* Hollow and degradable polyelectrolyte nanocapsules for protein drug delivery. *Acta Biomaterialia* **6**, 210-217.

33 Sukhorukov, G., Fery, A. & Möhwald, H. Intelligent micro-and nanocapsules. *Progress in Polymer Science* **30**, 885-897, (2005).

34 Wang, Y., Bansal, V., Zelikin, A. N. & Caruso, F. Templated Synthesis of Single-Component Polymer Capsules and Their Application in Drug Delivery. *Nano Letters* **8**, 1741-1745, (2008).

35 Stöber, W., Fink, A. & Bohn, E. Controlled growth of monodisperse silica spheres in the micron size range. *Journal of Colloid and Interface Science* **26**, 62-69, (1968).

36 Brunauer, S., Emmett, P. H. & Teller, E. *Journal of American Chemical Society* **60**, 309, (1938).

37 Pratten, M. K. & Lloyd, J. B. Pinocytosis and phagocytosis: The effect of size of a particulate substrate on its mode of capture by rat peritoneal macrophages cultured in vitro. *Biochimica et Biophysica Acta - General Subjects* **881**, 307-313, (1986).

38 Sivakumar, S. *et al.* Degradable, Surfactant-Free, Monodisperse Polymer-Encapsulated Emulsions as Anticancer Drug Carriers. *Advanced Materials* **21**, 1820-1824, (2009).

39 Mehta, K., Pantazis, P., McQueen, T. & Aggarwal, B. B. Antiproliferative effect of curcumin (diferuloylmethane) against human breast tumor cell lines. *Anticancer Drugs* **8**, 470–481, (1997).

40 Lamprecht, A. & Benoit, J.-P. Etoposide nanocarriers suppress glioma cell growth by intracellular drug delivery and simultaneous P-glycoprotein inhibition. *Journal of Controlled Release* **112**, 208-213, (2006).

5.6 Appendix

5.6.1 Tabular summaries of the silica template particles and chitosan nanocapsules fabricated

Template	Description	Core Size (nm)	MP Shell Thickness (nm)	Surface Area (m^2 g^{-1})	Pore Size in Shell (nm)	Pore Volume (mL g^{-1})
	Solid Cores					
$TempC_1$	Small diameter	170 ± 12	-	25.86	-	-
TempC	Medium Diameter	290 ± 24	-	14.37	-	-
$TempC_2$	Large Diameter	490 ± 14	-	8.50	-	-
	Solid Cores, Mesoporous Shell					
$TempC_1SP$	Medium Diameter, Medium Shell Thickness, Medium Pores Size	290 ± 24	46 ± 7	252.6	3.68	0.27
TempCSP	Small diameter, Medium Shell Thickness, Medium Pore size	170 ± 12	49 ± 16	300.0	5.12	0.44
$TempC_2SP$	Large Diameter, Medium Shell Thickness, Medium Pore Size	490 ± 14	42 ± 13	164.2	3.30	0.16
$TempCS_1P$	Medium Diameter, Small Shell Thickness, Medium Pores Size	290 ± 24	31 ± 21	144.1	3.83	0.16
$TempCS_2P$	Medium Diameter, Large Shell Thickness, Medium Pores Size	290 ± 24	55 ± 12	308.7	3.33	0.30
$TempCSP_1$	Medium Diameter, Medium Shell Thickness, Small Pores Size	290 ± 24	42 ± 9	184.0	2.90	0.13
$TempCSP_2$	Medium Diameter, Medium Shell Thickness, Large Pores Size	290 ± 24	48 ± 14	253.1	4.85	0.33

Table 5.4: A summary of the structural characteristics of the SC/MS silica template particles fabricated throughout the chapter.

Capsule	Description	Capsule Diameter (nm)	Shell Wall (nm)	Chitosan Loading (mg g-1)	Curcumin Loading (fg/capsule)
CapCSP	Medium Diameter, Medium Wall Thickness, Medium Porosity	270	45	76.35	2.155
$CapC_1SP$	Small Diameter, Medium Shell Thickness, Medium Porosity	220	47	97.73	0.163
$CapC_2SP$	Large Diameter, Medium Wall Thickness, Medium Porosity	440	40	73.36	23.492
$CapCS_1P$	Medium Diameter, Thin Wall Thickness, Medium Porosity	235	28	65.84	0.748
$CapCS_2P$	Medium Diameter, Thick Wall Thickness, Medium Porosity	325	56	83.25	6.870
$CapCSP_1$	Medium Diameter, Medium Wall Thickness, High Porosity	269	40	47.11	0.851
$CapCSP_2$	Medium Diameter, Medium Wall Thickness, Low Porosity	283	42	81.26	4.507

Table 5.5: A summary of the structural characteristics and loading capabilities of the chitosan nanocapsules fabricated throughout the chapter.

5.6.2 Quantifying of the number of capsules

As used in the previous chapter, the number of capsules was quantified by calculating the relative number of silica template particles based on the number of large spheres counted by a sample method. After the number of large particles was known, this value could be used to calculate the number of the other templates. As the diameters of the spheres were known, their volumes could be calculated and used to estimate the relatively number of particles in the samples of templates with three different core sizes (where the silica source/mass of particles fabricated was constant but the number of particles produced varied with size). Furthermore, as the weights of the samples varied greatly after the mesoporous shell growth, these values had to be recalculated and recalibrated to take into account the new weights. This was achieved by measuring the templates before and after shell growth. The number of capsules could then be correlated back to the weight of the templates that were used during capsule fabrication so that drug loading and toxicity could be represented with regards to a single capsule.

As stated in the previous chapter, this method of quantification allows for potential error to occur, however as there was no other method of counting the number of particles required for a sufficient comparison of the capsule types, the method and its potential error was accepted.

CHAPTER 6

CONCLUSIONS

This chapter provides a summary of the key findings of this thesis, and also elaborates on the potential for future work.

6.1 Summary of Accomplished Work

Although current cancer treatments help to reduce or eliminate cancerous cells from the body, they are not always effective, efficient and often cause adverse side effects. For example, chemotherapeutic drug do not greatly differentiate between healthy and cancerous cells, consequently they attack both types and cause systemic toxicity. Furthermore, the free circulating drug molecules are often rapidly eliminated from the body before carrying out their desired function.

Drug delivery systems (DDS) which confine an anticancerous drug within a carrier vehicle have proven enhanced cell toxicity, targeting, and retention time in the body, with fewer adverse side effects to the patient.[1,2] The aim of this thesis was to develop a DDS with improved structural and physio-chemical characteristics that could impose the desired cytotoxic effects ideal for cancer therapy applications. This was achieved through the fabrication of drug-loadable polymeric nanocapsules by employing monodispersed silica nanoparticles with tunable physico-chemical properties as templates.

Before the capsules were fabricated, fine control over the size and monodispersity of the silica template particles was established. To achieve this control, the effects of solvent, temperature, ammonia and water concentration on silica nanoparticle synthesis were investigated through single variable experiments, where it was determined that the solvent and temperature had major influences on the rate of particle nucleation, while the ammonia and water concentrations effected the reaction mechanisms in a dynamic and complex manner. An Artificial Neuron Network (ANN) was then applied to simulate the effects of these experimental parameters over a more comprehensive, 3-dimensional parameter range. Using

additional, multivariable experiments, a forecasting model of particle size with regards to temperature, ammonia and water concentration was generated. When compared with the single experimental results the forecast model was found to be relatively accurate, and allows for the prediction of the approximate experimental conditions required for the fabrication of silica template particles of a defined size.

These silica nanoparticles were then used as sacrificial templates to generate polymeric nanocapsules. The two template-facilitated fabricating approaches SC/MS and LbL were employed along with the polymers chitosan, poly(allylamine hydrochloride), poly(sodium 4-styrenesulfonate) to generate four unique capsules. The capsules fabricated using the SC/MS approach demonstrated an increased amount of polymer loading and increased capsule wall thickness, while also undergoing less aggregation when compared with the capsules fabricated using the LbL approach. Although it was found that the drug loading capability was found to be influenced by the polymeric material, the cytotoxicity efficiency of the capsules was predominantly governed by the degree of aggregation that occurred on exposure of capsules to mammalian cells. It was found that the combination of chitosan and the SC/MS fabrication method generated the capsules with the most desirable characteristics for a drug delivery system, warranting further investigation.

The SC/MS templates in combination with chitosan polymer were further adapted to fabricate seven structurally unique chitosan nanocapsules. Three sizes of the solid core of the SC/MS templates were fabricated based on previous investigations into experimental condition and silica size, to produce chitosan capsules with three different internal diameters. The shell thickness and porosity of the mesoporous shell of the templates were also modified

to create capsules with dissimilar capsule wall thicknesses and porosities. The effect of the structural changes in the template on the physio-chemical characteristics of the capsules such as polymer loading, drug loading, and cytotoxic efficiency against P815 mastocytoma cells was investigated. It was found that, although the amount of drug loading was proportional to the capsule size and wall thickness, it is the decrease in capsule diameter that increases the capsule's cytotoxic efficiency.

Through systematic investigation, a highly controlled, chitosan-based nanocapsular drug delivery system has been developed for the first time. Through a template assisted approach that demonstrated improved results, the fabrication of robust, near monodispersed, chitosan-based nanocapsules with a variety of structural and physio-chemical characteristics have been successfully generated. This thesis illustrates that through the modification of SC/MS template particles, nanocapsules can be turned based on their required properties such as capsule polymeric material, size, shell thickness, porosity, drug loading capability and cytotoxic efficiency, with the intention of applying these materials in future cancer therapies.

6.2 Possible Future Endeavours

Considering the vast possibilities that the work contained within this thesis could be applied to, a select number of suggested investigations for the future have be briefly discussed.

The SC/MS template-facilitated approach to nanocapsule synthesis can be applied to any ionic polymeric material which is below the dimensions to be able to infiltrate the pores of the template shell. As a result, it would be worthwhile fabricating nanocapsules of a

negatively charged polymer such as poly(L-glutamate), and investigating the effects of a negatively charged nanocarrier on its ability to act as a DDS. This may have important implications in drug delivery as cell membranes are negatively charged.[3,4] It would be interesting to study that whether negatively charged capsules will show reduced uptake due to electrostatic repulsion or the polymeric charge would not significantly influence capsule uptake, as endocytotic forces may dominate over electrostatic forces. It was indeed observed previously that physical form of polymer may have significant influence on their biological uptake profile.[5]

Another very advantageous endeavour with the presented drug delivery system would be to conjugate targeting ligands or antibodies onto the surface of the capsules to enhance specific uptake by tumour cells. Furthermore, non-fouling polymers such as polyethylene glycol (PEG) can also be conjugated to the surface to improve the stealth characteristics and increase retention time. Once again, the endocytotic cellular uptake profile of nanocapsules post-functionalization with targeting ligands or non-fouling polymers may be very different than those of non-modified systems.[6]

Finally, the incorporation of additional materials such as magnetic nanoparticles or fluorescent quantum dots into the template particles could lead to the development of multifunctional drug delivery systems. The combination of these materials would result in a controllable drug delivery system that would demonstrate enhanced targeting and imaging capabilities for theranostic (therapy and diagnostic) applications.

There remain many more fabrication methods and materials which could offer advantages over the drug delivery system presented in this thesis, but it is hoped that the

knowledge generated in this thesis contributes to the ongoing research in finding an effective tool in the fight against grievous illnesses like cancer.

6.3 References

1 Kumar, C. *Polymeric Nanomaterials*. Vol. 10 (Wiley-VCH, 2011).

2 Moghimi, S. M., Hunter, A. C. & Murray, J. C. Long-circulating and target-specific nanoparticles: Theory to practice. *Pharmacological Reviews* **53**, 283-318, (2001).

3 Foged, C., Brodin, B., Frokjaer, S. & Sundblad, A. Particle size and surface charge affect particle uptake by human dendritic cells in an in vitro model. *International Journal of Pharmaceutics* **298**, 315-322, (2005).

4 Jung, T. *et al.* Biodegradable nanoparticles for oral delivery of peptides: is there a role for polymers to affect mucosal uptake? *European Journal of Pharmaceutics and Biopharmaceutics* **50**, 147-160, (2000).

5 Wang, Y., Bansal, V., Zelikin, A. N. & Caruso, F. Templated Synthesis of Single-Component Polymer Capsules and Their Application in Drug Delivery. *Nano Letters* **8**, 1741-1745, (2008).

6 Bahmani, B., Gupta, S., Upadhyayula, S., Vullev, V. I. & Anvari, B. Effect of polyethylene glycol coatings on uptake of indocyanine green loaded nanocapsules by human spleen macrophages in vitro. *Journal of Biomedical Optics* **16**, 051303-051303, (2011).

CHAPTER 7

APPENDIX

7.1 Publications

Cover page, E. C. Goethals, A. Elbaz, A. L. Lopata, S. K. Bhargava, V. Bansal. Size Dictates Drug Delivery Efficiency of Curcumin-Infiltrated Chitosan Nanocapsules. *Langmuir*, **29**, 2, 511-859 (January 15 2013).

E. C. Goethals, A. Elbaz, A. L. Lopata, S. K. Bhargava, V. Bansal. Decoupling the Effects of the Size, Wall Thickness, and Porosity of Curcumin-Loaded Chitosan Nanocapsules on Their Anticancer Efficacy: Size Is the Winner. *Langmuir*, **29,** 2, 658-666, (2012).

E. C. Goethals, A. Elbaz, A. L. Lopata, S. K. Bhargava, V. Bansal. Templated synthesis of size controlled chitosan nanocapsules for drug delivery. Proceedings of the 2012 *International Conference on Nanoscience and Nanotechnology* (ICONN 2012), Perth, Australia, pp. 766-1-2 (Feb 2012).

E. C. Goethals, V. Bansal, S. K. Bhargava. Templated synthesis of chitosan nanocapsules with controllable shell thickness and porosity, in *Chemeca 2010: Engineering at the Edge*; 26-29 September 2010, Hilton Adelaide, South Australia. Barton, A.C.T.: Engineers Australia, 2845-2854, (2010)

E. C. Goethals, A. Esmaielzadeh Kandjani, S. K. Bhargava, V. Bansal. Optimized Synthesis of Ordered Macroporous Carbon Materials Using Size Controlled Silica Templates With Artificial Neural Network. *Communicated*

E. C. Goethals, R. Shukla, V. Mistry, S. K. Bhargava, V. Bansal. Role of the templating approach in influencing the suitability of polymeric nanocapsules for drug delivery: LbL vs SC/MS. *Communicated*

Langmuir
The ACS Journal of Surfaces and Colloids

JANUARY 15, 2013
VOLUME 29, NUMBER 2
pubs.acs.org/Langmuir

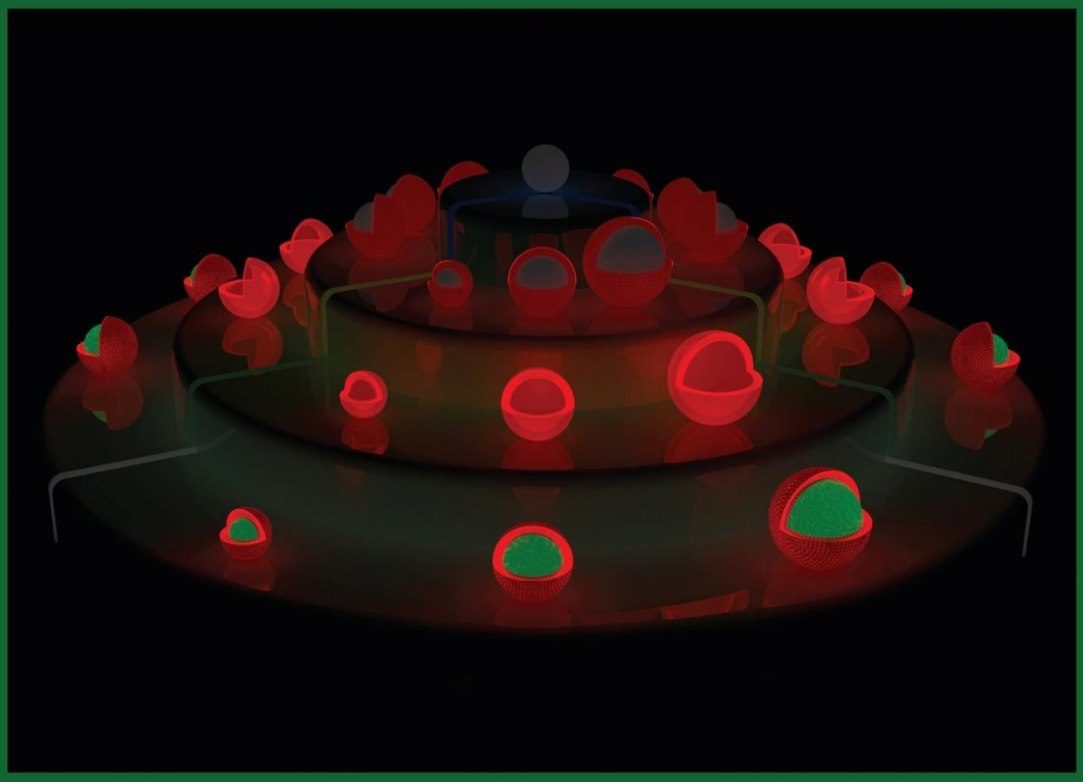

Size Dictates Drug Delivery Efficiency of Curcumin-Infiltrated Chitosan Nanocapsules

(see p. 5A)

ACS Publications
MOST TRUSTED. MOST CITED. MOST READ.

www.acs.org